ROYAUME DU MAROC
Université Mohammed V
- RABAT -
جامعة محمد الخامس
– الرباط –
Faculté des sciences
كلية العلوم
CENTRE D'ÉTUDES DOCTORALES - SCIENCES ET TECHNOLOGIES

N° d'ordre : 3939

THÈSE

en vue de l'obtention du : **DOCTORAT**

Centre de Recherche : Centres des Etudes Doctorales Sciences et Techniques (CEDOC-ST)
Structure de Recherche : Laboratoire de Matière Condensée et Sciences Interdisciplinaires(LAMCSCI)
Discipline : Physique Informatique
Spécialité : Physique Appliquée

Présentée et Soutenue le : *06 / 07 / 2024*
par :

Amal EZ-ZAHAR

Intelligent Traffic Management Strategies: Exploring the Impact of U-Turns and Adaptive Traffic Lights on Traffic Flow, Energy Dissipation, and Environmental Outcomes at Circular Intersections through Cellular Automaton Models

Devant le JURY :

Abdallah El Kenz	PES, Université Mohammed V, Faculté des Sciences, Rabat	Président
Abdelaziz Mhirech	PES, Université Mohammed V, Faculté des Sciences, Rabat	Rapporteur/ Examinateur
Youssef El Amraoui	PES, Université Mohammed V, Faculté des Sciences, Rabat	Rapporteur/ Examinateur
Ismail Essaoudi	PES, Université Moulay Ismail, Faculté des Sciences, Meknès	Rapporteur/ Examinateur
Abdelilah Benyoussef	PES, Expert, Académie Hassan II des Sciences et Techniques, Rabat	Examinateur
Hamid Ez-zahraouy	PES, Université Mohammed V, Faculté des Sciences, Rabat	Directeur de thèse

Année Universitaire : 2023 - 24

"This thesis is dedicated to my parents, who have always loved and supported me, guiding me through life. To my siblings, with whom I've shared many happy memories and laughter. And to my husband and son, who inspire me daily to be the best I can be. I also dedicate this to all my professors and friends, whose guidance, support, and companionship have been invaluable to me. With immense gratitude and love, thank you all."

Acknowledgments

This thesis was conducted at the Laboratory of Condensed Matter and Interdisciplinary Sciences (LAMScI) at the Faculty of Sciences, Mohammed V University in Rabat. The research was supervised by Mr. **Hamid EZ-ZAHRAOUY** and co-supervised by Mr. **Noureddine LAKOUARI**.

Firstly, I would like to express my sincere gratitude to Mr. **Hamid EZ-ZAHRAOUY**, Professor of Higher Education at the Faculty of Sciences in Rabat, for supervising my thesis at the Faculty of Sciences in Rabat. His constant support and guidance throughout my research were invaluable. I am deeply grateful for his willingness to share his time and expertise, which greatly contributed to the success of my work. I feel fortunate to have had the opportunity to work under his supervision in this laboratory.

I would like to express my heartfelt thanks to Mr. **Noureddine LAKOUARI**, Professor at the Instituto Nacional de Astrofísica, Óptica y Electrónica in Puebla, Mexico, for serving as my co-director and imparting valuable knowledge and expertise in this area. His guidance, encouragement, and inspiring qualities have had a significant impact on my research career, and I feel privileged to have collaborated with him.

I am sincerely grateful to Mr. **Outmane Oubram** and Mr. **J. G. Velásquez-Aguilar**, Professors at the Universidad Autónoma del Estado de Morelos (UAEM), Mexico, for providing me with an invaluable internship opportunity at UAEM. I would like to extend special thanks to Mr. **Outmane** for his warm welcome, guidance, and support throughout my internship. The skills and knowledge I acquired during this experience will undoubtedly be beneficial to my future academic and professional pursuits.

I would like to express my sincere gratitude to Mr. **Abdellah EL KENZ**, Professor of Higher Education at the Faculty of Sciences Rabat, for accepting the role of chairing the thesis jury.

I extend my gratitude to Mr. **Abdelaziz MHIRECH**, Professor of Higher Education at the Faculty of Sciences Rabat, for agreeing to serve as the rapporteur and a member of the jury for this examination.

My sincere thanks go to Mr. **Youssef EL AMRAOUI**, Professor of Higher Education at the Faculty of Sciences Rabat, for accepting to serve as the rapporteur and a member of the jury for this examination.

I would like to express my heartfelt gratitude to Mr. **Ismaïl ESSAOUDI**, Professor of Higher Education at the Faculty of Sciences in Meknes, for agreeing to serve as the rapporteur and a member of the jury for this examination.

I extend my heartfelt thanks to Mr. **Abdelilah Benyoussef**, Professor of Higher Education at the Faculty of Sciences, Rabat, and member of the Hassan II Academy, Rabat, for agreeing to participate in this jury as an examiner.

Lastly, I am immensely grateful to my parents, siblings, husband, and friends for their unwavering support throughout my academic journey. Their love and guidance have been my strength.

Abstract

Circular intersections, such as roundabouts and traffic circles, are increasingly being used globally to improve safety and manage traffic flow, reducing collisions. However, challenges persist, including minimizing environmental impact, ensuring pedestrian safety, understanding vehicle behavior, and alleviating traffic congestion. Despite significant investments, expanding infrastructure may not be sufficient. Effective resource management is essential, and modeling and simulation can play a crucial role. Traffic flow theories and models, such as the Nagel and Scherkenberg model of cellular automata (CA), can describe vehicle-to-vehicle and vehicle-to-infrastructure interactions, making CA models particularly well-suited for this purpose.

This thesis contributes to the field of traffic modeling at circular intersections by examining the effects of complete turning movements, such as U-turns and continuous turning without a specific direction, in single-lane roundabout systems. The study investigates the impact of increasing the number of vehicles performing these movements on traffic flow characteristics, CO_2 emissions, and energy dissipation. Additionally, the research explores conflicts arising from vehicles not adhering to safe gaps when entering the circulating lane and their impact on the roundabout's capacity. The findings reveal that this practice decreases the system's efficiency. To mitigate these issues, we propose the use of traffic lights to control vehicle flow, minimize conflicting interactions, and enhance traffic flow.

In the final section of the thesis, an intelligent strategy is proposed to manage and optimize traffic flow in traffic circles. This strategy employs a hybrid simulation model based on cellular automata for traffic control, which integrates traffic lights and priority rules specific to traffic circles. The model evaluates traffic flow in circulating lanes, using traffic density, satisfaction rate, average speed, time headway, and the density of stopped cars as feedback parameters. The results of the study indicate that these parameters effectively eliminate the gridlock phase that typically characterizes traffic flow in traffic circles without lights, thereby significantly improving throughput and efficiency in traffic circles.

Keywords: Cellular Automaton, Roundabout, Phase Diagram, Full Turn, Energy Dissipation, Safety Gap, CO_2 Emissions, Traffic Circle, Adaptive Traffic Lights.

Résumé

Les intersections circulaires, telles que les ronds-points et les carrefours giratoires, sont de plus en plus utilisées dans le monde entier pour améliorer la sécurité et la gestion du trafic, réduisant ainsi le nombre de collisions. Cependant, des défis persistent, notamment la minimisation de l'impact environnemental, la garantie de la sécurité des piétons, la compréhension du comportement des véhicules et la réduction de la congestion du trafic. Malgré des investissements importants, l'expansion de l'infrastructure peut ne pas être suffisante. Une gestion efficace des ressources est essentielle, et la modélisation et la simulation peuvent jouer un rôle crucial. Les théories et les modèles de circulation, tels que le modèle de cellular automata (CA) de Nagel et Scherkenberg, peuvent décrire les interactions entre les véhicules et entre les véhicules et l'infrastructure, ce qui rend les modèles CA particulièrement adaptés à cette fin.

Cette thèse contribue au domaine de la modélisation du trafic aux intersections circulaires en examinant les effets des manœuvres de virage, tels que les U-tours et les virages continus sans direction spécifique, dans les systèmes de ronds-points à une seule voie. L'étude examine l'impact de l'augmentation du nombre de véhicules effectuant ces manœuvres sur les caractéristiques du trafic, les émissions de CO_2 et la dissipation d'énergie. En outre, la recherche explore les conflits résultant du non-respect des écarts de sécurité par les véhicules lorsqu'ils entrent dans la voie circulaire et leur impact sur la capacité du rond-point. Les résultats révèlent que cette pratique réduit l'efficacité du système. Pour atténuer ces problèmes, nous proposons l'utilisation de feux de circulation pour contrôler le flux de véhicules, minimiser les interactions conflictuelles et améliorer la fluidité du trafic.

Dans la dernière section de la thèse, une stratégie intelligente est proposée pour gérer et optimiser le flux de circulation dans les carrefours giratoires. Cette stratégie utilise un modèle de simulation hybride basé sur les automates cellulaires pour le contrôle de la circulation, qui intègre des feux de circulation et des règles de priorité spécifiques aux carrefours giratoires. Le modèle évalue le flux de circulation dans les voies circulaires, en utilisant la densité, le taux de satisfaction, la vitesse moyenne, le temps de séparation entre les véhicules (time headway) et la densité des véhicules à l'arrêt comme paramètres de rétroaction. Les résultats de l'étude indiquent que ces paramètres éliminent efficacement la phase de blocage total (gridlock) qui caractérise typiquement le flux de circulation dans les carrefours giratoires sans feux de circulation, ce qui améliore considérablement le débit et l'efficacité dans les carrefours giratoires.

Mots-clés : Automate Cellulaire, Rond-point, Diagramme de Phase, Tour complet, Dissipation d'Énergie, Intervalle de Sécurité, Émissions de CO_2, Carrefours giratoires. Feux de Circulation Adaptatifs.

Résumé détaillé

Dans cette thèse, notre objectif est d'explorer en profondeur la dynamique du trafic aux intersections circulaires, considérées comme l'une des stratégies les plus efficaces pour réguler le trafic à l'échelle mondiale. Notre étude exhaustive couvre deux types distincts d'intersections circulaires : les ronds-points et les carrefours giratoires. Nous avons effectué une analyse complète des nombreux facteurs qui influencent leurs performances respectives, et nous avons développé des méthodes intelligentes pour améliorer la productivité tout en préservant l'environnement.

Au cœur de notre recherche se trouve une approche de simulation sophistiquée, basée sur un modèle d'automates cellulaires (AC) Nagel-Schreckenberg (NaSch). Ce modèle a été soigneusement intégré dans un environnement informatique Fortran, choisi pour ses capacités robustes en calcul numérique et scientifique.

Avant de présenter notre travail, nous avons mené une recherche bibliographique approfondie sur la théorie du trafic routier. Nous avons d'abord retracé l'histoire de cette théorie, puis présenté les principales variables qui influencent le flux de trafic, tant au niveau microscopique que macroscopique. Nous avons ensuite exploré les modèles empiriques de la circulation routière, notamment l'analyse de la formation des embouteillages, le diagramme fondamental, l'hystérésis et la métastabilité.

Nous avons présenté différents modèles utilisés pour modéliser la circulation routière: les modèles macroscopiques, qui considèrent le trafic comme un fluide compressible; les modèles mésoscopiques, qui associent le trafic à un espace de phases analogue à la cinétique des gaz; et les modèles microscopiques, qui décrivent les interactions entre les véhicules en utilisant le principe stimulus-réponse. Ces modèles sont regroupés en deux approches différentes: l'approche du diagramme fondamental et la théorie des trois phases.

Selon l'approche du diagramme fondamental, les différentes observables du trafic, en particulier le flux, sont supposées être une fonction de la densité. Par conséquent, la dispersion observée dans le diagramme fondamental empirique est considérée comme des fluctuations statistiques, qui peuvent être ajustées à l'aide d'une courbe lisse. Cependant, la théorie des trois phases stipule que le flux n'est pas toujours une fonction de la densité. De plus, la dispersion dans le diagramme fondamental empirique ne peut pas être considérée comme des fluctuations statistiques dans les phases métastables et congestionnées. Ces dispersions reflètent la présence d'une dynamique complexe, nécessitant que les différentes observables soient représentées en tenant compte des configurations spatiotemporelles.

Nous avons consacré une section au modèle d'automate cellulaire Nagel-Schreckenberg (NaSch), en détaillant ses principes fondamentaux, ses conditions aux limites, ainsi que les diverses extensions proposées pour améliorer sa représentativité et sa précision. Par ailleurs, nous avons abordé l'impact environnemental du trafic routier, en mettant en lumière la dissipation d'énergie et les émissions de dioxyde de carbone (CO_2). En outre, nous avons analysé en détail les caractéristiques des éléments d'infrastructure routière, tels que les autoroutes, les intersections à X et Y voies, et les intersections circulaires.

Enfin, nous avons discuté de la simulation de Monte Carlo et de son rôle dans la modélisation des systèmes de trafic complexes. Nous avons présenté les principes de base de cette méthode, ses applications dans la simulation du trafic, ainsi que les avantages

qu'elle offre pour l'analyse statistique et la prédiction des comportements du trafic.

Après avoir présenté les différents modèles et approches de l'analyse du trafic, nous nous sommes concentrés sur l'étude de la dynamique des flux de trafic dans les ronds-points. Tout d'abord, nous avons examiné l'impact des véhicules effectuant des manœuvres de virage, tels que les U-tours ou les virages continus sans direction spécifique, sur la dynamique du trafic et les facteurs environnementaux, comme les émissions de CO_2 et la dissipation d'énergie. Notre étude approfondie a montré une corrélation importante entre ces manœuvres de conduite et l'accroissement de la congestion sur les voies d'entrée, due aux règles de priorité. Cela entraîne des files d'attente prolongées et affecte négativement le flux de trafic ainsi que l'impact environnemental sur toutes les voies du rond-point.

Ensuite, nous avons examiné les effets du non-respect de l'écart de sécurité à l'entrée des voies de circulation par les véhicules sur la capacité du système de rond-point. Cette pratique réduit l'efficacité globale du rond-point. Pour atténuer ces problèmes, nous suggérons l'utilisation de feux de circulation aux entrées des ronds-points. Cela permettrait de mieux contrôler le flux de véhicules, de réduire les interactions conflictuelles et d'améliorer la fluidité du trafic.

Nous avons également étudié l'impact de la différence entre les durées des périodes de feu vert et de feu rouge sur la capacité du système de rond-point. Une mauvaise gestion de la durée des feux de signalisation peut entraîner une congestion accrue et une réduction de la capacité du système. Par conséquent, nous recommandons l'utilisation de systèmes de gestion du trafic avancés pour optimiser la durée des feux de signalisation en fonction des conditions de trafic.

De plus, nous avons proposé d'introduire une stratégie intelligente pour gérer le trafic aux carrefours giratoires en installant des feux de circulation adaptatifs aux voies d'entrée. Cette approche vise à optimiser la fluidité et la sécurité du trafic en temps réel. Nous avons étudié l'impact de ces feux adaptatifs sur le débit de trafic des carrefours giratoires. L'objectif de l'étude était de respecter les règles de priorité traditionnelles des carrefours giratoires tout en évitant les blocages dus aux embouteillages mutuels qui peuvent se produire lorsque les véhicules se retrouvent coincés dans un cycle de congestion. Pour ce faire, nous avons développé un modèle hybride de simulation basé sur des automates cellulaires pour le contrôle du trafic. Ce modèle intègre des feux de circulation et des règles de priorité spécifiques aux carrefours giratoires. Les feux de circulation aux voies d'entrée sont régulés en fonction de la densité du trafic, du taux de satisfaction, de la vitesse moyenne, du temps de séparation entre les véhicules (headway) et de la densité des véhicules à l'arrêt, qui servent de rétroaction pour ajuster le flux de véhicules entrant dans la voie circulaire du carrefour giratoire.

Le fonctionnement du système est le suivant : le flux de circulation dans la voie circulaire est continuellement analysé par des capteurs supposés. Ces capteurs calculent ces paramètres et en fonction de leurs valeurs, les feux de circulation aux voies d'entrée peuvent passer au rouge pour réduire temporairement le trafic entrant. Cette régulation permet de prévenir la saturation de la voie circulaire et de maintenir une circulation fluide. Cette stratégie améliore la fluidité du trafic en réduisant l'accumulation de véhicules dans la voie circulaire. Cela facilite les interactions entre les véhicules, réduit les temps d'attente, et permet à un plus grand nombre de véhicules de traverser le carrefour giratoire en toute sécurité et efficacité.

En conclusion, l'implémentation de feux de circulation adaptatifs aux carrefours giratoires constitue une avancée majeure dans la gestion du trafic en milieu urbain. Cette solution innovante permet non seulement d'optimiser la fluidité et la sécurité routière,

mais aussi de réduire les embouteillages et les risques d'accidents.

En général, cette thèse apporte une contribution significative à la compréhension de la dynamique du trafic aux intersections circulaires et propose des méthodes innovantes pour améliorer la gestion du trafic en milieu urbain. En examinant en profondeur les différents types d'intersections circulaires, tels que les ronds-points et les carrefours giratoires, nous avons identifié les principaux facteurs influençant leur performance et proposé des solutions pour optimiser leur fonctionnement. Les résultats de cette étude ont des implications importantes pour la conception et la gestion des intersections circulaires, ainsi que pour la réduction de l'impact environnemental du trafic routier.

List of Figures

1.1 Greenshields' Pioneering Photographic Method for Traffic Flow Study in the 1930s [5]. . . . 7
1.2 Illustrative diagram of the parameters involved in the calculation of time and distance headway. . . . 8
1.3 In this illustration, the left-lane cars are traveling twice as fast while maintaining the same headway [21]. . . . 10
1.4 A space-time diagram in which the trajectories of individual vehicles on a multi-lane highway are represented by each line. The dashed lines denote lane changes [22]. . . . 13
1.5 Various Shapes of the Fundamental Diagram. . . . 14
1.6 The empirical fundamental diagram from a Canadian Freeway, with data averaged over 5 minutes [23]. . . . 14
1.7 An Empirical Hysteresis Loop, with flow and density averaged over 5 minutes [23]. . . . 15
1.8 The Fundamental Diagram depicting metastability (in the region ($\rho_1 < \rho < \rho_2$). . . . 16
1.9 The empirical results of the distribution of inter-vehicular times in the phases of free-flowing traffic (a) and congested traffic (b) [24]. . . . 17
1.10 The mean velocity as a function of distance headway [25]. . . . 18
1.11 The spatiotemporal evolution of the mean velocity and current on a specific freeway [26]. . . . 20
1.12 Illustration du modèle NaSch . . . 24
1.13 Periodic boundary conditions. . . . 25
1.14 Fundamental Diagrams (a) for different values of the maximum speed V_{max} with $P_b = 0$, (b) for different values of the braking probability P_b with $V_{max} = 5$. . . . 25
1.15 Standard open conditions. . . . 26
1.16 Expanded open conditions ($V_{max=2}$). . . . 26
1.17 Phase diagrams of the NaSch model under open conditions with $P_b = 0.5$, $V_max = 5$. (a) Standard injection terminals, (b) Expanded injection terminals [27]. . . . 27
1.18 Flowchart of the Monte Carlo simulation for the NaSch model. . . . 33

2.1 (a) Sketch of the traffic circle system, (b) Regulations for entry and exit. . . . 37
2.2 Phase diagram in the (α, β) plane for three lanes: (a) circulating, (b) entry, and (c) exit, both with and without the impact of vehicles turning completely inside the circulation lane. . . . 39
2.3 Capacity as a function of the proportion of turning vehicles, for the circulating lane and entry/exit lanes. . . . 40

2.4 Energy dissipation as a function of the rates of injection α and extraction β: (a) Circulating Lane, (b) Entry Lane, and (c) Exit Lane—all without the effect of vehicles turning completely in the circulation lane. (d) Circulating Lane, (e) Entry Lane, and (f) Exit Lane - with the impact of vehicles making a complete turn in the circulation lane. 41
2.5 Maximum CO_2 emissions as a function of the percentage of vehicles making a U-turn. For the three lanes of the roundabout(circulating, entry and exit lanes. 42
2.6 Phase diagram for different percentages of vehicles turning in the roundabout's circulation lane without a specific direction, in the (α, β) plane. For three lanes: (a) circulating, (b) entry, and (c) exit. 42
2.7 Capacity as a function of the percentage of vehicles that keep turning in the circulating lane. For circulating lane and entry/exit lanes. 43
2.8 Energy dissipation with 10% of vehicles continuing to turn in the circulation lane as a function of injection α and extraction β rates. (a) Entry lane, (b) exit lane, and (c) circulating lane. In an additional instance, 35% of vehicles keep turning in the circulation lane. (d) Entry lane, (e) circulating lane, and (f) exit lane. 44
2.9 Maximum CO_2 emission as a function of the percentage of the vehicles that keep turning in the circulating lane. For the three lanes of the roundabout (circulating, entry, and exit lanes. 45
2.10 Current as a function of injection α and extraction β rates for the following lanes: (a) Circulating lane; (b) Entry lane; and (c) Exit lane. Phase diagram for (d) the circulating lane, (e) the entry lane, and (f) the exit lane in the (α,β) plane. 47
2.11 Space-time plots for the roundabout. For circulating lane ((b),(e),(h)) For entry lane ((a), (d),(g)). For exit lane ((c), (f), (i)). Black corresponds to vehicles while free space is presented in white. 48
2.12 Capacity as a function of the percentage of vehicles that do not respect the safety gap to enter the circulating lane. For the three lanes of the roundabout (circulating, entry, exit lanes. 49
2.13 The current in the roundabout system with the traffic light: (a) circulating lane, (b) entry lane, and (c) exit lane as a function of α for various β. Phase diagram for (d) circulation lane, (e) entry lane, and (f) exit lane in the (α, β) plane. 50
2.14 Space-time plots for the roundabout system with traffic light. For ($\alpha = 0.1$, $\beta = 0.6$) (a) Entry lane, (b) Circulating lane, (c) Exit lane. For ($\alpha = 0.27$, $\beta = 0.6$) (d) Entry lane, (e) Circulating lane, (f) Exit lane. For ($\alpha = 0.6$, $\beta = 0.1$) (g) Entry lane, (h) Circulating lane, (i) Exit lane. For ($\alpha = 0.6$, $\beta = 0.6$) (j) Entry lane, (k) Circulating lane, (l) Exit lane. Black corresponds to vehicles while free space is presented in white. 51
2.15 Capacity as a function of the ratio of green signal time to the cycle time T. For the three lanes of the roundabout (circulating, entry, and exit lanes). . 52

3.1 (a) Sketch of the traffic circle system, (b) Regulations for entry and exit. . 55
3.2 (a) Current as a function of injection α and extraction β rates in a circulating lane, (b) Phase diagram in the (α,β) plane. 58

3.3 Density in the circulating lane as a function of α for $\beta = 0.2$, $\beta = 0.4$, and $\beta = 0.6$. 58
3.4 Current as a function of α for various β, when the circulating lane's density values are varied and the adaptation criterion is applied: (a) $\rho_c = 0.8$, (c) $\rho_c = 0.6$, and (e) $\rho_c = 0.4$. Phase diagrams for (b) $\rho_c = 0.8$, (d) $\rho_c = 0.6$, and (f) $\rho_c = 0.4$ in the (α, β) plane. 60
3.5 Space-time diagrams for the traffic circle system with density $\rho_c = 0.8$ for: (a) $\beta = 0.6$ and $\alpha = 0.05$, (b) $\beta = 0.12$ and $\alpha = 0.6$, (c) $\beta = 0.6$ and $\alpha = 0.6$, and (d) $\beta = 0.1$ and $\alpha = 0.6$. White color represents free space, whereas black color represents vehicles. 61
3.6 The capacity of the entry/exit and circulation lanes as a function of density ρ_c. 62
3.7 The duration of the red light in each entry lane, as a function of α and β, for the following cases: (a) $\rho_c = 0.8$, (b) $\rho_c = 0.6$, and (c) $\rho_c = 0.4$. 63
3.8 Current as a function of α for various β, when the circulating lane's satisfaction rate values are varied and the adaptation criterion is applied: (a) $\eta_c = 0.2$, (c) $\eta_c = 0.5$, (e) $\eta_c = 0.75$. Phase diagrams for (b) $\eta_c = 0.2$, (d) $\eta_c = 0.5$, (f) $\eta_c = 0.75$ in the (α, β) plane. 64
3.9 Space-time diagrams for the traffic circle system with satisfaction rate $\eta_c = 0.2$ for (a) $\alpha = 0.05$ and $\beta = 0.5$, (b) $\alpha = 0.5$ and $\beta = 0.5$, (c) $\alpha = 0.05$ and $\beta = 0.5$. White color represents free space, whereas black color represents vehicles. 65
3.10 The capacity of the entry/exit and circulation lanes as a function of the critical satisfaction rate η_c. 66
3.11 The duration of the red light in each entry lane, as a function of α and β, for the following cases: (a) (a) $\eta_c = 0.2$, (b) $\eta_c = 0.5$, and (c) $\eta_c = 0.75$. . . 67
3.12 Current as a function of α for different β where the adaptation criterion is done with different mean velocity values in circulating lane (a) $\langle V \rangle_c = 1.4$, (c) $\langle V \rangle_c = 2.5$, (e) $\langle V \rangle_c = 3$. Phase diagram in the (α, β) plane (b) $\langle V \rangle_c = 1.4$, (d) $\langle V \rangle_c = 2.5$, (f) $\langle V \rangle_c = 3$. 68
3.13 Capacity as a function of mean velocity $\langle V \rangle_c$ for the circulating lane and entry/exit lanes. 69
3.14 Carbon dioxide emission as a function of α and β where the adaptation criterion is done with different mean velocity values in circulating lane (a) $\langle V \rangle_c = 1.4$, (b) $\langle V \rangle_c = 2.5$ (c) $\langle V \rangle_c = 3$. 70
3.15 Time-to-collision distributions under various critical mean velocity values in the circulating lane (a) $\langle V \rangle_c = 1.4$, (b) $\langle V \rangle_c = 2.5$, (c) $\langle V \rangle_c = 3$. 71
3.16 Space-time diagram for ($\alpha = 0.5$ and $\beta = 0.5$) where the adaptation criterion is done with different mean velocity values in the circulating lane (a) $\langle V \rangle_c = 1.4$, (b) $\langle V \rangle_c = 2.5$, (c) $\langle V \rangle_c = 3$. Black color corresponds to vehicles while free space is presented by white color. 71
3.17 The time needed to remain red light in all entry lanes as a function of α and β, for (a) $\langle V \rangle_c = 1.4$, (c) $\langle V \rangle_c = 2.5$, (e) $\langle V \rangle_c = 3$. 72
3.18 Current as a function of α for different β where the adaptation criterion is done with different time headway values in circulating lane (a) $t_{hc} = 15$, (c) $t_{hc} = 8$, (e) $t_{hc} = 3$. The phase diagram in the (α, β) plane (b) $t_{hc} = 15$, (d) $t_{hc} = 8$, (f) $t_{hc} = 3$. 73

3.19 Capacity as a function of time headway t_{hc} for the circulating lane and entry/exit lanes. 74
3.20 Carbon dioxide emission as a function of α and β where the adaptation criterion is done with different time headway values in circulating lane (a) $t_{hc} = 15$, (b) $t_{hc} = 8$, (c) $t_{hc} = 3$. 75
3.21 Time-to-collision distributions under various critical mean velocity values in circulating lane (a) $t_{hc} = 15$, (b) $t_{hc} = 8$, (c) $t_{hc} = 3$. 76
3.22 Space-time diagram for ($\alpha = 0.5$ and $\beta = 0.5$) where the adaptation criterion is done with different time headway values in circulating lane (a) $t_{hc} = 15$, (b) $t_{hc} = 8$, (c) $t_{hc} = 3$. Black color corresponds to vehicles while free space is presented by white color. 76
3.23 The time needed to remain the red light in all entry lanes as a function of α and β, for (a) $t_{hc} = 15$, (b) $t_{hc} = 8$, (c) $t_{hc} = 3$. 77
3.24 Current as a function of α for different β where the adaptation criterion is done with different density of stopped cars values in circulating lane (a) $f = 80\,\%$, (c) $f = 55\,\%$, (e) $f = 20\,\%$. The phase diagram in the (α, β) plane (b) $f = 80\,\%$, (d) $f = 55\,\%$, (f) $f = 20\,\%$. 78
3.25 Capacity as a function of density of stopped cars f for circulating lane and entry/exit lanes. 79
3.26 Carbon dioxide emission as a function of α and β where the adaptation criterion is done with different density of stopped cars values in circulating lane (a) $f = 80\,\%$, (b) $f = 55\,\%$, (c) $f = 20\,\%$. 80
3.27 Time-to-collision distributions under various critical densities of stopped car values in circulating lane (a) $f = 80\%$, (b) $f = 55\%$, (c) $f = 20\%$. . . . 80
3.28 Space-time diagram for ($\alpha = 0.5$ and $\beta = 0.5$) where the adaptation criterion is done with different densities of stopped cars values in circulating lane (a) $f = 80\%$, (b) $f = 55\%$, (c) $f = 20\%$. Black color corresponds to vehicles while free space is presented by white color. 81
3.29 The time needed to remain red light in all entry lanes as a function of α and β, for (a) $f = 80\%$, (b) $f = 55\%$, (c) $f = 20\%$. 81

List of Tables

1.1 Emission functions for the 2010 fleet of urban traffic [28]. 30

2.1 Parameters of the model used in the simulation 38

3.1 Parameters of the model used in the simulation 57

Contents

Acknowledgements ii

Abstract iii

Résumé iv

Résumé détaillé vii

List of Figures xi

List of Tables xii

General introduction 1

1 A Comprehensive Overview of Exploring Traffic Flow Dynamics: From Theory to Modeling 5

1.1 Introduction . . . 5
1.2 History of traffic flow theory . . . 5
1.3 The main variables of traffic flow . . . 7
1.3.1 Microscopic Variables . . . 7
1.3.1.1 Instantaneous velocity . . . 7
1.3.1.2 Time headway . . . 7
1.3.1.3 Distance headway . . . 8
1.3.1.4 The correlation . . . 8
1.3.2 Macroscopic Variables . . . 9
1.3.2.1 The flow . . . 9
1.3.2.2 The mean velocity . . . 9
1.3.2.3 The density . . . 11
1.3.2.4 Occupancy . . . 11
1.4 The empirical patterns of traffic flow . . . 11
1.4.1 Analysis of traffic jam formation and characteristics . . . 11
1.4.2 The fundamental diagram . . . 13
1.4.3 The Hysteresis . . . 15
1.4.4 The Metastability . . . 16
1.4.5 Inter-vehicular time and space distribution . . . 17
1.4.5.1 Inter-vehicular time distribution . . . 17
1.4.5.2 Inter-vehicular space distribution . . . 17
1.5 The modeling approaches in traffic analysis . . . 18
1.5.1 The fundamental diagram approach . . . 18
1.5.2 The three-phase theory . . . 19

1.6 Road traffic modeling . . . 20
1.6.1 The macroscopic models . . . 21
1.6.2 The microscopic models . . . 21
1.6.3 The mesoscopic models . . . 22
1.6.4 Cellular automata model . . . 22
1.6.4.1 Nagel and Schreckenberg model . . . 23
1.6.4.2 The boundary conditions . . . 24
1.6.4.3 Extensions of the NaSch model . . . 27
1.7 Environmental impact . . . 28
1.7.1 Energy dissipation . . . 28
1.7.2 Traffic Emission Model . . . 29
1.8 Characteristics of Road Infrastructure Elements . . . 29
1.8.1 Highways . . . 30
1.8.2 Intersections . . . 30
1.8.3 Circular Intersections . . . 31
1.9 Monte Carlo Simulation . . . 32
1.10 Conclusion . . . 34

2 Investigating the Impact of Vehicle Behavior on Roundabout Performance: A Simulation Study of Full-Turn Maneuvers and Safe Gap Adherence 35
2.1 Introduction . . . 35
2.2 Model Development and Simulation . . . 36
2.2.1 Motion rules . . . 36
2.2.2 Entry/exit rules . . . 36
2.2.3 The boundaries rules . . . 37
2.2.4 Traffic light control . . . 37
2.2.5 Simulation Parameters . . . 38
2.3 Effects of Full-Turn Maneuvers on Roundabout Traffic Dynamics . . . 38
2.3.1 Impact of vehicles making U-turns . . . 38
2.3.2 Impact of Directionless Vehicle Inflow in Circulation Lane . . . 40
2.4 Effects of Adhering to Safe Gaps on Roundabout Traffic Dynamics . . . 46
2.4.1 Traffic patterns in a roundabout system . . . 46
2.4.2 Roundabout system with traffic lights . . . 49
2.5 Conclusion . . . 52

3 Assessing the Impact of Adaptive Traffic Lights on Traffic Circle Throughput: A Simulation and Modeling Study 54
3.1 Introduction . . . 54
3.2 Model Development and Simulation . . . 55
3.2.1 The motion rules . . . 55
3.2.2 The priority rules . . . 55
3.2.3 Traffic lights rules . . . 56
3.2.4 Time-to-Collision Concept . . . 56
3.2.5 Simulation Parameters . . . 57
3.3 Unsignalized traffic circle . . . 57
3.4 Effects of adaptive traffic lights . . . 59
3.4.1 Effect of density . . . 59
3.4.2 Effect of satisfaction rate . . . 63

3.4.3 Effect of average speed 67
3.4.4 Effect of time headway 72
3.4.5 Effect of density of stopped cars 77
3.5 Conclusion 82

General conclusion **83**

A List of Publications and Presentations **86**

General introduction

Transportation systems are essential for shaping global economic and social landscapes. As populations grow rapidly, the demand for transportation infrastructure and traffic increases. However, building new infrastructure like urban streets, roundabouts, intersections, and highways faces significant cost challenges. Limited land availability and the current infrastructure's inability to handle increasing traffic worsen the issue. Additionally, the high costs of constructing new transportation infrastructure often lead to compromises in quality or delays, further exacerbating traffic and safety problems.

The environmental impact of expanding transportation networks, such as increased emissions and habitat fragmentation, requires more attention. For instance, burning diesel fuel releases 2.69 kg CO_2 per liter, while gasoline (98 ROZ) releases 2.39 kg CO_2 per liter [1]. Heavy traffic and congestion also increase noise pollution, with cars producing 55% of all urban noise [2]. Noise levels in cities range from 55.1 dB to 87.3 dB, contributing to various health issues [3]. Congestion-related stress can cause chronic lung diseases, elevated blood pressure, and a higher risk of heart attacks and strokes for those living near congested areas.

Economically, the state of transportation infrastructure significantly affects investment decisions and economic growth by facilitating the movement of people and goods. Congestion increases fuel consumption and complicates future developments, wasting billions of dollars annually. The financial costs to governments include both time lost and fuel wasted. For example, the Texas Transportation Institute estimates that traffic congestion costs the country 62.3 $ billion annually [4].

Understanding the fundamental causes of traffic congestion is essential for accurately forecasting and addressing its occurrence and the problems it poses. Physicists have gained insights into traffic by analyzing it as a physical system. Researchers have developed various models to simulate traffic flow dynamics, using concepts from statistical mechanics and nonlinear physics. These models not only replicate real-world scenarios but also provide valuable insights into how traffic patterns evolve and how interventions can be optimized.

Road traffic simulations, used in some of these models, enable a comprehensive study of traffic behavior under different conditions, illustrating how vehicles move collectively. These simulations also assess the potential impacts of proposed changes to the road network, offering valuable guidance to policymakers and urban planners in decision-making.

Cellular automata (CA) have emerged as a key model for understanding the complexities of road traffic since the 1930s. CAs are discrete dynamic systems consisting of identical cells, each holding a distinct state. These cells transition between states based on well-defined rules influenced by neighboring cells. In road traffic simulation, the roadway is discretized into cells, where each cell can be empty or occupied by a single vehicle. CAs provide detailed representations of vehicle interactions, enabling connections to macroscopic traffic metrics like flow rates and average speeds. They excel at capturing the nuanced behaviors of real-world traffic, including lane changes, vehicle diversity, accidents, and acceleration/deceleration patterns.

The genesis of CA-based traffic models can be traced back to Cremer's work in 1986 and Nagel and Schreckenberg's contributions in 1992. The Nagel-Schreckenberg model is a leading methodology in traffic research, offering valuable insights into traffic dynamics and paving the way for innovative solutions to mitigate congestion and enhance transportation efficiency.

In addition to traffic models, various road infrastructure elements, including freeways, intersections X and Y, and circular intersections, play essential roles in regulating traffic flow. Circular intersections, such as roundabouts and traffic circles, are specifically designed to enhance traffic flow efficiency and safety.

The objective of this thesis is to investigate the dynamics of traffic flow at circular intersections. Although they are effective, these intersections face challenges such as managing traffic volume, driver behavior, pedestrian safety, and environmental impacts. The study utilizes traffic flow theories and models, particularly cellular automata, to analyze vehicle interactions and their interactions with infrastructure.

To understand and manage these parameters to ensure the smooth operation of circular intersections, we will attempt to answer the following fundamental questions in this thesis:

1. What are the primary factors affecting traffic dynamics and how have empirical patterns in traffic flow evolved over time?

2. How do full-turning movements, such as U-turns and continuous turning without a specified direction, affect traffic flow characteristics and environmental factors within single-lane roundabout systems?

3. How do conflicts arising from vehicles not maintaining safe gaps influence disruptions to traffic flow, and what potential solutions can alleviate congestion and enhance traffic flow at roundabouts?

4. How can a hybrid simulation model based on cellular automata, integrating traffic circle priority rules and adaptive traffic lights, optimize traffic flow and prevent gridlock in traffic circles?

To address the preceding questions, this thesis is structured as follows:

- The first chapter of this thesis presents a comprehensive overview of traffic flow theory and analysis. It delves into the historical development of traffic flow theory, tracing its evolution and the key milestones that have shaped our understanding of traffic behavior. The chapter discusses the primary variables of traffic flow, including microscopic and macroscopic variables, and explores empirical patterns observed in traffic flow, such as traffic jam formation, hysteresis, and metastability. Furthermore, the chapter examines traffic flow research using macroscopic, microscopic, and mesoscopic modeling approaches, with a focus on the Nagel-Schreckenberg cellular automaton model, which provides valuable insights into traffic behavior through its fundamental principles and extensions.

  The chapter also emphasizes the role of road infrastructure elements in managing traffic flow and mitigating congestion. It discusses the design of freeways, intersections, and circular intersections, such as roundabouts and traffic circles, to optimize traffic movement, enhance safety, and reduce environmental impacts. The effectiveness of traffic lights in regulating traffic flow is also examined, highlighting their role in improving overall traffic efficiency.

In addition, the chapter introduces Monte Carlo simulation and its role in modeling complex traffic systems. It emphasizes the importance of simulation techniques in understanding and predicting traffic behavior under various conditions.

In summary, the first chapter lays the foundation by providing a thorough understanding of traffic flow theory and analysis, paving the way for further exploration in subsequent chapters. These chapters will investigate the dynamics of traffic flow at circular intersections and explore potential solutions to enhance traffic flow efficiency.

- The second chapter of this thesis examines the effects of full-turning movements, such as U-turns and continuous turning without a specified direction, on traffic flow characteristics within single-lane roundabout systems. It investigates how these maneuvers influence traffic dynamics, including changes in CO_2 emissions and energy dissipation, thus impacting the environment. The chapter also addresses conflicts that arise from vehicles not maintaining safe gaps, which can disrupt traffic flow and affect overall traffic efficiency and safety.

  By utilizing traffic flow theories and cellular automata models, the research provides a comprehensive understanding of vehicle interactions within roundabouts and their influence on traffic performance. The chapter explores various modeling approaches to simulate traffic behaviors and their implications for roundabout operations. Moreover, it discusses potential solutions, such as traffic light control strategies, aimed at alleviating congestion and enhancing traffic flow efficiency.

  In summary, the second chapter extends the study's investigation into the dynamics of traffic flow at circular intersections, focusing on single-lane roundabout systems. It provides insights into the environmental impacts of traffic behaviors, addresses challenges related to traffic flow disruptions, and explores innovative solutions to improve roundabout performance.

- The last chapter of this thesis investigates traffic flow dynamics within traffic circle systems using a sophisticated strategy for traffic management. This approach employs a hybrid simulation model based on cellular automata, integrating traffic circle priority rules and adaptive traffic lights. The model assesses traffic flow in circulating lanes using density, satisfaction rate, average speed, time headway, and the density of stopped cars as feedback mechanisms.

  To prevent gridlock caused by mutual obstruction in the circulating lane, the traffic lights in the entry lanes will turn red based on the traffic conditions in that lane, but only when traffic quality worsens. This strategy preserves the key advantage of traffic circles, which is the rules of priority, allowing uninterrupted traffic movement and enhancing the intersection's efficiency.

  Furthermore, the chapter explores the impacts of this hybrid simulation model on traffic flow dynamics, evaluating its effectiveness in optimizing traffic movement, reducing congestion, and improving overall traffic efficiency. It discusses the integration of adaptive traffic signals as a solution to enhance traffic management in traffic circle systems, providing valuable insights for future traffic engineering and urban planning strategies.

  In summary, the last chapter extends the study's exploration into traffic flow dynamics at circular intersections, focusing on innovative strategies for traffic management

and the application of advanced simulation models to improve traffic flow efficiency and safety.

Chapter 1

A Comprehensive Overview of Exploring Traffic Flow Dynamics: From Theory to Modeling

1.1 Introduction

In this chapter, we will explore the advancements in traffic flow modeling using tools and insights from statistical mechanics and nonlinear physics. We will delve into the foundational concepts, state-of-the-art methodologies, and key breakthroughs that have contributed to our understanding of traffic dynamics.

1.2 History of traffic flow theory

Traffic flow theories and models are designed to offer a precise mathematical description of how drivers, vehicles, and infrastructure interact. These theories and models are essential for managing and designing roads and highways, as well as for improving the predictability of the overall transportation system. The scientific study of traffic began in the early 20th century, with researchers developing various models to explain its movement. Greenshields, a pioneer in this field, established the foundational theories of traffic flow in 1934. His research primarily focused on the relationship between flow and velocity. Greenshields' theories were based on a traffic capacity study conducted by the Traffic Bureau of the Ohio State Highway Department, led by H. E. Neal, Traffic Engineer, and J. J. Darnall, Superintendent of Traffic Surveys. The study employed a photographic method, as shown in Figure 1.1 of the Proceedings of the Highway Research Board [5].

Following World War II, urban societies experienced a significant increase in automobile usage and road users, along with the expansion of the highway network. This led to a heightened interest in studying traffic characteristics and the development of theories and models related to traffic flow. In 1952, J.G. Wardrop [6] explored various aspects of road traffic behavior and distribution. His focus was on understanding the factors that influence traffic flow and their effects on average journey speed, capacity, delays, and vehicle distribution along roads. He also devised a method to determine the frequency of vehicle overtaking relative to traffic flow.

In 1956, P.I. Richards [7] developed a simple theory of traffic flow by establishing an empirical relationship between speed and density and replacing individual vehicles with continuous densities. This theory revealed significant characteristics, such as a straightforward method to track the progression of traffic waves over time and the frequent occurrence of shock waves.

In December 1959, the General Motors Research Laboratories in Warren, Michigan

hosted the First International Symposium on the Theory of Traffic Flow [8]. This symposium marked the beginning of a triennial series of recurring symposia dedicated to the study of traffic flow and transportation theory. Over time, the field of transportation and traffic flow theory has expanded significantly, encompassing a broad range of subjects. Consequently, the topic has become too extensive to be adequately covered in a single type of meeting. As a result, numerous additional symposia and specialized conferences focusing on various traffic-related topics are now regularly organized to address the diverse aspects of this discipline.

The first macroscopic model emerged in the latter half of the 20th century, using Lighthill and Whitham's hydrodynamic theory to depict a traffic stream as a fluid [4]. They explained the apparent similarities between traffic flow and fluid dynamics on a larger scale by employing kinematic principles to elucidate traffic waves. However, this model did not account for deviations from the equilibrium speed-density relationship, leading to several limitations and unsatisfactory outcomes in various dynamic traffic situations. Prigogine then introduced the innovative use of the kinetic technique to predict traffic flow [9]. However, this approach was constrained by several overly rigid assumptions and was unsuccessful at high densities, only producing excellent results at low densities.

Statistical models based on this method are more complex than continuum models but provide a more thorough understanding of the traffic stream dynamics. These statistical models offer more detailed data and a deeper comprehension of the nature of traffic flow. In a more recent development, Payne [10] developed a continuous model that allows deviations from equilibrium by employing car-following theory. It's important to note that all continuum models rely on establishing a functional relationship between equilibrium speed and density, which must be derived from external sources or experimental data. Continuum models cannot directly determine the speed-density relationship and instead require a statistical analysis similar to that used in the kinetic theory of gases to establish this connection.

Later, A. Aw and M. Rascle [11] introduced a new "second-order" traffic flow model that addresses the limitations of previous "second-order" models, as mentioned in the work by Daganzo [13]. The non-physical phenomena observed in the earlier models, which involved two equations (mass and "momentum"), were likely due to their attempt to mimic the equations of gas dynamics. An exaggerated relationship between acceleration and the space derivative of "pressure" led to these phenomena. Aw and Rascle proposed a simple modification to address this, which would replace the space derivative with a convective derivative. The results show that the inconsistencies in the previous models are resolved by making this modification. Furthermore, the revised model accurately predicts instability near the vacuum state, which corresponds to extremely light traffic conditions.

In the late 20th century, there were significant advancements in the field of traffic flow modeling. The first cellular automata model specifically designed for traffic flow analysis was introduced by Cremer et al. [15]. This model served as a foundation for subsequent developments, notably the work of Nagel and Schreckenberg [16], who created a simpler version with fewer rules. Simultaneously, car-following models also experienced significant improvements. The intelligent driver model, proposed by Treiber et al. [17], is a prominent modern model in this category. These advancements in car-following models and cellular automata have deepened our understanding of traffic flow dynamics.

The fundamental diagram method, which includes the traffic flow models mentioned earlier, traditionally considers flow as a continuous function of density. However, at the beginning of the 21st century, a new approach to traffic flow modeling emerged—the

three-phase theory—pioneered by Kerner [18]. This innovative concept introduced a fresh perspective and conceptual framework for understanding traffic flow dynamics. It provided a more comprehensive explanation of traffic phenomena and improved traffic flow modeling techniques by introducing the concept of three distinct phases.

Figure 1.1: Greenshields' Pioneering Photographic Method for Traffic Flow Study in the 1930s [5].

1.3 The main variables of traffic flow

1.3.1 Microscopic Variables

1.3.1.1 Instantaneous velocity

To determine the instantaneous speed of a vehicle, detectors with two inductive loops are required. The instantaneous speed of a vehicle, represented as i, as it passes through a detector with two inductive loops, is calculated by:

$$V_i = \frac{\Delta x}{t_{d2} - t_{d1}} \tag{1.1}$$

Where Δx represents the distance between the two inductive loops. The instances denoted as t_{d1} and t_{d2} refer to the time when the front of vehicle i approaches the first loop and the second loop, respectively. The distance traveled in a certain amount of time is known as speed, and it is typically measured in kilometers per hour (km/h).

1.3.1.2 Time headway

The time difference between the arrivals of the front ends of two consecutive vehicles is known as the time headway. This measurement is useful in modeling individual vehicle behavior and provides insights into the overall traffic flow quality. It is important in studies related to road safety, such as the development of gap regulation devices and anti-collision systems. Additionally, some traffic light intersection algorithms in urban

areas use this time headway. On highways, the concept of "gap regulation" is increasingly being employed as an operational strategy. The time headway is often referred to as the microscopic representation of the current traffic situation.

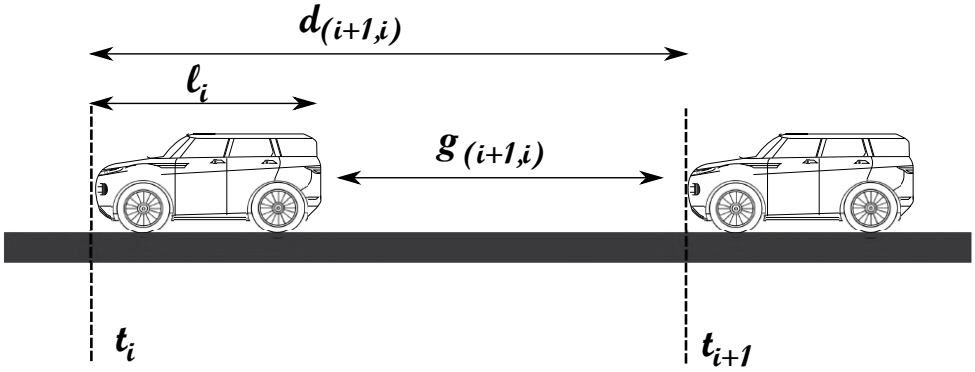

Figure 1.2: Illustrative diagram of the parameters involved in the calculation of time and distance headway.

The time headway is the time difference between two consecutive vehicles, i and $i+1$. It is determined by the following relationship:

$$t_{h(i+1,i)} = t_{i+1} - t_i \tag{1.2}$$

Generally, the unit is provided as (veh/s).

1.3.1.3 Distance headway

The headway, denoted as $d_{((i=1,i))}$, is the space between two vehicles traveling one after the other in the same lane. In other words, it represents the gap between the front ends of two consecutive vehicles, $i+1$ and i. The following mathematical relation is used to determine this distance:

$$d_{(i+1,i)} = t_{h(i+1,i)} \cdot V_i \tag{1.3}$$

Therefore, we can also determine the spatial window, which is the gap between vehicle i and the following vehicle $i+1$. This gap measures the distance from the back of vehicle i to the front of vehicle $i+1$. The following relationship is used to compute it:

$$g_{(i+1,i)} = d_{(i+1,i)} - l_i \tag{1.4}$$

It is important to note that all spatial quantities (distances, vehicle length l_i) are accurate only when the speed V_i is constant during the measurement.

1.3.1.4 The correlation

The correlation coefficient is used to measure the connection or relationship between two observables [19]. These variables are characterized by a mean and a variance. Therefore, the correlation function can be expressed as follows:

$$\mathrm{CC}_{X,Y} = \frac{\langle XY \rangle - \langle X \rangle \langle Y \rangle}{\sqrt{\langle X^2 \rangle - \langle X \rangle^2}\sqrt{\langle Y^2 \rangle - \langle Y \rangle^2}} \tag{1.5}$$

The variables X and Y can represent the current J, density ρ, speed V, etc. The angular brackets $\langle\rangle$ indicate that this is an average value calculated over a time span T or a series of N vehicles, and so on.

The correlation coefficient is a dimensionless measure that ranges from -1 to 1. If $\mathrm{CC}_{X,Y} \approx 0$, it suggests that there is no linear relationship. However, if $\mathrm{CC}_{X,Y} \approx -1$ or $\mathrm{CC}_{X,Y} \approx +1$, it indicates a strong linear relationship. For example, when dealing with two numeric variables, a positive coefficient implies a direct relationship, while a negative coefficient signifies an inverse relationship. In the field of road traffic, the correlation coefficient provides valuable insights into the spatio-temporal patterns of traffic states [20]. Its application is used to identify and quantify coupling effects between variables.

1.3.2 Macroscopic Variables

1.3.2.1 The flow

The term "traffic flow" or "flux" refers to the number of vehicles, denoted as N, that pass through a loop or sensor during a specific time interval Δt. It is usually represented by the symbol J.

$$\langle J \rangle_T = \frac{N}{T} \tag{1.6}$$

The unit for traffic flow is usually written as (veh/h) or (veh/s).

To simplify notation, we will often use J instead of $\langle J \rangle_T$. The relationship between the mean time headways $\langle t_{h(i+1,i)} \rangle$ and the current J is established through the following connection:

$$J = \frac{1}{\langle t_{h(i+1,i)} \rangle} \tag{1.7}$$

1.3.2.2 The mean velocity

To assess the average speed of a specific traffic situation, two types of mean velocity can be utilized: the mean velocities of time and space.

The time mean velocity

The term 'time mean velocity' refers to the average speed of vehicles passing by a detector at a specific location over a predetermined amount of time. It is calculated by determining the arithmetic mean of the instantaneous speeds (V_t) of the vehicles during that duration.

$$V_t = \frac{\sum_{i=1}^{N} V_i}{N} \tag{1.8}$$

Where N is the total number of vehicles detected by the sensor.

The space mean velocity

The space mean velocity, also known as the harmonic mean velocity, is an average calculated based on the number of vehicles on a road segment of length L at a specific time t. The formula is expressed as follows:

$$V_s = \frac{N}{\sum_{i=1}^{N} \frac{1}{V_i}} \tag{1.9}$$

The difference between the two mean velocities

Time mean velocity and space mean velocity differ in their calculation methods and the characteristics they consider. The time mean velocity is calculated using the vehicle velocities that occur during a specific time period. It provides information about the average speed of moving vehicles over time. On the other hand, space mean velocity, also known as the harmonic mean velocity, is determined by counting the number of vehicles on a particular road segment at a specific time. It is especially useful for understanding the dynamics of traffic flow at specific locations since it considers the geographical distribution of velocities.

To illustrate the difference between the two types of mean velocities, we can look at the diagram in Figure 1.3. Assuming that vehicles on both lanes maintain identical time headways, the use of time mean velocity would result in an equal flux. This is because the detectors on both lanes identify the same number of vehicles passing within a collective time interval [21]. Consequently, the detectors register a time mean velocity of $V_t = 108\,\mathrm{km/h}$. However, when using the space mean velocity, the result is:

$$V_s = \frac{2}{3} \times 72\,\mathrm{km/h} + \frac{1}{3} \times 144\,\mathrm{km/h} = 92\,\mathrm{km/h} \tag{1.10}$$

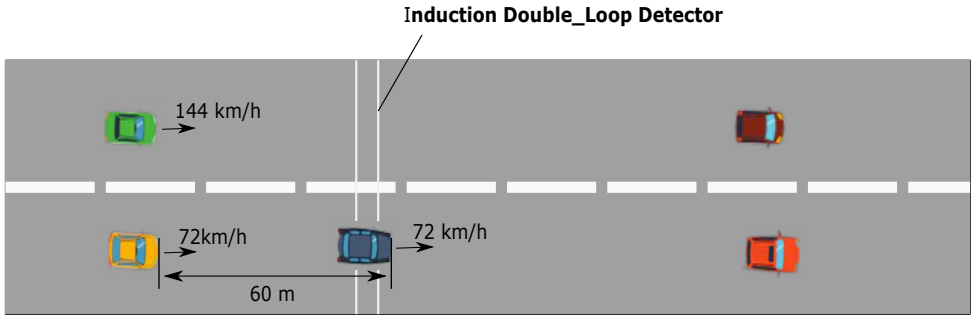

Figure 1.3: In this illustration, the left-lane cars are traveling twice as fast while maintaining the same headway [21].

Therefore, the space mean velocity tends to underestimate the average speed. On the other hand, because cross-sectional detectors tend to detect faster vehicles more frequently than slower ones, using temporal averages from these detectors introduces systematic errors. This results in a bias toward higher speed values [12, 21], demonstrating the need to use the space mean velocity for the measurement of traffic variables.

The relationship between the two mean velocities

The relationship between the two speeds, temporal V_t and spatial V_s as defined by Wardrop [6], is established as follows:

$$V_t = V_s + \frac{\sigma_s^2}{V_s} \tag{1.11}$$

Where σ_s is the standard deviation of the velocity distribution in space.

1.3.2.3 The density

Density or concentration is one of the parameters that can provide immediate insights into the traffic situation. The density refers to the number of vehicles on a specific length of road at a given time. It can be calculated using the following relationship:

$$\rho = \frac{N}{L} \tag{1.12}$$

At a more aggregated (macroscopic) level, density is related to the headway distance. The relationship between density and average headway distance in this case is inversely proportional, and it can be expressed as follows [14]:

$$\rho = \frac{1}{\langle d_{(i+1,i)} \rangle} \tag{1.13}$$

1.3.2.4 Occupancy

Occupancy quantifies the time interval during which the electromagnetic loop detects a magnetic signal or registers the presence of a vehicle, and it can also be used as an alternative to density [29]. It is calculated using the following relationship:

$$\Delta t_i = \frac{(L_i + d)/v_i}{T} \tag{1.14}$$

Where T is the time during which the calculation is performed, v_i is the vehicle's velocity, and L_i and d are the length of the vehicle and the detector, respectively.

The average occupancy rate Δt_m is determined using the following formula:

$$\Delta t_m = \frac{1}{\Delta T} \sum_{i=1}^{N} \Delta t_i \tag{1.15}$$

The vehicle density (ρ) can be derived from this quantity using the following relationship:

$$\Delta t_m = (l_m + d) \times \rho \tag{1.16}$$

Where l_m is the mean vehicle length throughout the given time interval ΔT.

1.4 The empirical patterns of traffic flow

This section will provide a comprehensive examination of several notable traffic phenomena that have been extensively studied and are well-known in the field. Through in-depth research and explanation, we aim to shed light on the complexities of these occurrences and offer valuable insights into the dynamics of traffic flow.

1.4.1 Analysis of traffic jam formation and characteristics

The dynamics of traffic jam formation are one of the most extensively researched traffic phenomena due to their prevalence and the daily frustration they cause. For physicists, the collective behavior observed when all drivers try to move as quickly as possible serves as a

clear indication of the significant role played by collective phenomena, complex dynamics, and emergent properties. A single, comprehensive definition has not yet been developed. Generally speaking, a traffic jam is described as [19]:

- An area of space with the highest density.
- An area of space where the system's mean velocity is lower than it is elsewhere.
- Some authors link gaps traveling against the direction of traffic flow to traffic jams [19, 30].

In addition to traffic jams, there is another more all-encompassing and commonly used term: traffic congestion. All the states connected to high density are included in this concept. Then, a traffic jam indicates a condition in which the average speed is almost zero, and the number of vehicles is almost as high as a road can support (in a specific area of space). There are two primary types of traffic congestion that can be identified as the cause of jams:

Bottleneck-induced Traffic Congestion: This type of congestion occurs when certain sections along a road experience localized reductions in capacity. When the volume of traffic entering these bottleneck areas surpasses their capacity, traffic jams ensue. Bottlenecks commonly occur due to lane reductions, merge points, or accidents, including incidents on ramps. Typically, the front of a traffic jam caused by a bottleneck forms at the beginning of the bottleneck, with the length of congestion varying based on incoming traffic flow [31]. Additional factors contributing to bottleneck effects include weather conditions, accidents, and inclines. American authorities estimate that approximately 15% of congestion can be attributed to adverse weather conditions. Theoretical studies have investigated bottlenecks caused by adverse weather or accidents [32, 33], and research has also explored the impact of highway slopes on traffic flow dynamics [34].

Spontaneous traffic jams: These jams manifest suddenly, devoid of any apparent external cause, and can occur even in homogeneous traffic systems. When a certain threshold is surpassed, a minor local fluctuation has the potential to escalate, ultimately leading to the onset of congestion [22]. This type of traffic jam is triggered by speed fluctuations [35] or by a relatively small disturbance occurring in an area where vehicles are closely spaced (such as a lane change by a vehicle) [12].

Treiterer [22] conducted an empirical study on the phenomenon of spontaneous traffic jams using a series of aerial photos of a multi-lane freeway. Figure 1.4 shows the evolution of each vehicle's position along the route over time. The paths followed by individual cars using highway lanes are represented by each line in the figure. This arrangement demonstrates the initiation and spread of traffic congestion over time using this spatial-temporal model.

Initially, the trajectories of the vehicles show significant separation, as depicted in the space-time diagram. However, over time, a congested area emerges, leading to a traffic congestion. This congestion temporarily subsides before suddenly dissipating without a clear cause. The graphic illustrates the spontaneous formation of phantom traffic jams and their tendency to expand in the opposite direction of the way that vehicles are traveling. Additionally, multiple traffic jams can coexist on a single roadway.

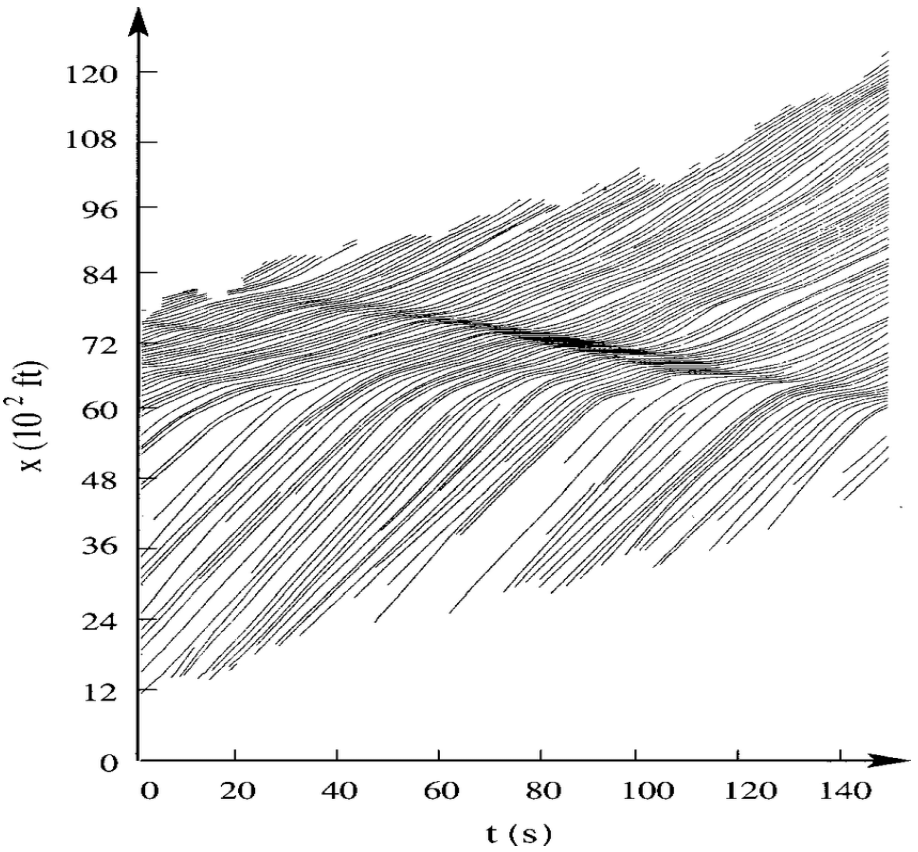

Figure 1.4: A space-time diagram in which the trajectories of individual vehicles on a multi-lane highway are represented by each line. The dashed lines denote lane changes [22].

1.4.2 The fundamental diagram

The fundamental diagram is the most important tool utilized by researchers and traffic engineers to illustrate the flow of traffic. It is defined by the relationship $J(\rho)$ between the traffic density ρ and the flow J. This relationship is analogous to a concept in hydrodynamics:

$$J = \rho \cdot V \tag{1.17}$$

In this context, different representations of the fundamental diagram are shown (see Figure 1.5). The relationship between density and the corresponding flow is displayed in Figure 1.5 (a). The first branch represents the free flow regime ($\rho < \rho_c$), where the flux J increases with density ρ. The maximum point ($\rho = \rho_c$) signifies the traffic capacity, and the second branch is reached, where J decreases with increasing ρ, indicating congested regimes ($\rho > \rho_c$). The Speed-density diagram is shown in Figure 1.5 (b). When the density ρ is low enough, vehicles are too far apart to interact significantly, and the average speed $< V >$ is mainly independent of ρ. Therefore, there are essentially no restrictions on movement at low vehicle densities. Congestion occurs when vehicles have to slow down significantly due to increasing interaction as the density rises above a critical threshold ρ_c. The relationship between speed and flow can be characterized as follows: Flow is either zero due to the absence of vehicles or excessive congestion preventing movement. At maximum flow, speed lies between zero and free flow speed. This relationship is depicted in Figure 1.5 (c).

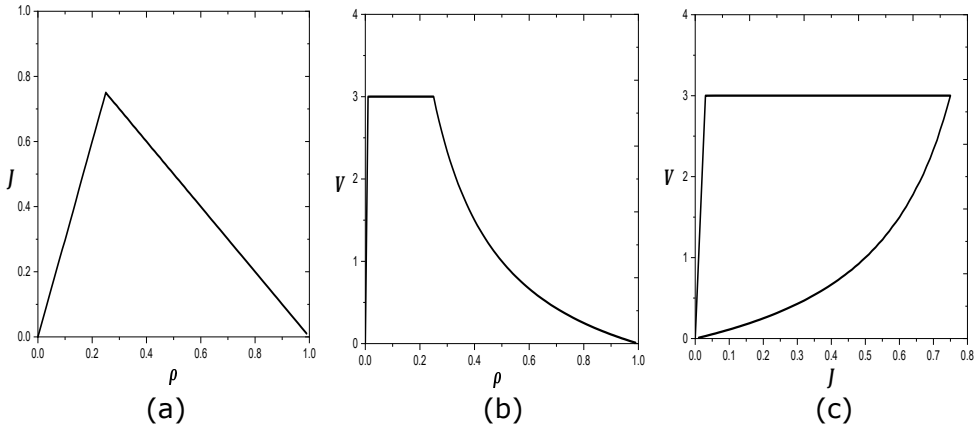

Figure 1.5: Various Shapes of the Fundamental Diagram.

The previously mentioned fundamental diagrams aim to replicate the empirical data presented in Figure 1.6 by considering the scattered dots as statistical fluctuations. The goal is to complete the fitting process and obtain the appropriate function.

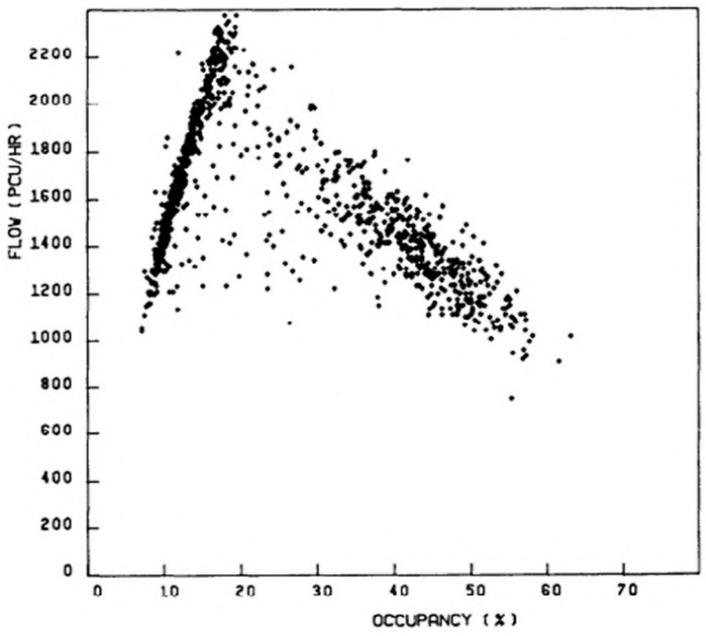

Figure 1.6: The empirical fundamental diagram from a Canadian Freeway, with data averaged over 5 minutes [23].

The results indicate that the relationship between flow and density is linear at low densities. However, there are significant fluctuations in the high-density zone, making it difficult to determine the functional form directly. Figure 1.6 also displays typical values for the primary characteristics of the flux-density relationship. A maximum of 2500 automobiles per hour can be accommodated. The maximum is achieved at vehicle densities of about 30 per kilometer, or an occupancy rate of about 20%. The nuage of points obtained in the empirical fundamental diagram is nothing more than statistical fluctuations around mean values [12,23]. These variations are due to the traffic's instability. Therefore, it is necessary to adjust this nuage to obtain a unidimensional current graph

with density. This will provide a simplified picture of reality while better aligning with experimental data. This image will then be used as the foundation for traffic models. This is the approach of the fundamental diagram.

Various analytical forms have been proposed to represent the fundamental diagram. The simplest version considers basic characteristics, featuring two linear branches forming a triangular shape, as illustrated in Figure 1.5. Neubert et al. [20] demonstrated a range of possible fundamental diagram forms, adjusting them based on empirical data presented in Figure 1.6. Across all proposed forms, two distinct regions are evident within the fundamental diagram. In the first region, at low densities, the traffic flow current J increases as density ρ rises, representing the free traffic regime. In the second region, current J decreases with increasing density ρ, indicating congestion. Additionally, in all these forms, current J reaches a single maximum value at an intermediate density. Persaud et al. [36] noted that this state is unstable, lasting only a few minutes before transitioning to the congested state (second branch). In other words, within this density range, traffic exhibits instability. A discontinuity is evident at a critical density ρ_c in various fit forms.

1.4.3 The Hysteresis

The first investigations of hysteresis were carried out by Treiterer and Myers [22], and it is a crucial aspect in the theory of road traffic. Figure 1.7 shows a hysteresis cycle that was obtained experimentally. For the same density, we have two distinct values of the current J. A high value for J signifies the state of free flow, while a second value indicates congestion.

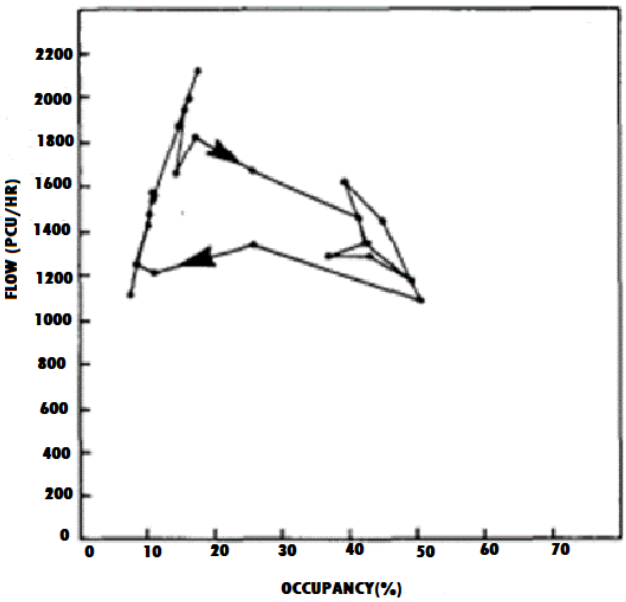

Figure 1.7: An Empirical Hysteresis Loop, with flow and density averaged over 5 minutes [23].

Hysteresis is the term used to describe the phenomenon in road traffic where the flow measurement is dependent on the initial traffic state. If the flow measurement J begins in the regime of freely flowing traffic, then an increase in density ρ results in an increase in flow J. Conversely, if the measurement starts in a congested condition, then flow J decreases as density ρ rises. This illustrates how the behavior of flow depends on the

traffic's historical state and shows how previous circumstances can influence current traffic dynamics.

1.4.4 The Metastability

Within thermodynamics, the term "metastability" refers to the presence of an unstable phase within a stable phase. When we apply this concept to road traffic, we can differentiate between two distinct phases of traffic: free flow and congested. Free-flowing traffic, where vehicles move smoothly and without disruption, represents the stable phase. In contrast, the early onset of the congestion phase is triggered by the occurrence of congestion conditions, such as phantom congestion. This early change leads to the formation of traffic platoons and hinders the efficient movement of vehicles. As a result, these two phases—the stable, free-flowing traffic and the unstable, congested state—compete against each other within the system. This dynamic interplay highlights the delicate balance between stability and instability within road networks and underscores the complexity of traffic dynamics.

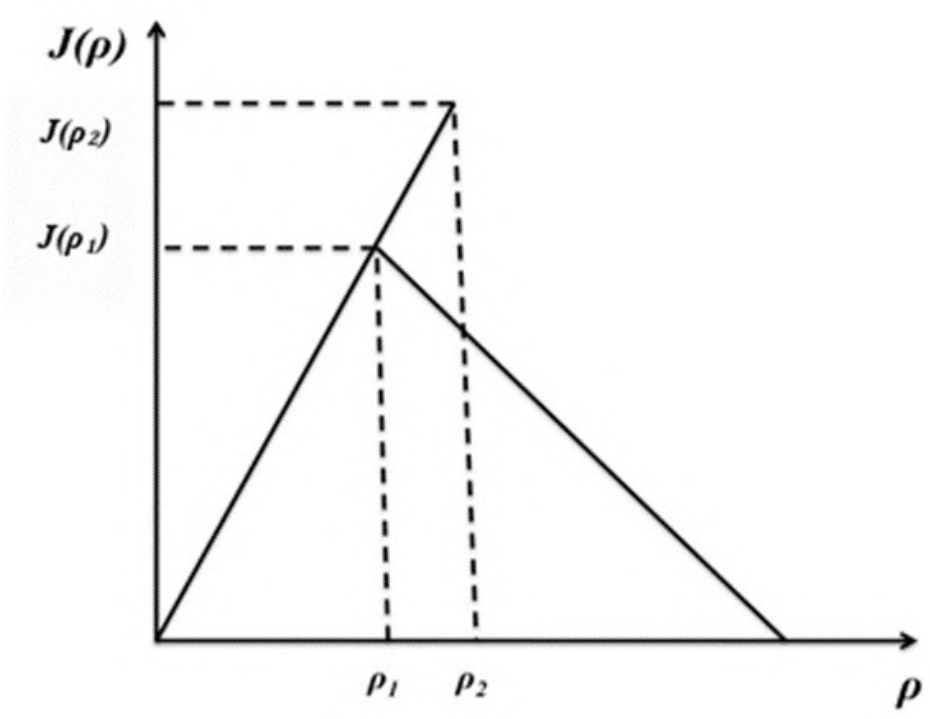

Figure 1.8: The Fundamental Diagram depicting metastability (in the region ($\rho_1 < \rho < \rho_2$).

In the free phase, an increase in density results in an increase in flow; however, at a certain density, an additional increase in density leads to a sudden decrease in flow (capacity drop) and the emergence of traffic jams. The inverse version of "λ" can be found in the equivalent fundamental diagram (Figure 1.8).

1.4.5 Inter-vehicular time and space distribution

1.4.5.1 Inter-vehicular time distribution

The inter-vehicular time is the time gap between the fronts of two consecutive vehicles. This aspect provides a detailed understanding of the traffic situation at a micro-level. The empirical results of the inter-vehicle time distributions in two traffic conditions are shown in Figure 1.9. During the free-flowing traffic phase, the main inter-vehicular time is $t_h = 0.8s$ for any density (see Figure 1.9 (a)). During this period of free-flowing traffic, drivers travel at their preferred speeds, causing vehicles to form platoons and move closely together, reducing the time between vehicles.

The inter-vehicular time is less predictable in the congested phase, as it varies with density (see Figure 1.9 (b)). It consistently exceeds the value of 0.8 seconds, which represents the value of t_h in free-flowing traffic. Drivers must be cautious and make an effort to maintain a safe distance behind the vehicle in front of them, especially considering the increased volume of vehicles on the road during this period.

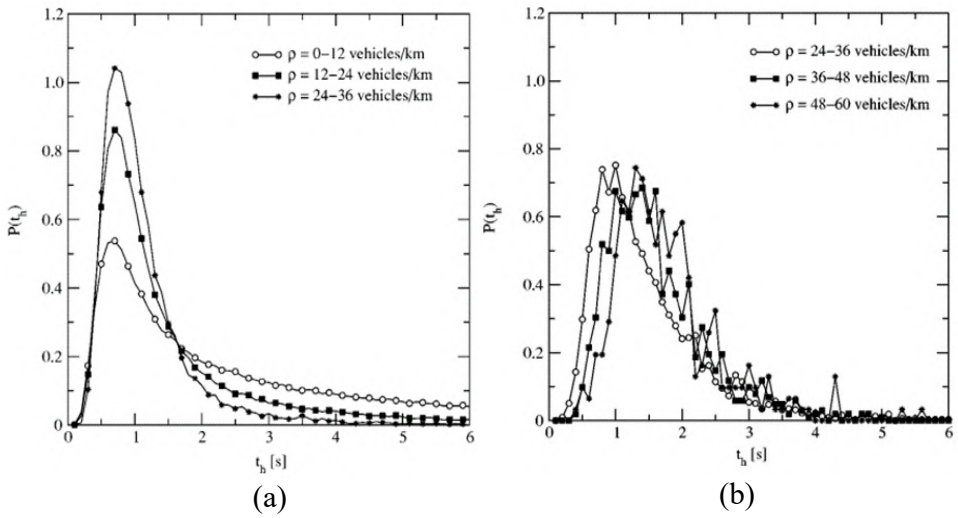

Figure 1.9: The empirical results of the distribution of inter-vehicular times in the phases of free-flowing traffic (a) and congested traffic (b) [24].

1.4.5.2 Inter-vehicular space distribution

The inter-vehicle space refers to the gap between the fronts of two successive vehicles (i and $i-1$) at a specific time within the same traffic lane. This measurement is crucial in understanding road traffic dynamics and behavior [37]. Analyzing the distribution of vehicle spacing is important in various aspects of traffic analysis, including traffic flow modeling, congestion management, and safety assessments. An empirical study on the characterization of vehicle spacing was conducted and documented in reference [25], providing valuable insights into the distribution and patterns of vehicle spacing on the road.

Figure 1.10 shows that during the free-flow phase, vehicles can achieve high velocities even over short distances as they move freely. However, as interactions between vehicles increase, the asymptotic velocity significantly decreases.

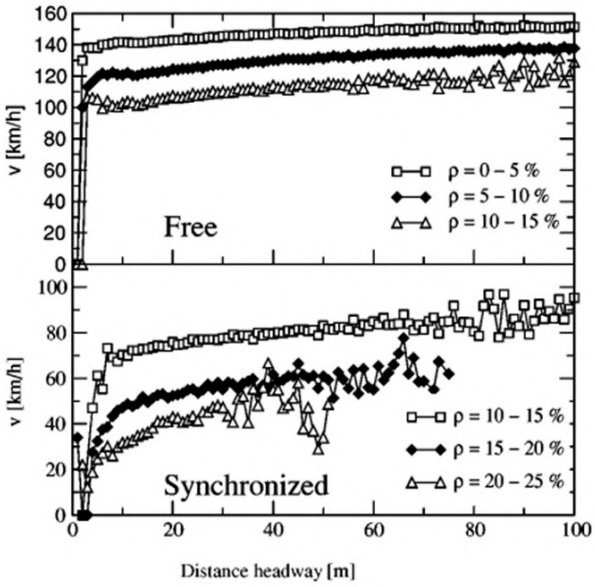

Figure 1.10: The mean velocity as a function of distance headway [25].

1.5 The modeling approaches in traffic analysis

1.5.1 The fundamental diagram approach

We use the concept of concentration, or density, along the route to understand how traffic conditions evolve within the context of the fundamental diagram method. This foundational concept was established by the pioneers of traffic modeling, who clarified that the fundamental premise of this theory is a functional relationship between two crucial parameters: flow, measured in vehicles per hour, and concentration, quantified in cars per mile. The foundation of the fundamental diagram is this fundamental relationship, which asserts that these variables are connected at every point along a road.

In steady-state traffic, especially in the free-flow regime, vehicles maintain a consistent distance from one another and travel at the same speed. However, when traffic becomes congested, we rely on the empirical fundamental diagram to understand how traffic behaves under these conditions. This diagram enables us to observe the average characteristics of the complex patterns seen in traffic flow [38]. In real-world traffic, there are fluctuations, often referred to as statistical quirks, which are natural deviations from the norm in any dynamic system. These fluctuations are evident in traffic behavior.

The fundamental diagram technique has significantly advanced our understanding of traffic dynamics. Firstly, it successfully integrated the concept of shock waves—resulting from the collective behavior of vehicles—into previous macroscopic models [4]. Real-world traffic situations frequently exhibit these shock waves, which are especially noticeable in congested flow patterns that arise upstream of freeway bottlenecks. Secondly, stability analysis, employing both automobile following models and optimal velocity models, has extensively explored the dynamics of moving jam emergence [21]. Typically, researchers start with a fixed configuration of cars and then introduce localized perturbations to certain vehicles in terms of location or velocity. By examining how other vehicles respond to these disturbances, researchers can identify the critical threshold at which traffic jams occur. Additionally, a lot of research has been done on the idea of traffic flow metastability. Several

simulations have demonstrated that, depending on initial conditions, there exists a density range where traffic remains in a metastable state [39, 40]. This sensitivity underscores the complexity of traffic behavior. Moreover, studies have investigated the factors contributing to the development and breakdown of traffic jams within this metastable zone [41], providing insight into the intricate dynamics involved in situations involving crowded traffic.

However, the fundamental diagram approach has limitations, such as its inability to explain empirical results in the congested phase. Furthermore, statistical fluctuations alone cannot account for the dispersion of points on the fundamental diagram (refer to Figure 1.6) as these fluctuations might be averaged out to produce a smooth line. Kerner proved this by focusing only on the analysis of empirical facts pertaining to wide jams [18]. He saw that scattered points continued when he compared his results to the basic diagram. Consequently, these dispersed spots originate from the intricate dynamics of synchronized flow patterns rather than statistical fluctuations.

1.5.2 The three-phase theory

The congestion phase within the fundamental diagram approach is divided into two distinct phases: "synchronized flow" and "moving jams" according to Kerner's three-phase theory [18]. This theory is based on phase transitions and spatiotemporal configurations. It's important to note that the free traffic phase is shared by both approaches. Within this theory, traffic is categorized into three distinct phases:

Free flow: In this phase, every vehicle moves at its desired speed, and interactions between vehicles are rare. Consequently, the flow increases linearly as the vehicle density increases.

Synchronized flow: The average speed in this phase is significantly lower than in free traffic, although the flow can still be significantly faster than in times of densely packed traffic. The primary attribute is the lack of a functional form connecting density and flux, meaning the empirical points are dispersed erratically along the flux-density plane. In this phase, the flow may increase or decrease in response to an increase in density, unlike the open traffic phase where the flow grows continuously. This irregularity can be measured using the cross-correlation function $\mathrm{CC}_{(\rho,J)}$ between the density ρ and the flow J [20]:

$$\mathrm{CC}_{(\rho,J)}(\tau) = \langle \rho(t) J(t+\tau) \rangle - \langle \rho(t) \rangle \langle J(t+\tau) \rangle \tag{1.18}$$

In the synchronized flow phase, the cross-correlation function $\mathrm{CC}_{(\rho,J)}(\tau)$ is nearly zero, indicating that density and flow are unrelated to one another [42]. In contrast, in free traffic, the cross-correlation function is close to one.

Wide-moving jams: are areas with comparatively low average flow or speed and very high density. These jams are significantly longer longitudinally than they are wide. They are an example of a traffic gridlock that travels against the direction of traffic flow, usually at a speed of about $15 km/h$ [43].

Kerner argues that instead of solely relying on the averaging process, as in the fundamental diagram approach, we should consider the spatiotemporal evolution of flow, mean velocity, density, and other traffic variables, as illustrated in Figure 1.11 [18].

The synchronized congestion pattern emerges from the synchronization of density and flow between lanes with relatively high traffic. When this synchronized congestion pattern occurs at a bottleneck, its downstream front usually remains stationary at the bottleneck [30, 38, 42]. This is different from the classical traffic jams observed in the

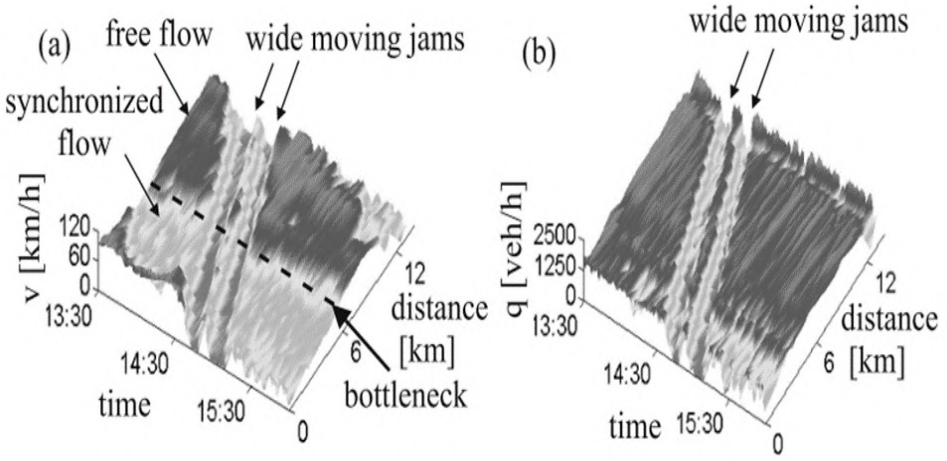

Figure 1.11: The spatiotemporal evolution of the mean velocity and current on a specific freeway [26].

fundamental diagram approach, which, once formed, propagate upstream. However, the upstream front of the synchronized congestion pattern might either move or remain constant (typically associated with intricate oscillations over time) [26, 36]. Consequently, the synchronized flow consists of multiple sub-patterns, such as the widening synchronized pattern, the localized synchronized pattern, and the moving synchronized pattern.

The three-phase theory provides reasonable explanations for many observable empirical phenomena, but it also has certain limitations. Firstly, alternative simpler models could be used to replicate the scattering observed in the fundamental diagram [1, 44]. Kerner attributes this dispersion to distinct traffic flow dynamics, particularly evident when using identical driver models. However, Helbing's macroscopic model [12] may replicate this dispersion when considering heterogeneity with multilane conditions. The scattering described earlier results from the varied behaviors and interactions of trucks and specific vehicles. Additionally, the synchronized flow comprises various sub-patterns, including the moving synchronized pattern and the widening synchronized pattern [44]. Interestingly, both propagate upstream at the same speed. Kerner distinguishes the "moving synchronized pattern" from the "wide moving jam" by noting that the former transforms into a different synchronized pattern upon encountering a bottleneck, such as an on-ramp, whereas the latter continues spreading through the bottleneck [26]. This poses a methodological challenge as it becomes difficult to differentiate between the moving synchronized pattern and the widening synchronized pattern.

1.6 Road traffic modeling

We use simulation to understand real-world scenarios by analyzing data, predicting outcomes, and evaluating experimental results to replicate the operation of dynamic traffic systems. Different classification criteria, such as the type of variables (continuous or discrete), the level of detail, and the representation of processes (deterministic or stochastic), are used in constructing traffic simulation models. In this thesis, we focus on classifying road traffic models according to the adopted level of detail, categorized as macroscopic, microscopic, and mesoscopic. This section begins with a brief overview of existing flow models, followed by a more detailed exploration of cellular automata models,

with particular emphasis on the Nagel and Schreckenberg model [16].

1.6.1 The macroscopic models

Macroscopic models, based on principles from fluid mechanics, aim to depict the collective behavior of traffic on a broader scale of analysis. The model was initially introduced by Lighthill and Whitham [4].

Generally, macroscopic models are fundamentally grounded in two key principles. The first principle, known as the "law of continuity," involves measuring traffic flow in terms of characteristics like speed, flow, and density. These three attributes (flow, speed, and density) constitute the primary features of movement. By examining the connection between density and flow velocity, mathematical models for continuous transport flow modeling have been developed, leading to precise and effective simulations.

The second principle, termed the "conservation law," dictates that there is neither dissipation nor creation of vehicles within the system. This principle contributes to a more thorough understanding of macroscopic traffic dynamics by emphasizing the preservation of the total number of vehicles in the traffic flow.

In macroscopic modeling, addressing the challenges of traffic involves grappling with various factors like citywide congestion, road traffic, assessing the efficiency of public transport routes, scheduling public transport, and modeling current and future traffic patterns [45]. However, the hypothesis of continuity in traffic, though a fundamental assumption in macroscopic models, faces challenges due to vehicle sizes, preventing an accurate depiction of local or individual phenomena like lane changes. Despite this limitation, macroscopic models, as detailed in [46], offer valuable insights into traffic dynamics.

1.6.2 The microscopic models

The microscopic model offers a detailed description of traffic flow and transport infrastructure, achieved through models depicting interactions among individual vehicles and their environment. The microscopic description relies on variables such as instantaneous speed and inter-vehicular time. The primary aim of microscopic modeling is to differentiate the behavior of individual vehicles and their interactions with other drivers across three distinct driving situations: pursuit behavior, change of direction behavior, and insertion behavior. Microscopic models gained popularity with the advent of powerful computers, given their need for extensive calculations. These models excel in portraying traffic dynamics and can be categorized into two types:

Car following models: In these models, braking and acceleration patterns are described, resulting from interactions with the vehicle in front. Vehicles perceive parameters such as distance or speed differentials perfectly from preceding vehicles and remain constantly attentive to acceleration control tasks. It is expected that all drivers will behave consistently, with each vehicle seeking a safe distance based on the relative speeds of the two vehicles ahead of it [47, 48]. Building upon this assumption, Bando et al. [49] propose the Optimal Velocity Model (OVM), where the driver regulates speed not only based on the vehicle being followed but also on a speed ensuring the avoidance of collision risk with the vehicle in front in the event of sudden braking.

Particle models: These models allow for a detailed analysis of how individual vehicles respond to various conditions. This includes lane changes, where drivers make decisions

based on factors like driver preferences, the current traffic in the lane they're in, and conditions in the target lane, including the speed of approaching vehicles and the available space in the adjacent lane. Additionally, particle models are applied to route choice, where drivers determine their paths from departure to destination and react to traffic conditions along the chosen route [50–52]. They prove particularly valuable for studying intricate traffic phenomena, including congestion patterns, traffic dynamics, and the impacts of diverse traffic management strategies.

1.6.3 The mesoscopic models

Mesoscopic models serve as an intermediate between macro models, which describe the overall characteristics of traffic flows, and micro models, which detail the movements of individual vehicles within those flows. While behavioral rules are specified at an individual level [46], vehicles and driver behavior are aggregated in mesoscopic models, focusing on groups with similar properties, such as origin and destination. Mesoscopic models strike a balance by preserving a high level of detail in simulating street-road networks while simplifying the representation of traffic flow dynamics. This preservation of detail allows for the expansion of the simulated network scale while ensuring a high simulation speed.

Mesoscopic models come in various forms, including gas-kinetic and headway distribution models [53–55]. Despite their complexities, mesoscopic models find applications in evaluating Traveler Information Systems. This modeling approach occupies a vital position between macro and micro models, offering detailed descriptions of the simulated street-road network and simplified dynamics of traffic flow.

1.6.4 Cellular automata model

After providing an overview of the most pertinent modeling approaches, we will delve into the selected modeling approach for this thesis: the cellular automata model.

Von Neumann [56] first established the mathematical notion of cellular automata in 1948 while using CAs to investigate biological processes. However, the primary applications in studying dynamical systems were conducted by Wolfram [57].

The speed and simplicity of this model make it an excellent choice for modeling various phenomena across different domains. Cellular automata, for instance, have been utilized to simulate the spread of forest fires [58], explore earthquakes [59], analyze stock market dynamics [60], examine epidemic diseases [61,62], and serve as an alternative to differential equations [63].

In road traffic modeling, the road is depicted as a series of sequential cells, or N sites. One vehicle (particle) or none at all may occupy each cell. The system's update depends on the chosen dynamics, which include a range of types [64,65]. Parallel dynamics, in which all sites are updated concurrently, is the most efficient dynamic for researching traffic on roads. Vehicle movement can either be deterministic or probabilistic. The simplicity of these rules enables the handling of large systems, facilitating the connection between microscopic scales (individual vehicle interactions) and correlating them with macroscopic road traffic metrics like flow and average speed. Additionally, CA models are more adept at simulating the nuances of actual traffic, such as lane changes, diversity of traffic, accidents, acceleration and deceleration, and more.

The first models utilizing cellular automata for studying road traffic were introduced by Cremer et al. in 1986 [15], then prototyped by Nagel and Schreckenberg in 1992 [16].

Since then, the latter has emerged as one of the most renowned models in the realm of road traffic.

1.6.4.1 Nagel and Schreckenberg model

Nagel and Schreckenberg (NaSch) selected a limited set of rules for their model [16] to emphasize the fundamental aspects of real traffic when simulating complex events in statistical physics. The NaSch model simulates the fundamental motions of one-dimensional traffic flow, which includes the driver's propensity to accelerate and attain the intended speed as well as to decelerate to avoid collisions with other vehicles.

The NaSch cellular automaton model is based on three discrete variables: time, space, and velocity. The road is represented as a one-dimensional chain of cells, with each cell either occupied or empty by a vehicle. The length of one cell is determined by $\Delta x = \rho_{\text{jam}}^{-1} = 7.5$ meters, where Δx represents the minimum space occupied by a vehicle [66]. Time is also discretized, with the time step corresponding to $\Delta t = 1$ second. Vehicle speed is constrained to discrete values $V = 0, 1, 2, ..., V_{\max}$, indicating the number of cells a vehicle can move in one time step.

Each vehicle aims to attain its maximum velocity while considering two constraints: the distance between adjacent vehicles and the various behaviors of drivers, including the spontaneous occurrence of congestion, quantified by a probability of spontaneous deceleration.

In traffic flow, these dynamics occur simultaneously, meaning that the velocities of each vehicle are updated concurrently at time t. As a result, the NaSch model characterizes vehicle motion at a given time t as follows:

R1: Acceleration: $V_i \rightarrow \min(V_i + 1, V_{\max})$

R2: Deceleration: $V_i \rightarrow \min(V_i, d_i)$

R3: Randomization: $V_i \rightarrow \max(V_i - 1, 0)$ with the braking probability P_b

R4: Movement: $x_i \rightarrow x_i + V_i$

Where x_i and V_i represent the position and speed of vehicle i, respectively. The variables $V_{\max}$ and d_i represent the maximum velocity and headway, respectively.

In the first rule (R1), if the vehicle hasn't reached its maximum speed $V_{\max}$, the driver accelerates and is prepared to brake to prevent accidents (R2). These rules establish a structure for optimal driver behavior and decision-making. The cellular automaton operates on deterministic principles, with its equilibrium contingent upon the initial setup. However, drivers in reality don't consistently exhibit this optimal behavior. Therefore, the introduction of the so-called random portion (R3) is necessary to offer a realistic description of traffic flow. This element simulates the complex interactions between vehicles, integrating three diverse models of individual driver behavior into a unified system [67]: speed fluctuations at maximum, lag in acceleration, and an exaggerated response to braking. The inclusion of non-deterministic acceleration and exaggerated deceleration is crucial for the spontaneous generation of traffic jams [68]. There are two possible scenarios in the NaSch model: $P_b = 0$ (P_b is the braking probability), then the

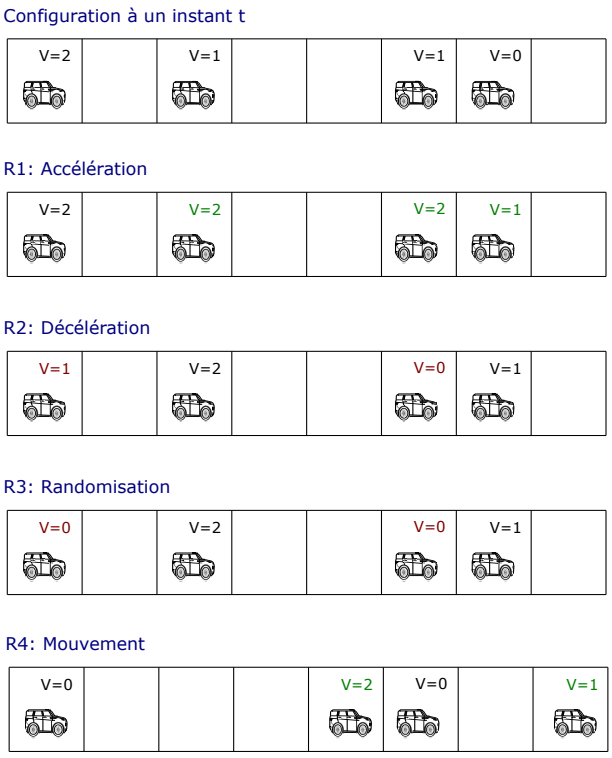

Figure 1.12: Illustration du modèle NaSch

dynamics are deterministic and parallel, and $P_b > 0$, the dynamics become parallel random (non-deterministic), meaning the movement of vehicles is probabilistic. After that, the vehicle moves forward according to the rule (R4) (see Figure 1.12). The NaSch model is versatile, accommodating both periodic (closed loop) [16] and open boundary conditions for modeling traffic flow in numerical simulations or analytical methods [27, 40].

1.6.4.2 The boundary conditions

To simulate traffic flow, researchers use different boundary conditions in numerical simulations or analytical methods. In this discussion, we will use the NaSch cellular automata model to represent traffic flow, incorporating two primary types of boundary conditions: periodic and open.

The periodic boundary conditions

In periodic boundary conditions, the road network is considered a closed loop, where vehicles follow the previously mentioned rules. Vehicles exit from one end of the road and re-enter from the other (see Figure 1.13), resulting in a constant density and a continuous flow without any sudden disruptions. This setup allows for the simulation of traffic flow on long and wide roads without needing to account for boundaries.

Periodic boundary conditions are often used to evaluate the significance of internal model effects, such as vehicle interactions within the system, in describing traffic phenomena. For example, they help in understanding the emergence of phantom traffic jams while disregarding external factors like ramps and intersections [69]. These conditions are instrumental in revealing the fundamental relationships between density, velocity, and traffic flow, and can be represented on the flow-density plane of the fundamental diagram.

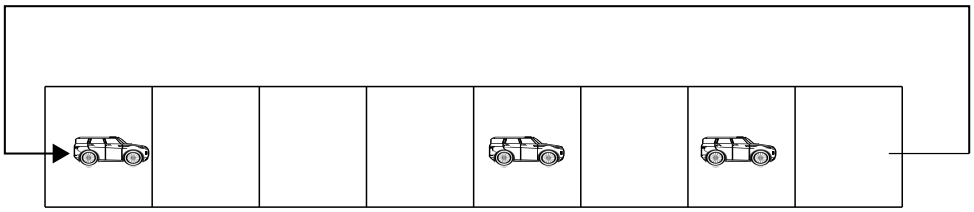

Figure 1.13: Periodic boundary conditions.

Figure 1.14 shows the fundamental diagrams for two cases: (a) the deterministic case where $P_b = 0$ and various values of V_{max}, and (b) the random case where $P_b > 0$ and $V_{max} = 5$. At low densities, all vehicles move at their maximum speeds V_{max}, and vehicle interactions are negligible, which increases the flow, corresponding to the free-flow phase. Vehicles continue to travel at their maximum speeds until reaching a critical density ρ_c. After that, the congested phase begins, where the flow starts to decrease, and vehicle interactions become more significant. In Figure 1.14 (a), we observe that when $V_{max} = 1$, the fundamental diagram is symmetrical with respect to $\rho_c = 1/2$. However, this symmetry breaks for all $V_{max} > 1$. Additionally, the flux increases with the increase in V_{max} in the region of low densities, and the maximum flux shifts to the left. This shift suggests that as V_{max} increases, the critical density ρ_c, which is the point at which the free phase and congested phase meet, decreases. Furthermore, when the probability of braking P_b increases, most drivers become more cautious and less linked to the vehicles in front of them, which results in a drop in flux and the critical density ρ_c (See Figure 1.14 (b)).

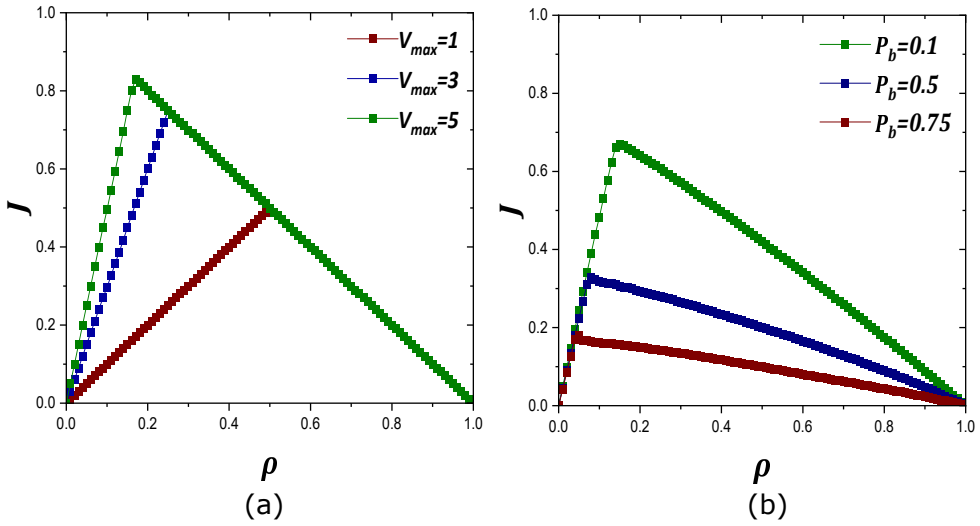

Figure 1.14: Fundamental Diagrams (a) for different values of the maximum speed V_{max} with $P_b = 0$, (b) for different values of the braking probability P_b with $V_{max} = 5$.

The open boundary conditions

Open boundary conditions are more practical and can provide a better understanding of the bulk properties of a dynamic model. In systems with open boundaries, the entry and exit points control the flow of vehicles, and the density is no longer constant, unlike in closed systems with periodic boundary conditions.

For the NaSch model, there are primarily two types of open boundary conditions: "standard" [27] and "expanded" [40]. The primary distinction between these types lies in the injection rule, while their extraction rule remains consistent. Vehicles are introduced into the lattice at the left boundary at a rate α, and removed from the right boundary at a rate β. This injection of vehicles can simulate traffic entering from sources such as traffic lights, intersections, or on-ramps. The extraction rate constraint may indicate the presence of disturbances or other obstructions.

Consider a chain of length L, where i is the index of the locations for which $1 \leq i \leq L$. To extract the vehicles from the final cell, at the end of the lane, we add one additional cell. There is a probability of β that these vehicles will exit the system. If not, there is a probability of $1 - \beta$ that the vehicles will slow down as they approach the end of the system and wait to be removed.

In the case of the standard injection rule, a vehicle with a probability of α and a speed of $V = V_{max}$ is formed at site $i = 0$ outside the system within a reservoir of size 1. This vehicle immediately adheres to the NaSch rules and begins to move. On the other hand, if site $i = 1$ is already occupied by another vehicle, the injected vehicle at site $i = 0$ will be removed (See Figure 1.15).

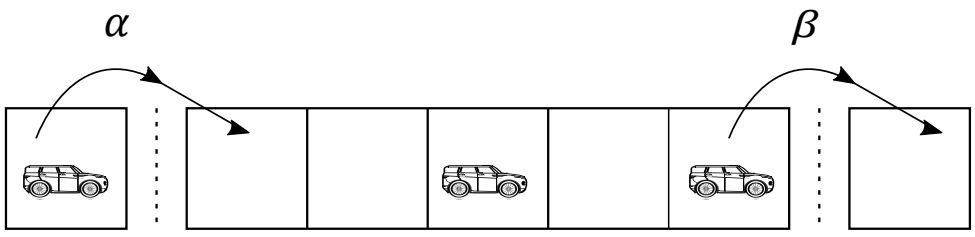

Figure 1.15: Standard open conditions.

In the expanded open boundary conditions, vehicles are added to the system at the left edge of the entry lanes. A mini-system (width $V_{max} + 1$) is connected in series with the entry lane at the left border. Vehicles in the mini-system are added with a probability of α in the following way: if a vehicle already exists, it must be removed. Then, with probability α, a vehicle with initial velocity V_{max} is added. Its distance from the first vehicle in the entry lane is at least the maximum speed V_{max}. Each vehicle's destination or escape path is chosen with an equal probability at the entry lane (See Figure 1.16).

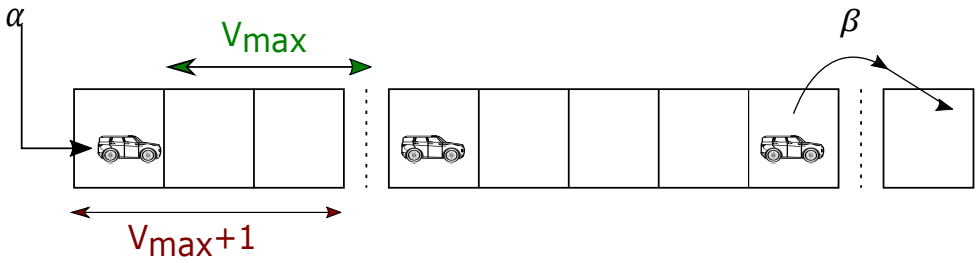

Figure 1.16: Expanded open conditions ($V_{max=2}$).

The open boundary conditions replicate a significant observed traffic phenomenon, specifically, the phase transitions induced by the boundaries [70].

Three flow regimes are observed (Figure 1.17), depending on the values of α, β, and P_b: the flow is free at $\alpha < \beta$. Conversely, a traffic congestion arises at the system's right

end and progressively extends across the entire system if $\alpha > \beta$. These two phases are separated by a first-order transition under expanded open conditions and a second-order transition with standard injection terminals. The current reaches its highest value in the third phase. In this final phase, known as maximum current, the system becomes independent of the extremities (the input and the output), relying only on the chain's length L and the probability of braking P_b.

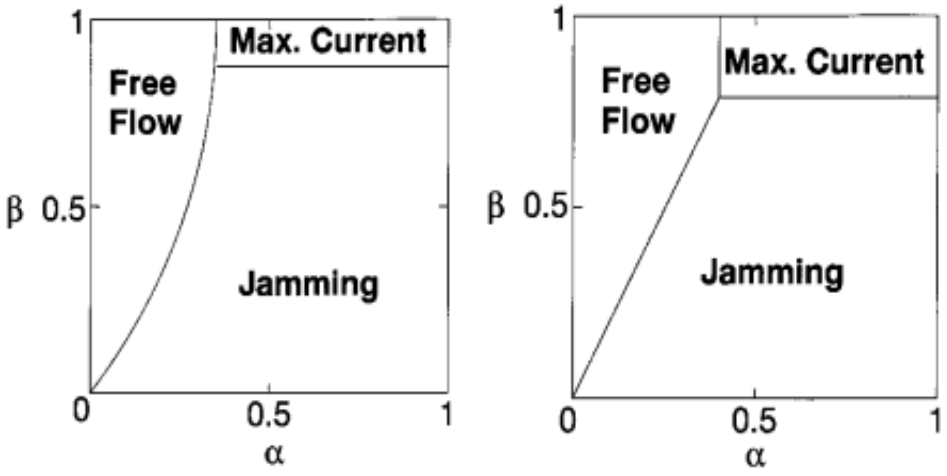

Figure 1.17: Phase diagrams of the NaSch model under open conditions with $P_b = 0.5$, $V_max = 5$. (a) Standard injection terminals, (b) Expanded injection terminals [27].

1.6.4.3 Extensions of the NaSch model

Nagel and Schreckenberg (NaSch) [16] developed a probabilistic cellular automaton (CA) several years ago to simulate traffic on single-lane highways. This model uses simple principles, such as linear acceleration (R1 of NaSch) and immediate stopping instead of gradual speed reduction (R2 of NaSch), to replicate basic phenomena observed in real-world traffic. In this model, vehicles consider the distance to the vehicles ahead of them instead of speed [71]. Moreover, the model incorporates the phenomenon of "jams out of nowhere" (R3 of NaSch), also known as phantom traffic jams [39].

Consequently, additional rules and modifications have been proposed to achieve a more realistic depiction of traffic flow [71, 72]. These modifications aim to capture a wider range of phenomena observed in actual traffic scenarios, such as ramps or multi-lane traffic, or to accurately depict finer details of traffic flow such as the existence of metastable states or synchronized circulation. Given the wide range of these proposed modifications, we have chosen to focus on the most widely adopted and effective ones, which introduce several intriguing aspects into the dynamics.

To enhance the realism of the NaSch model and better reflect real traffic conditions, numerous researchers have introduced additional rules to alter traffic behaviors. S. C. Benjamin et al. [73] incorporate a slow-to-start rule in their study of the cellular automaton model for highway traffic flow and investigate the effects of acceleration, disorder, and slow-to-start behavior on the length of the wait at the entry. R. Barlovic et al. [39] extend the Nagel-Schreckenberg model by introducing velocity-dependent randomization and examining a particular case of slow-to-start rules. This study uncovers metastable states and elucidates the conditions necessary for hysteresis effects in flow-density relationships.

Y. Xue et al. [68] utilize the Nagel-Schreckenberg (NaSch) model to investigate the impact of the order of evolutive rules on traffic flow. They demonstrate that the cellular automaton (CA) traffic model is sensitive to these orders and develop two modified models, noise-first and SDNaSch, by altering the evolutionary phases of the NaSch model. Boris S Kerner et al [71] modified the Nasch model to calculate the synchronization distance between the vehicles and the synchronization phase. M. Fukui and Y. Ishibashi [72] introduced a variation on the basic model that unveils a phase transition between moving and noise phases, where the speed increase in this transition may not be progressive, and only high-speed vehicles are subject to the stochastic delay. W. Knospe et al. [74] created a different cellular automata model that incorporates anticipation effects, decreased acceleration, and enhanced braking contact. This model effectively replicates real traffic phases and aligns well with empirical single-vehicle data, thus enhancing comprehension of elementary dynamics.

These initiatives enhance our understanding of traffic dynamics at a deeper level, thereby fostering the development of more efficient transportation systems and policies.

1.7 Environmental impact

1.7.1 Energy dissipation

A common statistic used by researchers to evaluate traffic conditions is energy dissipation. In the deterministic NaSch model, Zhang et al. [75] studied the impact of the energy dissipation rate on speed limitations and found relationships between braking probability, energy dissipation, and "stop and go" occurrences. To enhance Bando's optimal velocity model, Zhu et al. [76] explored the interaction between energy dissipation and signal control parameters. Laarej et al. [77] examined how slow cars affected energy dissipation and satisfaction rates using a two-lane cellular automaton model.

We use the following equation to calculate the kinetic energy that a vehicle gains while moving:

$$E_c = \frac{1}{2}mv^2 \tag{1.19}$$

Where v and m represent the vehicle's speed and mass, respectively.

The energy dissipated during deceleration is used to calculate the dissipation energy. Similarly, the kinetic energy (i.e., the energy gained during acceleration) and the energy dissipation (i.e., the energy dispersed due to the slowdown) are equal under the conservation of kinetic energy principle. In this model, only the energy dissipation resulting from the deceleration is considered, while other forms of energy dissipation are ignored [76, 78]. The dissipated energy ΔE of vehicle i between times $t-1$ and t is defined as follows:

$$\Delta E_i(t) = \begin{cases} \frac{1}{2}m[v_i^2(t-1) - v_i^2(t)] & \text{if } v_i^2(t-1) > v_i^2(t) \\ 0 & \text{Otherwise} \end{cases} \tag{1.20}$$

Therefore, the energy dissipation rate is:

$$E_d = \frac{1}{T}\frac{1}{N}\sum_{t=t_0+1}^{t_0+T}\sum_{i=1}^{N}\Delta E_i(t) \tag{1.21}$$

Where t_0 is the relaxation time, which is considered to be a sufficient amount of time for the system to reach its steady state, and N is the total number of cars in the system. The time interval used to calculate total energy dissipation is T.

1.7.2 Traffic Emission Model

To simulate traffic emissions, we use the emission model presented by Panis et al. [28]. This well-established model employs nonlinear multivariate regression techniques to determine emissions based on a vehicle's acceleration and instantaneous speed. Its empirically confirmed underpinnings and simplicity have led to its widespread acceptance by researchers. Notably, it was calibrated using data collected from real-world urban and highway driving conditions.

Building on this, Li et al. [79] used GPS data from Beijing taxis to develop a novel method for examining different patterns of emissions of nitrogen oxides (NOx), carbon dioxide (CO2), particulate matter (PM), and volatile organic compounds (VOCs). They also investigated the relationships between emissions and road densities. Similarly, Nyhan et al. [80] used GPS trajectory data from a large fleet of over 15,000 taxis to determine the necessary speeds and accelerations, which served as the foundation for predicting emissions of PM, CO2, NOx, and VOCs in Singapore's air.

In continuation of this discussion, Wang et al. [81] combined an empirical formula for vehicle exhaust emissions with a mixed NaSch traffic flow model to examine CO2, PM, VOC, and NOx emissions while considering variables like vehicle lengths, maximum velocity, movement conditions, and mixing ratios.

For our investigation, we will use the Int Panis et al. [28] model, where the emission function depends on the acceleration and instantaneous speed of the vehicle. This approach enables us to focus on the emissions of pollutants such as VOC, NOx, PM, and CO2 that have significant effects on both health and the economy. We used the following general formula for pollutant emission:

$$E_i(a_i(t), V_i(t)) = \max\left(0, f_1 + f_2 V_i(t) + f_3 V_i^2(t) + f_4 a_i(t) + f_5 a_i^2(t) + f_6 V_i(t) a_i(t)\right) \tag{1.22}$$

In the equation, $V_i(t)$ and $a_i(t)$ represent the instantaneous speed (in meters per second) and instantaneous acceleration (in meters per second squared) of vehicle i, respectively. Additionally, Table 1 contains the constants f_1 to f_6, which are specific to each type of vehicle.

We estimate emissions in grams per second per vehicle (g/s) to account for the frequent variations in vehicle speed in densely populated urban areas. This statistic is more relevant as it considers real-time emission levels, which might fluctuate greatly due to traffic congestion.

1.8 Characteristics of Road Infrastructure Elements

The aim of this section is to provide a comprehensive analysis of the various types of road infrastructure, including highways, intersections X and Y, and circular intersections

Table 1.1: Emission functions for the 2010 fleet of urban traffic [28].

Pollutant	Vehicle type	E_0	f_1	f_2	f_3	f_4	f_5	f_6
CO_2	**Petrol car**	0	$5.53e^{-01}$	$1.61e^{-01}$	$-2.89e^{-03}$	$2.66e^{-01}$	$5.11e^{-01}$	$1.83e^{-01}$
	Diesel car	0	$3.24e^{-01}$	$8.59e^{-02}$	$4.96e^{-03}$	$-5.86e^{-02}$	$4.48e^{-01}$	$2.30e^{-01}$
	LPG car	0	$6e^{-01}$	$2.19e^{-01}$	$-7.74e^{-03}$	$3.57e^{-01}$	$5.14e^{-01}$	$1.70e^{-01}$
	HDV	0	$1.52e^{+00}$	$1.88e^{+00}$	$-6.95e^{-02}$	$4.71e^{+00}$	$5.88e^{+00}$	$2.09e^{+00}$
	Bus	0	$9.04e^{-01}$	$1.13e^{+00}$	$-4.27e^{-02}$	$2.81e^{+00}$	$3.45e^{+00}$	$1.22e^{+00}$
NO_x	**Petrol car** ($a \geq -0.5\,\mathbf{m/s^2}$)	0	$6.19e^{-04}$	$8.00e^{-05}$	$-4.03e^{-06}$	$-4.13e^{-04}$	$3.80e^{-04}$	$1.77e^{-04}$
	Petrol car ($a < -0.5\,\mathbf{m/s^2}$)	0	$2.17e^{-04}$	$0.00e^{+00}$	$0.00e^{+00}$	$0.00e^{+00}$	$0.00e^{+00}$	$0.00e^{+00}$
	Diesel car ($a \geq -0.5\,\mathbf{m/s^2}$)	0	$2.41e^{-03}$	$-4.11e^{-04}$	$6.73e^{-05}$	$-3.07e^{-03}$	$2.14e^{-03}$	$1.50e^{-03}$
	Diesel car ($a < -0.5\,\mathbf{m/s^2}$)	0	$1.68e^{-03}$	$-6.62e^{-05}$	$9.00e^{-06}$	$2.50e^{-04}$	$2.91e^{-04}$	$1.20e^{-04}$
	LPG car ($a \geq -0.5\,\mathbf{m/s^2}$)	0	$8.92e^{-04}$	$1.61e^{-05}$	$-8.06e^{-07}$	$-8.23e^{-05}$	$7.60e^{-05}$	$3.54e^{-05}$
	LPG car ($a < -0.5\,\mathbf{m/s^2}$)	0	$3.43e^{-04}$	$0.00e^{+00}$	$0.00e^{+00}$	$0.00e^{+00}$	$0.00e^{+00}$	$0.00e^{+00}$
	HDV	0	$3.56e^{-02}$	$9.71e^{-03}$	$-2.40e^{-04}$	$3.26e^{-02}$	$1.33e^{-02}$	$1.15e^{-02}$
	Bus	0	$2.36e^{-02}$	$6.51e^{-03}$	$-1.70e^{-04}$	$2.17e^{-02}$	$8.94e^{-03}$	$7.57e^{-03}$
VOC	**Petrol car** ($a \geq -0.5\,\mathbf{m/s^2}$)	0	$4.47e^{-03}$	$7.32e^{-07}$	$-2.87e^{-08}$	$-3.41e^{-06}$	$4.94e^{-06}$	$1.66e^{-06}$
	Petrol car ($a < -0.5\,\mathbf{m/s^2}$)	0	$2.63e^{-03}$	$0.00e^{+00}$	$0.00e^{+00}$	$0.00e^{+00}$	$0.00e^{+00}$	$0.00e^{+00}$
	Diesel car ($a \geq -0.5\,\mathbf{m/s^2}$)	0	$9.22e^{-05}$	$9.09e^{-06}$	$-2.29e^{-07}$	$-2.20e^{-05}$	$1.69e^{-05}$	$3.75e^{-06}$
	Diesel car ($a < -0.5\,\mathbf{m/s^2}$)	0	$5.25e^{-05}$	$7.22e^{-06}$	$-1.87e^{-07}$	$0.00e^{+00}$	$-1.02e^{-05}$	$-4.22e^{-06}$
	LPG car ($a \geq -0.5\,\mathbf{m/s^2}$)	0	$1.44e^{-02}$	$1.74e^{-07}$	$-6.82e^{-09}$	$-8.11e^{-07}$	$1.18e^{-06}$	$3.96e^{-07}$
	LPG car ($a < -0.5\,\mathbf{m/s^2}$)	0	$8.42e^{-03}$	$0.00e^{+00}$	$0.00e^{+00}$	$0.00e^{+00}$	$0.00e^{+00}$	$0.00e^{+00}$
	HDV	0	$1.04e^{-03}$	$4.87e^{-04}$	$-1.49e^{-05}$	$1.27e^{-03}$	$2.10e^{-04}$	$1.00e^{-04}$
	Bus	0	$1.55e^{-03}$	$8.20e^{-04}$	$-2.42e^{-05}$	$1.86e^{-03}$	$3.21e^{-04}$	$1.36e^{-04}$
PM	**Petrol car**	0	$0.00e^{+00}$	$1.57e^{-05}$	$-9.21e^{-07}$	$0.00e^{+00}$	$3.75e^{-05}$	$1.89e^{-05}$
	Diesel car	0	$0.00e^{+00}$	$3.13e^{-04}$	$-1.84e^{-05}$	$0.00e^{+00}$	$7.50e^{-04}$	$3.78e^{-04}$
	LPG car	0	$0.00e^{+00}$	$1.57e^{-05}$	$-9.21e^{-07}$	$0.00e^{+00}$	$3.75e^{-05}$	$1.89e^{-05}$
	HDV	0	$2.14e^{-04}$	$3.35e^{-04}$	$-2.22e^{-05}$	$2.07e^{-03}$	$1.80e^{-03}$	$2.27e^{-04}$
	Bus	0	$2.23e^{-04}$	$3.47e^{-04}$	$-2.38e^{-05}$	$2.08e^{-03}$	$1.76e^{-03}$	$2.23e^{-04}$

such as traffic circles and roundabouts. A deep understanding of these different variations is essential to evaluate their usefulness, efficiency, and impact on traffic flow dynamics and safety protocols. By examining the unique features and operational intricacies of each infrastructure component, we can better understand their role in constructing the overall transportation landscape and guide strategic decision-making processes aimed at improving roadway efficiency and safety standards.

1.8.1 Highways

Highways are crucial components of the transportation network, serving as essential links for the movement of vehicles across borders and between states. These highways are typically constructed for long-distance connectivity and high-speed travel, enabling the efficient and rapid transportation of people and goods. The classification of highways varies, including major interstates, expressways, local and regional routes, each designed to handle specific traffic levels and travel demands. To ensure safe and efficient traffic flow, they incorporate standardized design elements such as grade separations, lane widths, and shoulder widths. Highways are equipped with various traffic control systems, including lane markings, signage, and traffic lights at intersections, to manage traffic and enhance safety. Moreover, highways often incorporate advanced technologies like tolling and intelligent transportation systems (ITS) [82–84].

1.8.2 Intersections

Intersections are critical points in a roadway network where various traffic streams connect, diverge, and converge. Each type of intersection serves a distinct purpose and presents

unique challenges for safety and traffic management. The first type of intersection is T-shaped or Y-shaped, where three arms of traffic typically intersect, with a minor road meeting a main route. To regulate vehicle movement and prioritize traffic flow, this configuration requires the implementation of traffic control measures such as rules of priority, stop signs, or traffic signals.

In an unsignalized T-shaped intersection, traffic flow remains uncontrolled, leading to potential conflicts between vehicles on the main road and those on the minor road. To mitigate the risk of collisions, two crash-avoidance rules are commonly employed: giving precedence to vehicles traveling straight ahead and allowing vehicles that arrive at the intersection first to proceed. However, the impact of these rules on intersection capacity varies depending on prevailing traffic conditions [85].

When stop signs or traffic signals are utilized at the intersection, they provide a structured approach to managing traffic flow and minimizing conflicts between vehicles. Stop signs require drivers to come to a complete stop before proceeding, allowing for orderly movement of vehicles through the intersection. Traffic signals, on the other hand, use a system of lights to control when vehicles from each direction may proceed, ensuring safe passage while minimizing congestion. The choice between stop signs and traffic signals depends on factors such as traffic volume, intersection geometry, and safety considerations. Stop signs are typically used at intersections with lower traffic volumes or where visibility is limited, while traffic signals are employed at intersections with higher traffic volumes and complex traffic patterns [86].

Intersection X is a type of intersection where four arms of traffic meet at a central point, also known as a four-way intersection. The flow control and optimization of this intersection are crucial for achieving global optimization in city networks. The first basic two-dimensional CA model for urban traffic systems was provided by BML (Biham, Middleton, and Levine) [52]. Additionally, the first model for simulating two crossing highways was proposed by Nagatani [87]. Most earlier studies have focused on two-road intersections with either open or typically closed border conditions. Marzoug et al. [88] investigated the impact of changing boundary conditions on a fundamental diagram and identified the optimal traffic flow control method for two intersecting roads.

Stop signs and traffic signals are also used to regulate this type of intersection, helping to minimize vehicle collisions and manage the increasing density of vehicles [89]. For traffic engineers and urban planners to develop suitable intersection designs and implement efficient traffic management techniques, they must have a comprehensive understanding of the features and operational requirements of crossroads. The design of an intersection should closely align with the operating characteristics of its users, considering factors such as safety, operational flexibility, vehicle capacity, and traffic management type. Efficient utilization of smaller lanes in urban intersections and optimizing approach capacity through lane configuration are pivotal elements that influence intersection performance for motor vehicles.

1.8.3 Circular Intersections

Circular intersections, such as roundabouts and traffic circles, are designed to improve traffic flow and safety. They operate under the principle that circulating traffic has priority, promoting continuous movement and minimizing stops and idle periods. Vehicles entering the traffic circle have the right of way over other vehicles, as this lane is intended to facilitate the acceleration of vehicles into the circulating lane for smoother passage. However, unlike

traffic circles, roundabouts typically feature a smaller center island, causing vehicles to slow down as they approach the circulating lane [90].

Research has consistently shown that both traffic circles and roundabouts offer substantial improvements in intersection capacity and efficiency, along with notable reductions in the severity of collisions [91–93]. Moreover, their ability to promote smoother traffic flow patterns often results in decreased fuel consumption and lower vehicle emissions. This can be attributed to the minimized idling and acceleration-deceleration cycles inherent in circular intersections, which contribute to overall environmental sustainability and air quality improvement efforts [94].

A noticeable increase in throughput and a decrease in traffic emissions can be observed when circular junctions are equipped with traffic lights [95]. This integration optimizes intersection operations by combining the efficiency of circular intersections with the control mechanisms provided by traffic lights. Therefore, this thesis will delve deeply into the investigation of circular intersections, exploring their design, functionality, and impact on traffic management and environmental sustainability.

1.9 Monte Carlo Simulation

In the field of transportation systems, particularly, digital simulation is a crucial tool for studying and understanding complex phenomena such as traffic. With this powerful instrument, researchers can explore the complexities of urban mobility and traffic flow, leading to valuable discoveries. The process involves using computer software to mathematically model transportation systems in accordance with accepted traffic simulation best practices.

In traffic systems, simulation is the process of using complex computer models that change over time to create dynamic representations of real-world situations. By replicating the behavior of vehicles, pedestrians, and infrastructure, researchers can investigate different scenarios, evaluate the effects of actions, and enhance system performance. This method improves our understanding of traffic dynamics and provides useful information for developing and implementing efficient transportation laws and infrastructure upgrades.

The Monte Carlo simulation method, introduced by Metropolis and Ulam in 1949 [96], is a powerful tool extensively used in numerical simulation for analyzing stochastic systems. This method involves generating random samples to approximate solutions to complex mathematical and physical problems. The term "Monte Carlo" originates from the well-known city of Monte Carlo in Monaco, famous for its casino culture. In Monte Carlo simulation, random variables are repeatedly sampled to model uncertainty and variability within a system, enabling researchers and engineers to explore a wide range of potential outcomes and assess the likelihood of different scenarios occurring.

Monte Carlo simulation is particularly well-suited for situations where deterministic approaches are impractical or infeasible due to the presence of stochastic elements [97, 98]. By simulating random quantities and running numerous iterations, this method provides a comprehensive understanding of the behavior of systems under uncertainty. It allows for the evaluation of probabilistic outcomes, the assessment of risk factors, and the optimization of decision-making processes in various fields such as finance, engineering, physics, and more.

Analytical approaches to cellular automata present challenges due to their discrete nature and parallel update system, leading to non-locality in dynamics. These models rely on dynamic rules with transition probabilities rather than a "Hamiltonian" and do

not conform to detailed balance conditions, making conventional methods unsuitable for analysis. The complexity of cellular automata analysis arises from their unique characteristics, requiring specialized analytical techniques to understand their behavior accurately.

We provide a brief introduction to simulating the NaSch model using the Monte Carlo method for parallel updating and incorporating periodic boundary conditions. The Monte Carlo method, widely used in simulations, consists of two main phases: the transient state and the steady state.

Transient State: This initial phase involves running the system for a designated period, denoted as T_{Cal}, without sampling the system's dynamic properties. This allows the system to stabilize and reach a steady state without interruptions from measurements or observations.

Steady State: Once the system has reached stability, it enters the steady state. Here, certain properties of the system remain constant over time (usually denoted as T_{Cal}). During this phase, the simulation focuses on observing and analyzing the system's behavior under stable conditions. The simulation concludes when it reaches the maximum time limit, denoted as T_{Max} (typically $t > T_{\mathrm{Max}}$), or when specific termination conditions are met.

In the context of cellular automata models, the Monte Carlo method involves implementing these steps to accurately simulate and study the behavior of the system over time. These procedures can be succinctly summarized as follows:

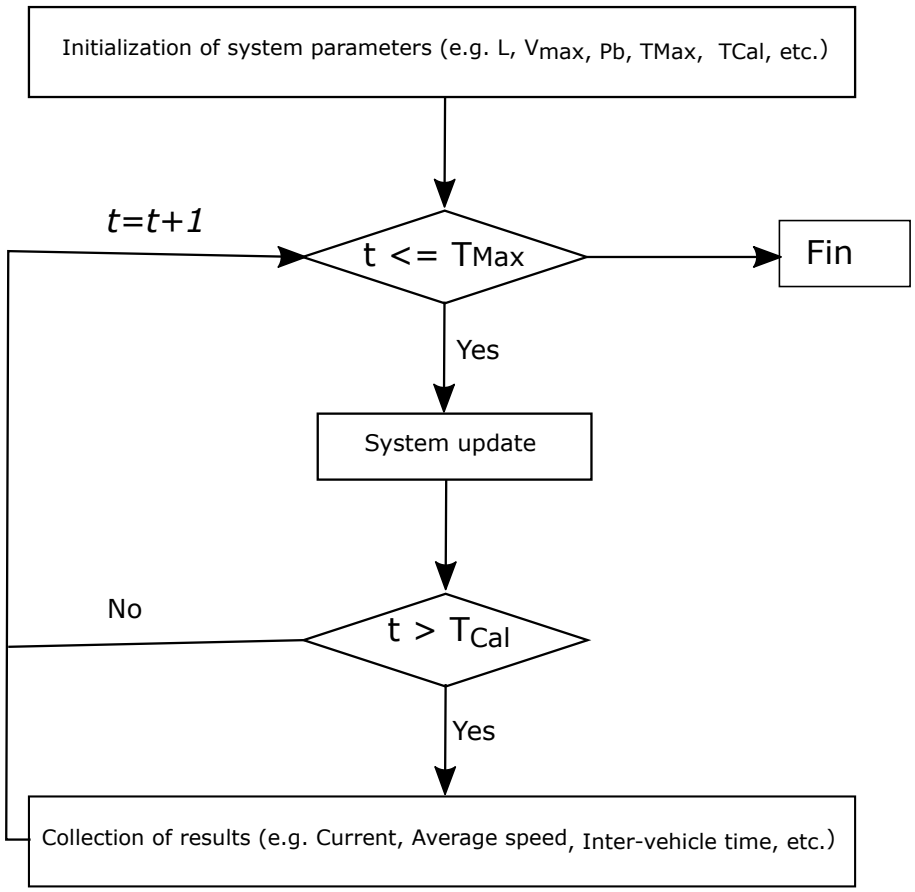

Figure 1.18: Flowchart of the Monte Carlo simulation for the NaSch model.

1.10 Conclusion

In this chapter, we presented an overview of the history of road traffic, emphasized the significant research in this field, and discussed the various empirical results, such as inter-vehicular time and space, the fundamental empirical diagram, and the phantom traffic jam. These results are replicated by theoretical models. We defined the different traffic flow observables and models, including macroscopic, mesoscopic, and microscopic models, to represent the dynamics of traffic flow. These models are categorized into two approaches: the fundamental diagram and the three-phase theory.

We conducted an in-depth analysis of various types of road infrastructure, such as highways, intersections, traffic circles, and roundabouts, to assess their efficiency, impact on traffic flow, and safety measures. The goal was to offer guidance for strategic decision-making to improve roadway efficiency and safety standards. This thesis will investigate the effect of circular intersections on traffic management and environmental sustainability using the cellular automata model, which can be adapted to include various factors as required. Additionally, computer simulations provide considerable flexibility in this respect.

Chapter 2

Investigating the Impact of Vehicle Behavior on Roundabout Performance: A Simulation Study of Full-Turn Maneuvers and Safe Gap Adherence

2.1 Introduction

The efficiency of intersections is vital for smooth traffic flow in cities. However, these nodal points often become congested due to issues like traffic lights and vehicle-pedestrian interference. Addressing these challenges is essential to improve intersection functionality. Circular intersections, such as roundabouts, play a significant role in managing these difficulties. Roundabouts are increasingly adopted as a type of intersection design due to their ability to enhance both safety and traffic throughput. Vehicles navigate around a central island, yielding to those already inside. This design encourages smoother traffic flow and reduces the incidence of high-speed collisions by prompting vehicles to slow down upon entry. The continuous flow of traffic minimizes delays and improves fuel efficiency [90].

Research conducted in the United States provides evidence for the effectiveness of this design, as it shows a notable decrease in accidents after the implementation of roundabouts [99]. The complex relationships between roundabout traffic systems have been the subject of numerous studies to identify potential issues and areas for improvement. This range of research shows that several factors, such as traffic volume fluctuations [100], pedestrian movements [101], and driving behavior [102, 103], are considered when assessing a roundabout's effectiveness. However, there seems to be a lack of research on the precise effects of the percentage of vehicles that complete a turn in a roundabout system and how this feature relates to the overall traffic flow and phase dynamics.

This chapter addresses a gap in the literature by examining the intricate connections between full-turn maneuvers and various metrics that reflect traffic flow and roundabout capacity. Our study explores the impacts of continuous vehicle circulation within the roundabout, specifically focusing on the energy dissipation patterns that result from this dynamic. The energy dissipation metric is crucial to our research because it provides important information about vehicle interactions within the roundabout by capturing the quadratic variances between initial and final vehicle speeds. Furthermore, we broaden the scope of our study to assess environmental effects, concentrating on the CO_2 emissions brought about by various vehicle behaviors at roundabout intersections. We also investigate how conflicts arising from vehicles in the entry lane not adhering to safe gaps in the circulating lane affect the roundabout's capacity. By adopting this comprehensive approach, our goal is to clarify the complex dynamics of roundabout traffic systems, thereby contributing to a deeper understanding of this field of study. To improve the

functionality of roundabout systems, we suggest introducing traffic lights to minimize vehicle interactions.

2.2 Model Development and Simulation

2.2.1 Motion rules

A single-lane roundabout system that we investigate consists of four entry and exit lanes connected to a central circular lane. We use periodic boundary conditions on the circular lane and open boundary conditions on the entry and exit lanes to simplify this. There are two types of sites in the spatial layout: L_1 sites are located in the circulation lane, and L_2 sites are located in the entry and exit lanes. A vehicle is defined by its position and speed at each time step. In accordance with the principles of the NaSch model, which are detailed in chapter 1, updates to vehicle positions and speeds are carried out simultaneously [16]. Vehicles travel in a counterclockwise direction around the circulating lane. At any given moment, a site may be vacant or occupied by a single vehicle. Each vehicle's speed can be represented by an integer value ranging from zero to its maximum speed.

2.2.2 Entry/exit rules

In the roundabout system, vehicles already present in the circulating lane have the right of way. This prioritization of oncoming vehicles reduces the probability of collisions between vehicles entering the roundabout (incoming vehicles) and those already in the circulating lane. As a result, incoming vehicles must slow down and assess the number of empty spaces separating them from the next vehicle in the circulating lane (designated as g_1 in Figure 2.1):

- If $g_1 \geq V_0 + 1$: the incoming vehicle can enter the circulating with speed $V_{\text{inc}} = \max(V_{\max}, V_{\text{inc}} + 1)$. In this case, V_{inc} and V_0 designate the speed of the incoming and oncoming vehicles, respectively.
- Otherwise, the vehicle cannot enter the circulating lane unless the oncoming vehicle uses the indicator when it approaches its required exit direction.

Meanwhile, the oncoming vehicle can exit the circulating lane to reach its intended destination (i.e., choosing one of the available exit lanes) if the following conditions are satisfied:

- In our model, the first site (exit point) of the exit lane must be vacant, as accumulation is not allowed.
- If the distance (g_3) between the oncoming vehicle and its intended exit cell is less than its current speed (V_0) (see Figure 2.1).

Otherwise, if the conditions are not satisfied, the vehicle must slow down and wait in the exit cell until the exit point is free.

2.2.3 The boundaries rules

The roundabout system allows vehicles to enter and exit based on the expanded open boundary conditions. A mini-system, with a width of $V_{max} + 1$, is connected in series with the left side of the entry lanes. The insertion of vehicles into the mini-system is governed by the following rules:

- If the mini-system is not empty, the vehicle must be removed from the mini-system before a new vehicle can be inserted with probability α and a maximum speed of $V_{\max}$. The distance between the vehicle in the mini-system and the one in the entrance lane must always be at least equal to $V_{\max}$.
- If the mini-system is empty, a vehicle is inserted with probability α and initial speed $V_{\max}$ in its first cell.

It is essential to remember that each vehicle's exit lane is assigned at the moment it enters the circulation lane and does not change. Moreover, this model accounts for a subset of vehicles that can circle the central island multiple times before choosing an exit lane.

Vehicles exit the system through the exit lanes, where a additional cell is placed at the end of the lane. If the vehicle's position exceeds the length of the exit lane (L_2), it will be removed with probability β. Otherwise, the vehicle will stop with probability $1 - \beta$ at the final exit lane cell for removal.

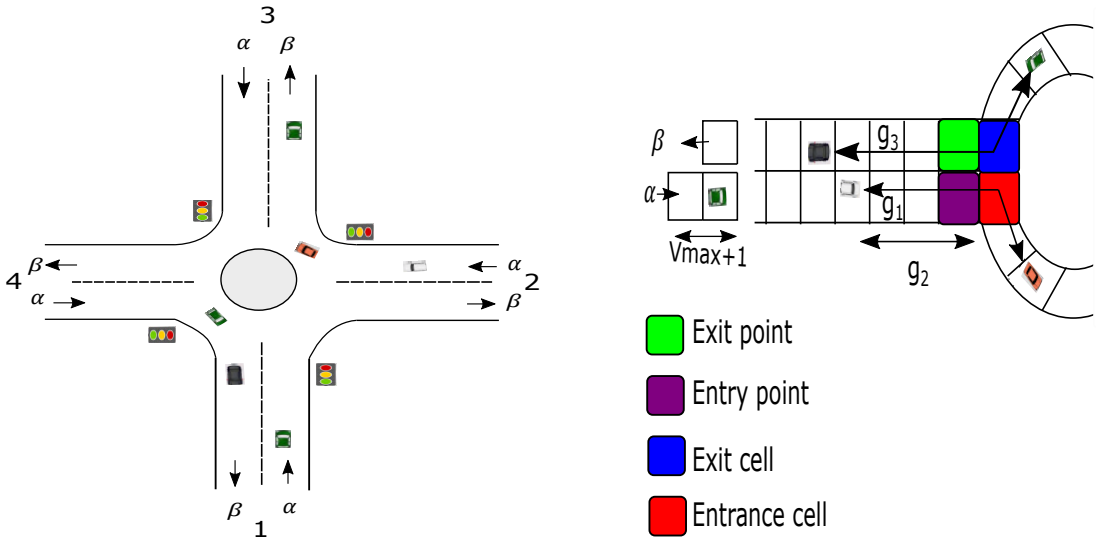

Figure 2.1: (a) Sketch of the traffic circle system, (b) Regulations for entry and exit.

2.2.4 Traffic light control

Traffic lights regulate the flow of vehicles entering the roundabout system from the entry lanes. These traffic lights are positioned at the entry lanes (refer to Figure 2.1). The lights switch periodically between green, with a duration of $(t_g \times T)$, and red, with a duration of $(1 - t_g) \times T$. The cycle time T, which encompasses both light phases, is represented here. The ratio of the green signal time (t_g) to the cycle time T is indicated. The signals operate in synchronization, so vehicles traveling in opposite directions will see the same light. Entry/exit lanes 1 and 3 have a green light, while entry/exit lanes 2 and 4 have a red light [95].

2.2.5 Simulation Parameters

Table 2.1 provides the parameters used in our numerical simulation. Furthermore, in this study, we analyzed the emissions of the pollutant carbon dioxide (CO_2). It was assumed that all vehicles in the simulation were fueled by petrol.

Table 2.1: Parameters of the model used in the simulation

Parameter	Symbol	Value
Size of the circulating lane	L_1	40
Size of the entry/exit lanes	L_2	100
NaSch braking probability	P	0
Maximum permissible speed	$v_{\max}$	2
Maximum Time Limit of Monte Carlo	T_{Max}	30 000
Calibration Time of Monte Carlo	T_{Cal}	10 000
Number of Independent Runs	T	100

2.3 Effects of Full-Turn Maneuvers on Roundabout Traffic Dynamics

2.3.1 Impact of vehicles making U-turns

In this section, we analyzed the impact of U-turns on traffic flow in all essential lanes of the roundabout: the entry, exit, and circulating lanes. First, we plotted a phase diagram, considering both scenarios where vehicles make complete U-turns in the circulating lane and instances where they do not. When there were no full-turn vehicles, each vehicle's position was determined relative to an exit and assigned a destination according to an equal probability distribution. This made it possible to choose each vehicle's destination in an orderly manner (see Figure 2.1 for a more detailed example).

Three distinct phases emerged in the traffic pattern of the roundabout, which we identified from Figure 2.2: Free Flow, Congestion, and Maximum Current. We observe a free flow phase when vehicles proceed at their desired speeds with minimal disruptions in cases where α is less than β. In contrast, the system enters a congestion phase when α exceeds β, resulting in a significant decrease in vehicle speeds due to increased movement constraints. Additionally, we found a maximum current phase, indicating a steady flow, where traffic current is independent of the α and β.

When we consider the actions of vehicles making complete U-turns, which account for 40% of the traffic, the dynamics shift significantly. Figure 2.2 illustrates how the maximum current phase expands, showing a wider range of steady traffic situations, while the free flow and congested phases diminish. Furthermore, a jammed phase that is visible in all of the roundabout's lanes is introduced with this inclusion. Interestingly, compared to the entry and exit lanes, the circulating lane has a larger free-flow phase. This phenomenon can be explained by the fact that vehicles making U-turns in the circulating lane create more opportunities for free-flowing traffic, resulting in a wider free-flow window.

To analyze the effect of vehicles making U-turns in the roundabout, we will examine how the lane capacity, or the maximum current in the lane, varies with the percentage of vehicles making U-turns in the three lanes. As shown in Figure 2.3, the capacity of

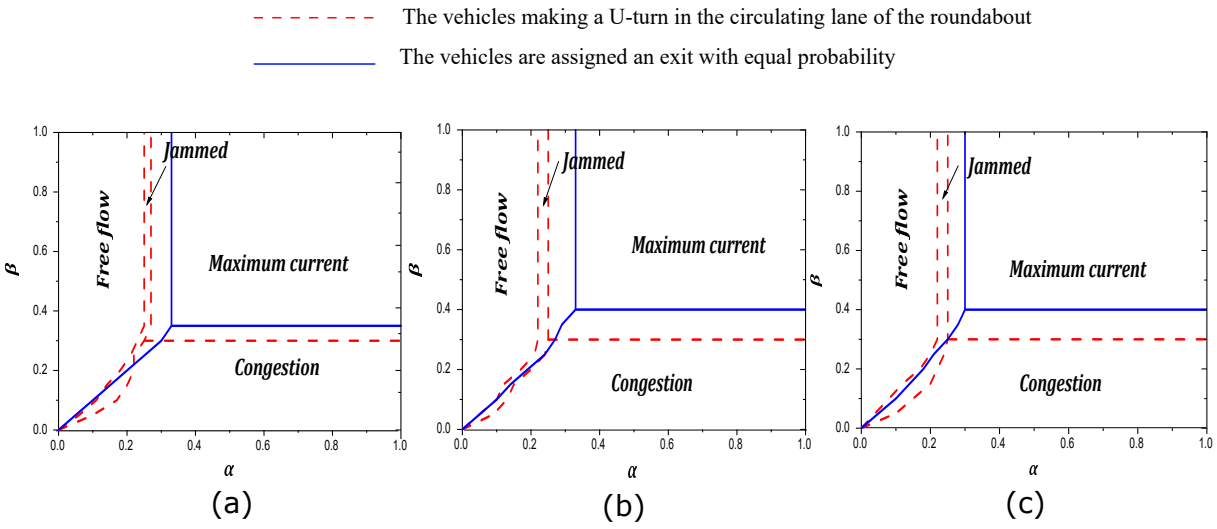

Figure 2.2: Phase diagram in the (α, β) plane for three lanes: (a) circulating, (b) entry, and (c) exit, both with and without the impact of vehicles turning completely inside the circulation lane.

the circulating lane slightly increases as a greater proportion of vehicles perform U-turns, while the capacity of the entry and exit lanes steadily decreases. The presence of U-turning vehicles reduces incoming traffic from the other entry lanes, thereby increasing the maximum current in the circulation lane and resulting in a slight improvement in capacity. The entry and exit lanes' capacity also exhibit similar patterns. This is because as the percentage of vehicles that complete full turns in the circulation lane increases, the number of vehicles in the exit lane decreases, and the line of stationary vehicles in the entry lane grows, which in turn lowers the capacity of both the entry and exit lanes.

To better understand how deceleration affects vehicle speed and the impact of U-turns in the roundabout's circulating lane, we examined the energy dissipation that occurs during this process. Figure 2.4 shows the energy dissipation as a function of the rates of injection (α) and extraction (β), including scenarios where vehicles make a full U-turn in the circulating lane.

In the circulating lane (Figure 2.4 (a)), there is less energy dissipation in both the free-flow ($\alpha < \beta$) and the congestion ($\alpha > \beta$) phases. This is due to the uniform speed that vehicles maintain during the free-flow phase and the near-standstill conditions in the extreme jam phase. However, as both α and β increase, we observe a gradual increase in energy dissipation, culminating in a plateau region where the peak energy dissipation reaches $E_d/m = 0.4$.

Figure 2.4 (b) illustrates a similar pattern in the entry lane, but the peak energy dissipation is significantly lower at $E_d/m = 0.15$. In the exit lane (Figure 2.4 (c)), the absence of the plateau region is due to the exclusion probability β, which causes a queue to form close to the final cell of the exit lane, where the maximum energy dissipation is lowered to $E_d/m = 0.10$.

The addition of U-turning vehicles to the system results in significant differences in energy dissipation between lanes, as shown in Figure 2.4 (d-f). The energy in the circulation lane is roughly constant at $E_d/m = 0.4$, but there is a significant decrease in the entry ($E_d/m = 0.10$) and exit ($E_d/m = 0.06$) lanes. This phenomenon can be explained by the high number of U-turning vehicles in the roundabout's circulating lane, which naturally

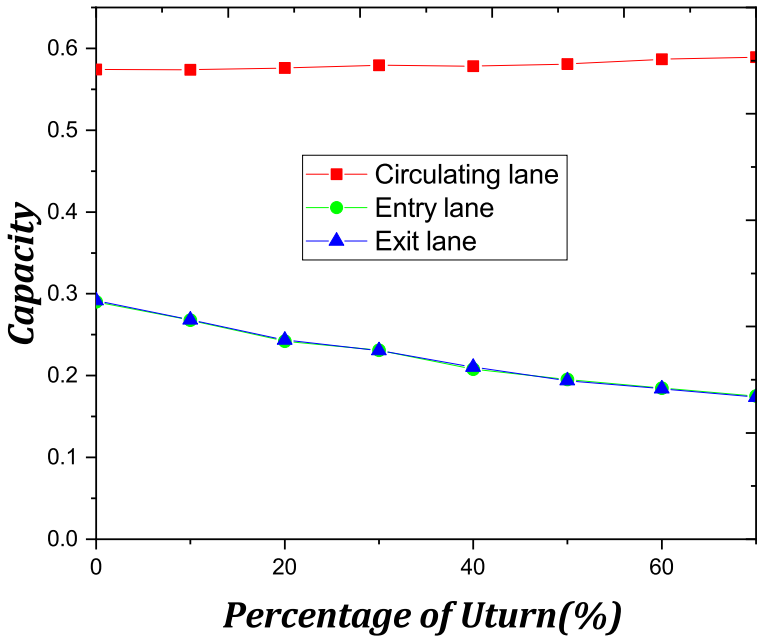

Figure 2.3: Capacity as a function of the proportion of turning vehicles, for the circulating lane and entry/exit lanes.

reduces the number of vehicles entering this lane. This, in turn, reduces the number of vehicles leaving the lane and, ultimately, the total amount of energy dissipated in both entry and exit lanes.

After analyzing energy dissipation, we now focus on the environmental implications, specifically concerning CO_2 emissions of carbon dioxide. Figure 2.5 shows the peak CO_2 emissions as a function of the percentage of vehicles executing U-turns in the three lanes for all combinations of α and β. As the percentage of vehicles doing U-turns in the circulating lane rises, we observe a slight increase in the maximum CO_2 emissions. This pattern can be attributed to the fact that the circulating lane is saturated with U-turning vehicles, which naturally reduces the number of vehicles entering this lane and consequently affects CO_2 emissions. When the circulating lane receives less traffic than the entering lane, lines form in the entry lanes, which raises CO_2 emissions. Regarding the exit lane, there is a decrease in CO_2 emissions as a result of a decrease in outflow as the number of vehicles making U-turns increases the journey of those vehicles in the circulating lane.

2.3.2 Impact of Directionless Vehicle Inflow in Circulation Lane

In this subsection, we analyze the impact on roundabout traffic flow of the rate of entering vehicles without a specific direction, or vehicles that continuously turn in the circulation lane. The fixed probability of selecting the closest exit point to depart the circulation lane is $P_{\text{exit}} = 0.01$. We have plotted a phase diagram, as shown in Figure 2.6, considering both scenarios with and without vehicles that continuously turn in the circulation lane. In the first part of the study, we examine the case where the vehicles are assigned an exit with equal probability. The results show that an increase in the proportion of vehicles that keep

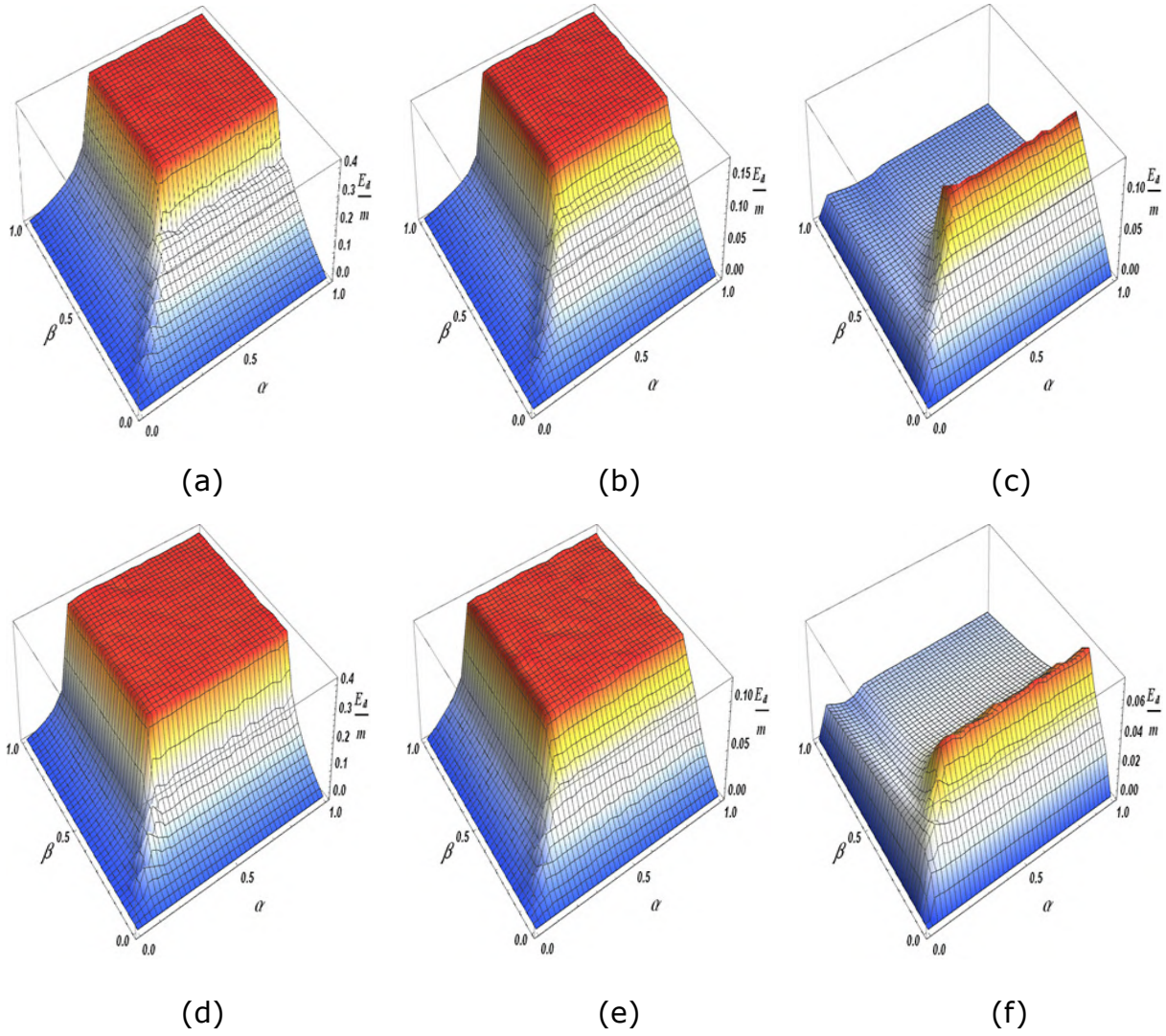

Figure 2.4: Energy dissipation as a function of the rates of injection α and extraction β: (a) Circulating Lane, (b) Entry Lane, and (c) Exit Lane—all without the effect of vehicles turning completely in the circulation lane. (d) Circulating Lane, (e) Entry Lane, and (f) Exit Lane - with the impact of vehicles making a complete turn in the circulation lane.

turning in the circulation lane leads to a decrease in the free flow and congestion phases, and an expansion of the maximum current phase in the three lanes of the roundabout system.

To further investigate the effects of these types of vehicles, Figure 2.7 displays the capacity as a function of different percentages of vehicles without a designated direction by illustrating the traffic peaks in the three lanes. The circulating lane has a higher capacity, mainly because vehicles continue to circulate around the central island of the roundabout in this lane. As a result of this saturation, the entry and exit lanes experience a reduction in their capacity, which also lowers the probability for vehicles in the entry lanes to find a safe gap to merge into the circulation lane. The capacity of entry lanes capacity decreases due to an increase in the queue of stopped vehicles. A decline in the number of vehicles exiting the circulating lane leads to a decrease in exit lanes' capacity.

As shown, vehicles that continuously turn can impact traffic flow in all lanes, thereby

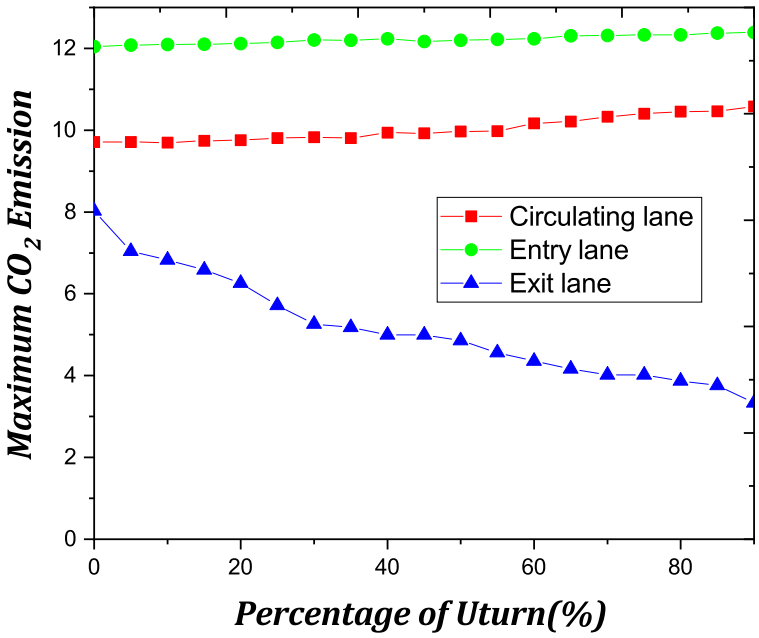

Figure 2.5: Maximum CO_2 emissions as a function of the percentage of vehicles making a U-turn. For the three lanes of the roundabout(circulating, entry and exit lanes.

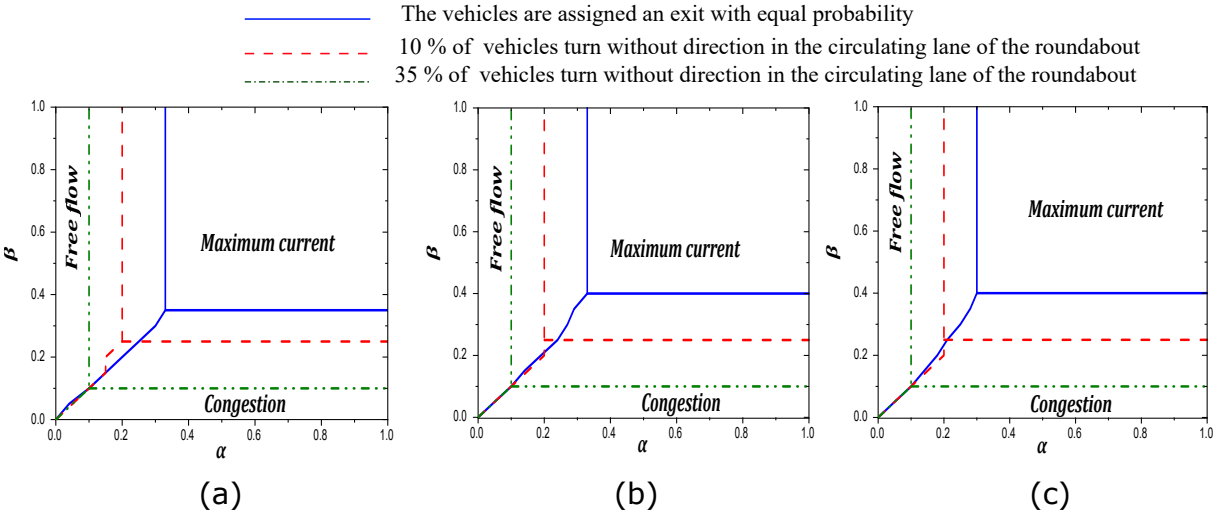

Figure 2.6: Phase diagram for different percentages of vehicles turning in the roundabout's circulation lane without a specific direction, in the (α, β) plane. For three lanes: (a) circulating, (b) entry, and (c) exit.

affecting vehicle speed. The energy dissipation resulting from vehicle deceleration is a valuable metric for analyzing heterogeneity in vehicle speeds. Figure 2.8 presents the dissipation energy as a function of injection rate α and extraction rate β for various percentages of vehicles that continue turning in the circulating lane of the roundabout.

Initially, we consider 10% of the vehicles that continue to turn in the circulating lane.

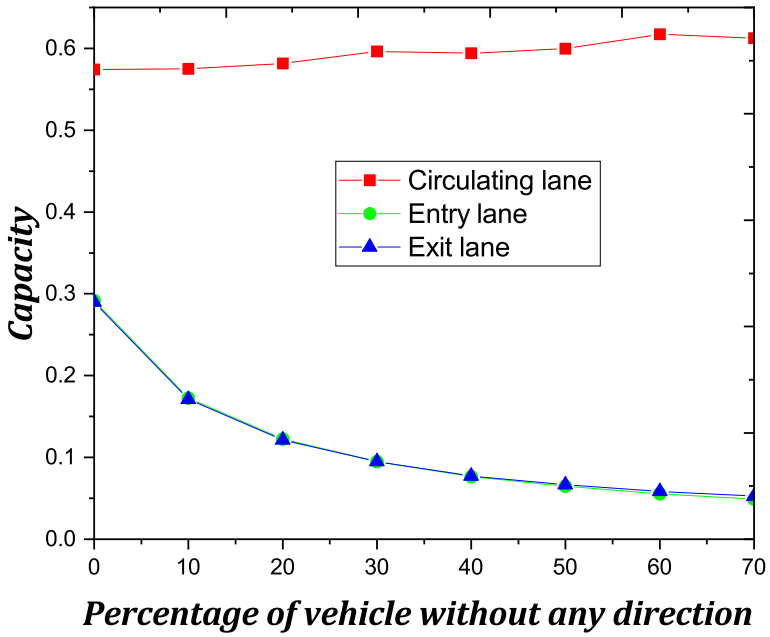

Figure 2.7: Capacity as a function of the percentage of vehicles that keep turning in the circulating lane. For circulating lane and entry/exit lanes.

A decrease in dissipated energy is observed for the entirely free-flow phase ($\alpha < \beta$) in the circulating lane (see Figure 2.8 (a)). During the congestion phase ($\alpha > \beta$), the system experiences a decrease in energy dissipation due to an increase in the number of stopped cars. Minimal energy dissipation is observed in situations where traffic is either highly congested or moving freely. The energy dissipation measure can be useful in determining whether local interactions are present. Specifically, free-flowing traffic arises when there is an increase in available space, while global congestion occurs when there is a significant decrease in the space between vehicles. Between these phases, a mix of moving and stopped vehicles in the traffic flow leads to increased energy dissipation. In this scenario, the plateau results from saturation, which occurs when energy dissipation becomes independent of variations in α and β. The peak of the energy dissipation seen in the circulating lane is $E_d/m = 0.4$.

As shown in Figure 2.8 (b), the entry lane exhibits a lower maximum dissipated energy of $E_{dmax}/m = 0.08$. This can be attributed to the lane's progressively growing queue of stopped vehicles. The maximum dissipated energy for the exit lane (as seen in Figure 2.8 (c)) is $E_{dmax}/m = 0.08$ when ($\alpha > \beta$). Traffic conditions in the exit lane improve as the extraction rate β increases, due to the decrease in dissipation energy.

To gain a clearer understanding of the effect of vehicles that continue to circulate within the lane on energy dissipation, we increased the percentage of these vehicles to 35%. The circulating lanes depicted in Figure 2.8 (a) and Figure 2.8 (d) both exhibit nearly identical patterns and attain the same maximum value of dissipated energy. However, compared to Figure 2.8 (a), the plateau region in Figure 2.8 (d) representing the maximum of the dissipated energy is larger. This occurs when more vehicles are persistently traveling around the island of the roundabout, which reduces the circulating lane's flow dependence

on α and β, thereby expanding the plateau region. Traffic conditions can change for the better or worse as one approaches the boundaries between distinct traffic phases. In particular, traffic conditions improve as one gets closer to the barrier that separates the maximum current from the free-flow phase, which lowers energy dissipation. On the other hand, when the boundary between the maximum current and the congestion phase approaches, traffic conditions worsen and there is a discernible decrease in energy dissipation. In the case of the entry lanes, the constant stream of vehicles causes the vehicle speed to drop, which in turn reduces energy dissipation. As can be seen in Figures 2.8 (b) and (e) above, the peak energy dissipation changes from $E_d/m = 0.08$ to $E_d/m = 0.04$ in this instance. As for the exit lanes, fewer vehicles leave the circulating lane as the percentage of consistently circulating vehicles rises to 35%. Consequently, the maximum energy dissipation in the exit lane shown in Figure 2.8 (f) is lower than that in Figure 2.8 (c).

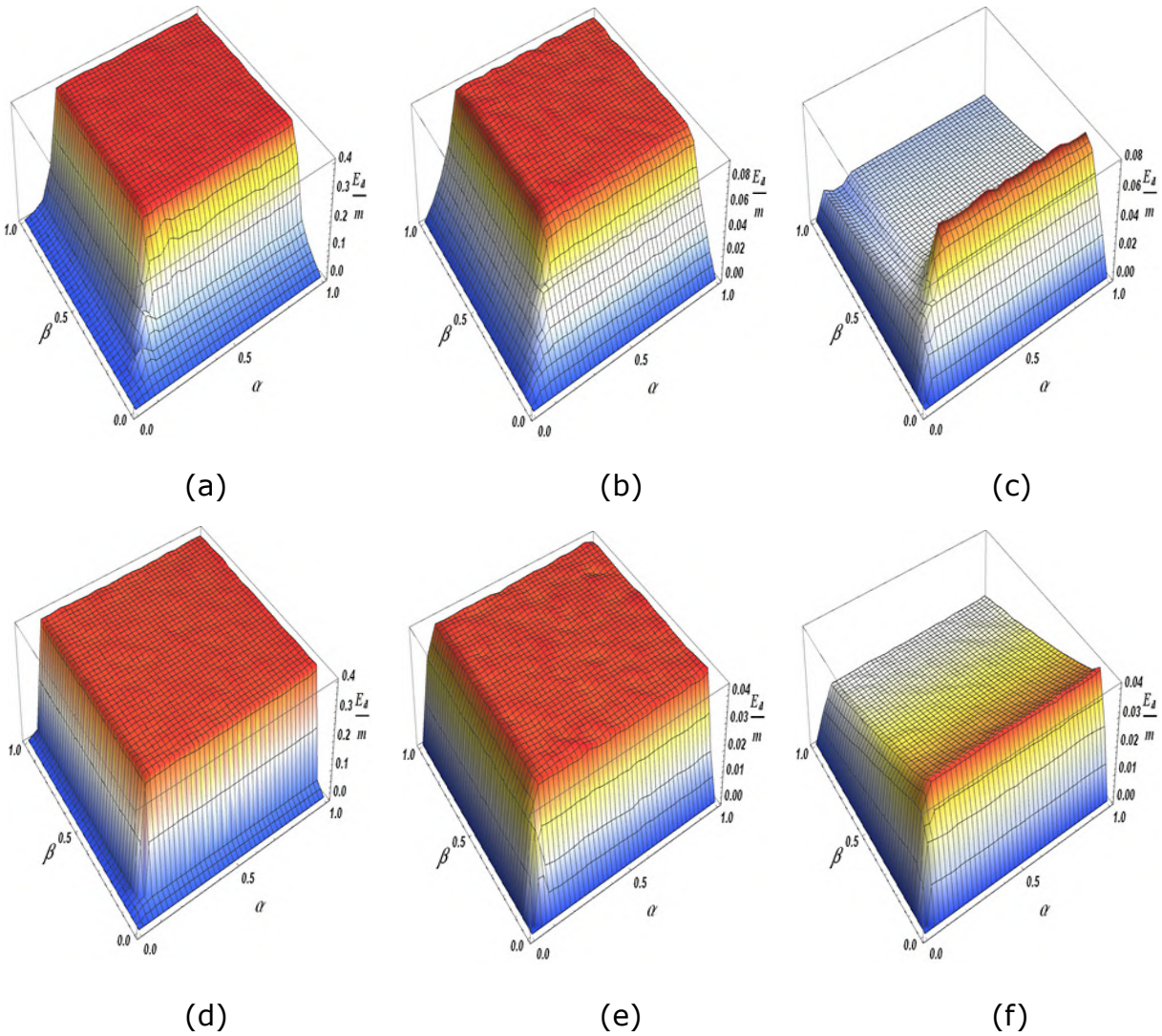

Figure 2.8: Energy dissipation with 10% of vehicles continuing to turn in the circulation lane as a function of injection α and extraction β rates. (a) Entry lane, (b) exit lane, and (c) circulating lane. In an additional instance, 35% of vehicles keep turning in the circulation lane. (d) Entry lane, (e) circulating lane, and (f) exit lane.

Subsequently, we presented the relationship between the percentage of directionless vehicles and the maximum CO_2 emissions. It can be observed that even with an increase in the percentage of vehicles that are continuously circulating, the maximum CO_2 emissions remain constant in Figure 2.9. This stability can be attributed to the majority of the vehicles in the circulating lane traveling at higher speeds, with the entry point being the origin of the speed heterogeneity. The situation differs concerning the entry lanes. First, the increase in the proportion of vehicles that continue to drive in the circulating lane amplifies the speed heterogeneities in that lane, which in turn increases CO_2 emissions. However, as the number of vehicles in continuous circulation rises, CO_2 emissions decrease. This reduction is a result of consistent queues of stopped vehicles that minimize acceleration and deceleration events; in other words, most vehicles are essentially stationary, which significantly lowers CO_2 emissions. For the exit lanes, as the proportion of consistently circulating vehicles in this lane increases, fewer vehicles are leaving from the circulating lane. This change improves traffic flow efficiency in the exit lanes, thereby reducing CO_2 emissions.

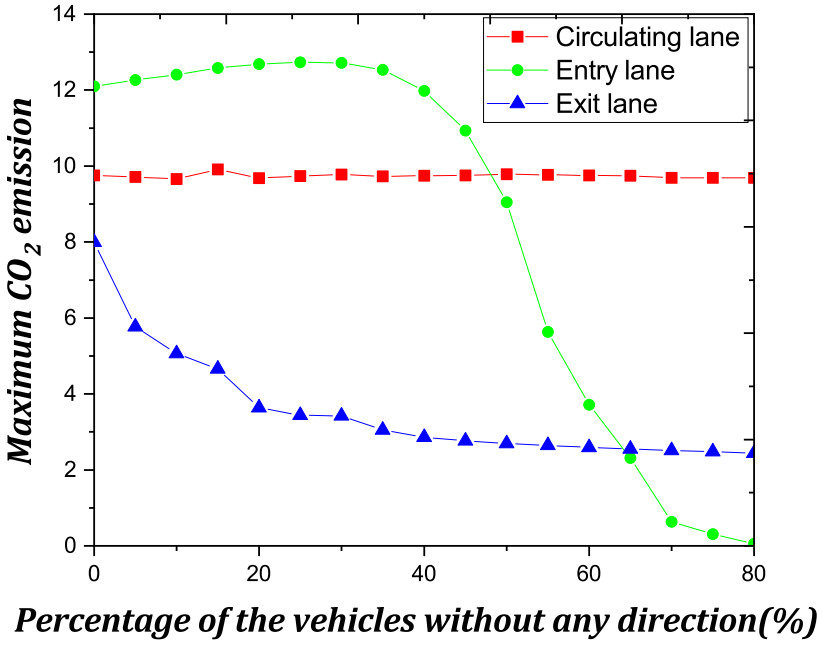

Figure 2.9: Maximum CO_2 emission as a function of the percentage of the vehicles that keep turning in the circulating lane. For the three lanes of the roundabout (circulating, entry, and exit lanes.

2.4 Effects of Adhering to Safe Gaps on Roundabout Traffic Dynamics

2.4.1 Traffic patterns in a roundabout system

In this section, we will study the flow characteristics in the roundabout system without traffic lights at the entry lanes. We will consider a scenario where the probability of a vehicle entering the circulating lane without considering the safety gap P_{sg} is set to 0. Figure 2.10 (a), (b), and (c) show the current in the circulating, the entry, and the exit lanes, respectively, as a function of the rates α (injection) and β (extraction).

In the three lanes of the roundabout system (the circulating, entry, and exit lanes), three phases are observed: free-flow, jammed, and maximum current. During the free-flow phase, each vehicle moves at its desired speed, and the current J depends on α. In the jammed phase, vehicles are compelled to slow down, and J depends on β. Consequently, the system reaches the maximum current phase, where J becomes independent of both α and β.

The boundaries of each phase are determined by the phase diagram depicted in Figure 2.10 (d), (e), and (f). In the phase diagram of the roundabout, three distinct phases are evident across its three lanes: Free flow, Jammed, and Maximum current. For α values less than or equal to 0.33 in both the circulating and entry lanes, and for α values less than or equal to 0.3 in the exit lane, traffic flows freely, with the current J being directly proportional to α. When β is less than or equal to 0.35 in the circulating lane, and when β is less than or equal to 0.4 in both the entry and exit lanes, the Jammed phase is encountered, characterized by a dependence of the current J on β. In the Maximum current phase, J becomes independent of both α and β.

To gain a better understanding of the microscopic interactions between vehicles, we plotted the space-time diagrams of the circulating, entry, and exit lanes in Figure 2.11. In the free-flow phase ($\alpha = 0.1$, $\beta = 0.6$), the space-time diagrams predominantly display white, representing free space, in all three lanes of the roundabout. However, the circulating lane appears slightly denser than the entry and exit lanes due to traffic entering from the four entry lanes. During this phase, vehicles freely enter and exit the circulating lane.

In the jammed phase ($\alpha = 0.6$, $\beta = 0.1$), the space-time diagrams are predominantly black, indicating the presence of jams in all three lanes. Jams occur in the entry lanes due to the roundabout's priority rules favoring oncoming vehicles, as well as the high injection probability α. Additionally, a queue of stationary vehicles forms at the end of the exit lane due to the low extraction rate β, which adversely affects traffic flow in the circulating lane.

In the maximum current phase ($\alpha = 0.6$, $\beta = 0.6$), jams persist in the entry lane because incoming vehicles are compelled to wait until finding a sufficient gap to enter the circulating lane of the roundabout. Meanwhile, traffic in the exit and circulating lanes improves due to the high extraction rate β.

Many drivers do not strictly adhere to traffic laws and exhibit unpredictable behavior while driving, making it challenging to understand the dynamics of traffic flow. In our research, we are particularly interested in the fluctuation of lane capacity within a roundabout, which is the maximum flow rate achieved in the lane. We aim to determine how the percentage of vehicles that disregard safety gaps when merging into the circulating lane affects the capacity of each lane. The distance between vehicles that allows for safe merging and maneuvering is known as a safety gap.

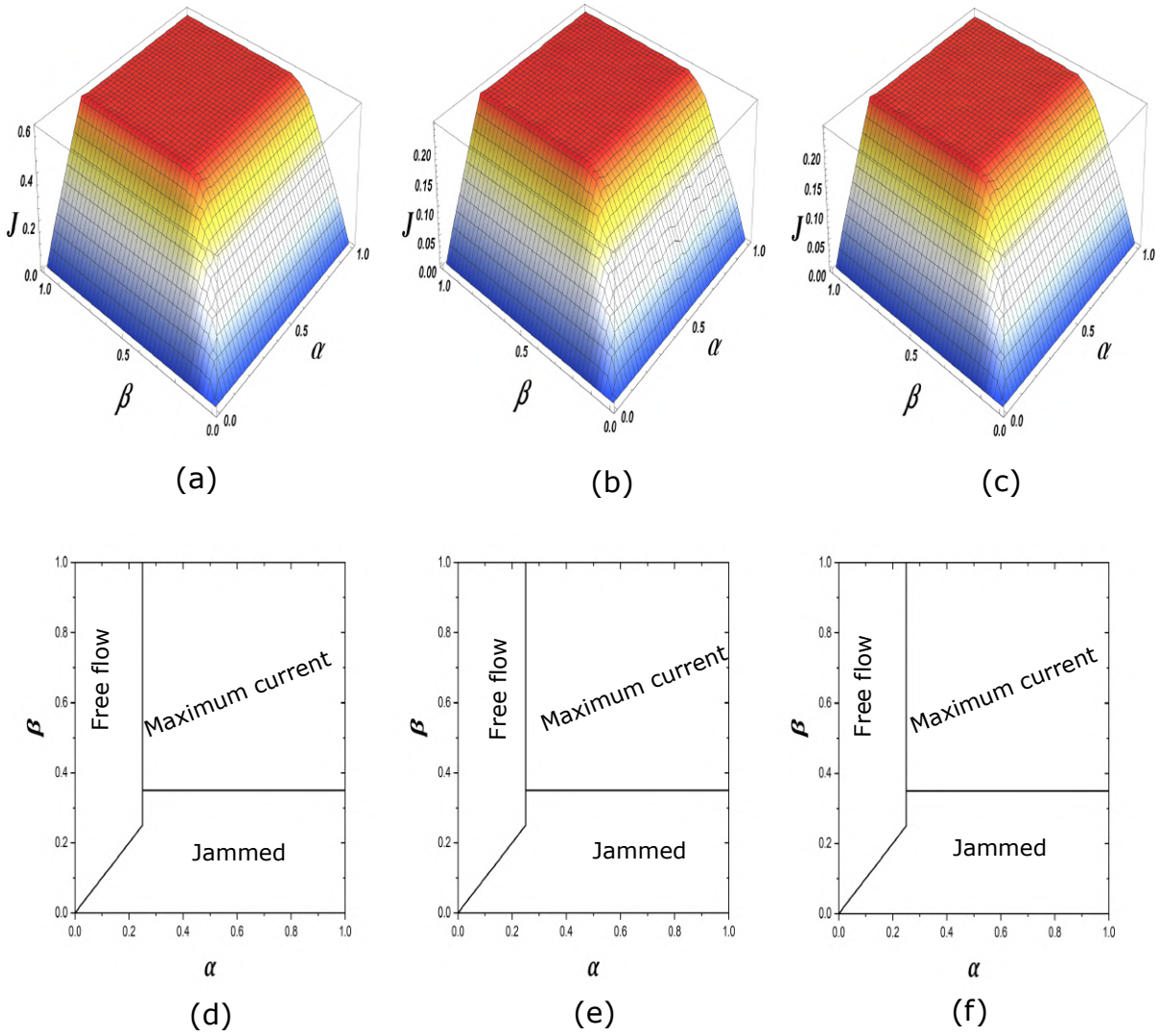

Figure 2.10: Current as a function of injection α and extraction β rates for the following lanes: (a) Circulating lane; (b) Entry lane; and (c) Exit lane. Phase diagram for (d) the circulating lane, (e) the entry lane, and (f) the exit lane in the (α,β) plane.

The results, shown in Figure 2.12, indicate that the capacity of the three lanes in the roundabout decreases as the probability P_{sg} increases. This probability represents the probability of vehicles not adhering to safety gap regulations when entering or exiting the roundabout. These violations disrupt traffic flow, leading to a gradual decrease in the entry and exit lanes' capacity and a more rapid decrease in the roundabout's circulating lane. Additionally, the capacity of the roundabout's circulating lane exceeds that of the entry and exit lanes because vehicles in the circulating lane are already in motion within the roundabout, allowing for a higher volume of traffic to pass through. In contrast, the entry and exit lanes involve vehicles entering and exiting the roundabout, which can disrupt traffic flow and reduce overall capacity. Moreover, the entry and exit lanes' capacity exhibits a similar pattern because they are both affected by the same probability of drivers disregarding safety gap regulations when entering the roundabout. Furthermore, the entry and exit lanes have similar traffic flow patterns as vehicles enter and exit the roundabout. Drivers who disregard the safety gap when entering the roundabout adversely impact

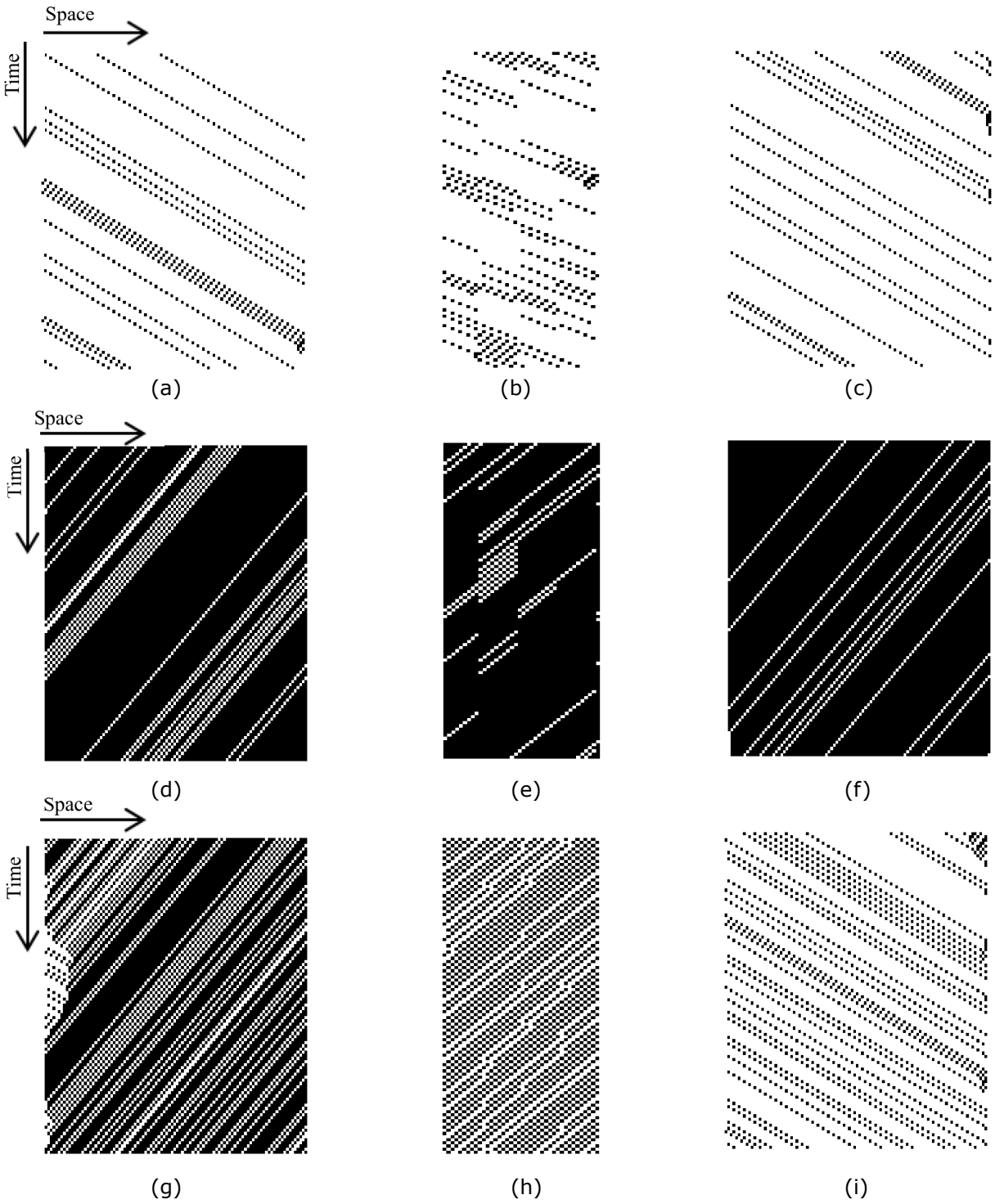

Figure 2.11: Space-time plots for the roundabout. For circulating lane ((b),(e),(h)) For entry lane ((a), (d),(g)). For exit lane ((c), (f), (i)). Black corresponds to vehicles while free space is presented in white.

its performance. To enhance traffic conditions within the roundabout system, we will explore the impact of traffic lights on the throughput of the roundabout in the subsequent subsection.

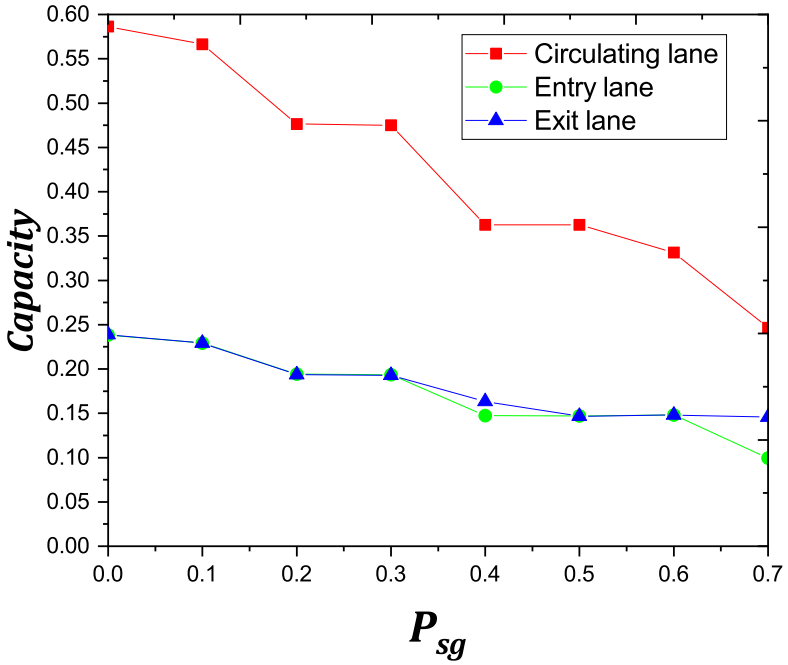

Figure 2.12: Capacity as a function of the percentage of vehicles that do not respect the safety gap to enter the circulating lane. For the three lanes of the roundabout (circulating, entry, exit lanes.

2.4.2 Roundabout system with traffic lights

In this section, we investigate the impact of traffic lights on the throughput of the roundabout system, considering the probability of vehicles entering the circulating lane of the roundabout without adhering to the safety gap $P_{\text{sg}} = 0.1$. Traffic lights can operate according to various strategies, but in this study, we focus on a strategy where the traffic lights' states in the entry lanes are synchronized. The cycle time is set to $T = 80$, with $t_g = 0.5$ (meaning the green and red lights have the same cycle time $T_G = T_R = t_g \times T = 40$), and the position of the signals in the lane is set to $X = 20$. Figure 2.13 illustrates the current as a function of α and β rates, along with the corresponding phase diagram in the (α, β) plane for the three lanes of the roundabout.

Compared to Figure 2.10, the results show that the free-flow and the jammed phases shrinks, while the maximum current phase expands. Additionally, a congestion phase appears in all lanes of the roundabout. However, the maximum current phase in the circulating lane appears wider than that of the entry and exit lanes, as traffic lights can reduce the number of conflict points when vehicles enter the circulating lane from adjacent entry lanes.

To gain a deeper understanding of the microscopic interactions among vehicles in different traffic phases, we illustrate the space-time configurations of these phases in Figure 2.14. In the free-flow phase ($\alpha = 0.1$, $\beta = 0.6$), vehicles move freely in the three lanes of the roundabout, except for the black lines marked at the entry lane. These lines indicate vehicles stopped due to a red traffic light. As we transition into the congestion phase ($\alpha = 0.27$, $\beta = 0.6$), traffic lights compress the free space ahead of them during the red cycle, resulting in an increased number of stopped vehicles in the entry lane and improving

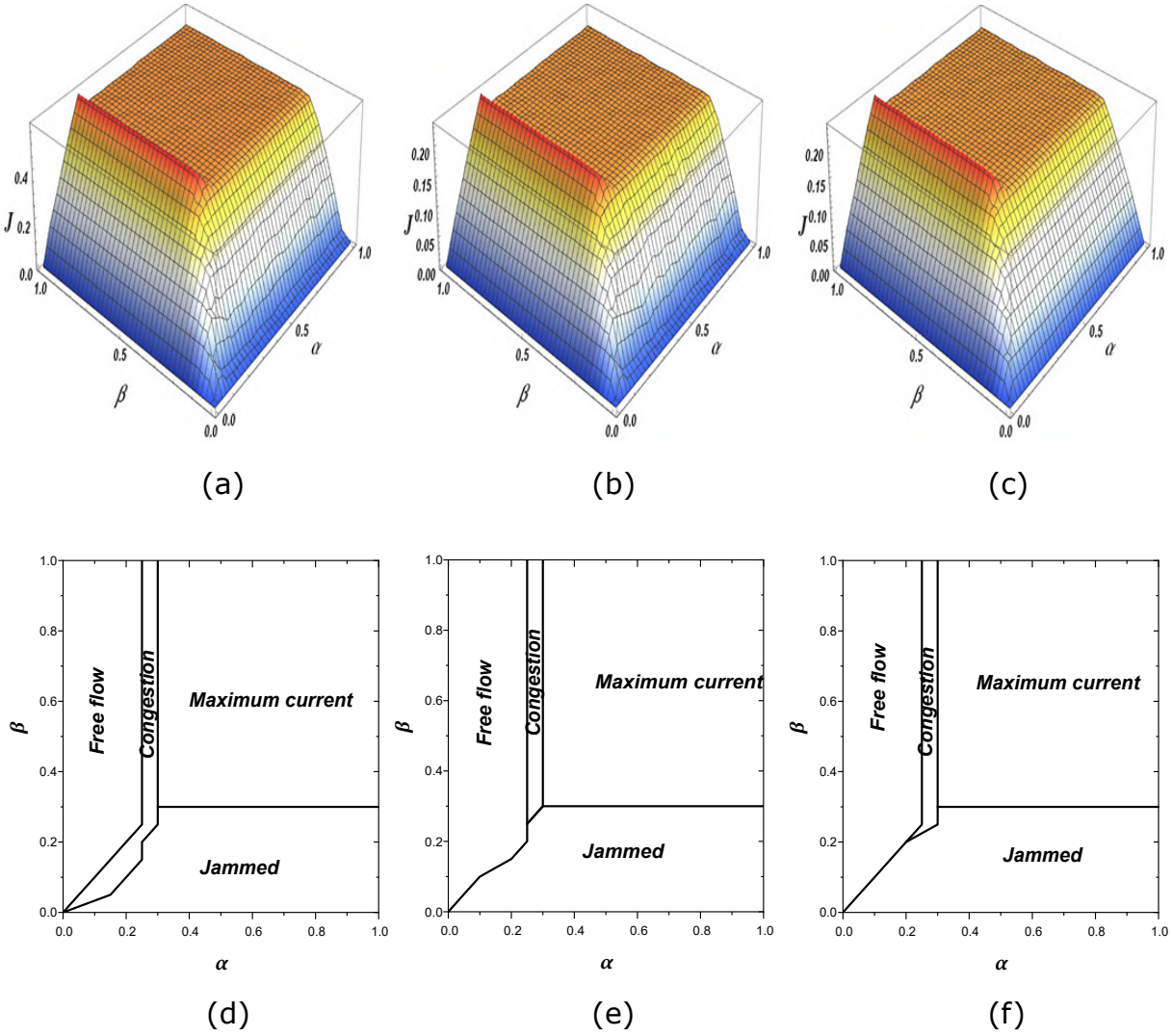

Figure 2.13: The current in the roundabout system with the traffic light: (a) circulating lane, (b) entry lane, and (c) exit lane as a function of α for various β. Phase diagram for (d) circulation lane, (e) entry lane, and (f) exit lane in the (α, β) plane.

flow in the circulating and exit lanes.

During the jammed phase ($\alpha = 0.6$, $\beta = 0.1$), queues of stationary vehicles are evident in all lanes of the roundabout system. Congestion forms in the entry lane due to the red cycle, while in the exit lane, it occurs due to the low extraction rate β, impacting the flow in the circulating lane. Additionally, in the circulating lane, the white space shifts backward in the opposite direction of traffic movement, indicating a congested traffic scenario.

In the maximum current phase ($\alpha = 0.6$, $\beta = 0.6$), congestion persists in the entry lane due to the red cycle of traffic lights. Meanwhile, traffic flow in the exit and circulating lanes improves due to the high extraction rate β.

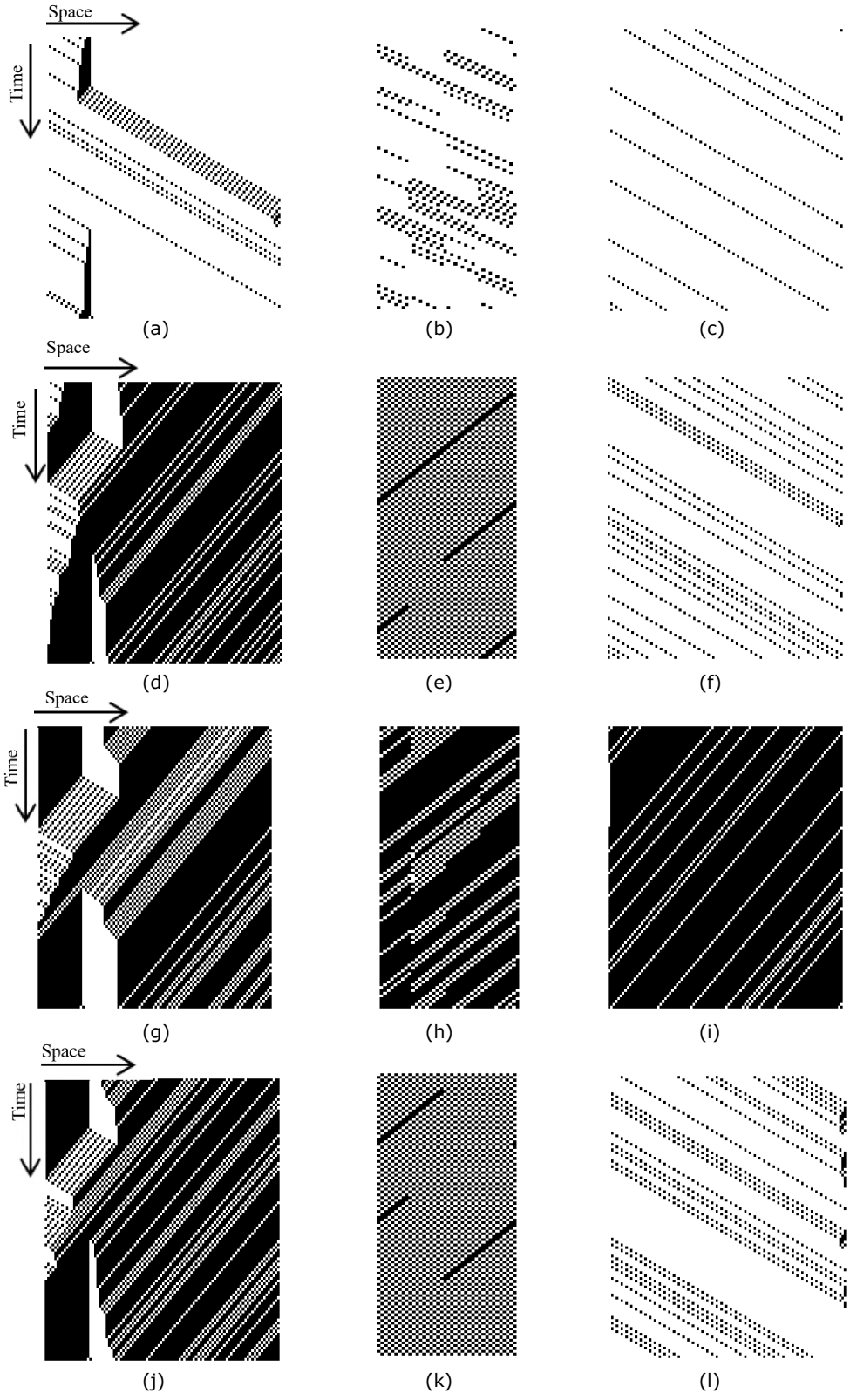

Figure 2.14: Space-time plots for the roundabout system with traffic light. For ($\alpha = 0.1$, $\beta = 0.6$) (a) Entry lane, (b) Circulating lane, (c) Exit lane. For ($\alpha = 0.27$, $\beta = 0.6$) (d) Entry lane, (e) Circulating lane, (f) Exit lane. For ($\alpha = 0.6$, $\beta = 0.1$) (g) Entry lane, (h) Circulating lane, (i) Exit lane. For ($\alpha = 0.6$, $\beta = 0.6$) (j) Entry lane, (k) Circulating lane, (l) Exit lane. Black corresponds to vehicles while free space is presented in white.

The results show that the addition of traffic lights improves the flow of traffic in the roundabout system. However, it is important to explore how the variation between the duration of green and red signal periods can influence the capacity, which refers to the maximum flow achievable in the lane, within the roundabout system. To address this question, we aim to investigate how the capacity fluctuates concerning the ratio of green signal time to the cycle time T (r_{green}), as illustrated in Figure 2.15. The findings demonstrate a rise in capacity across the three lanes of the roundabout (including the circulating, entry, and exit lanes) as the ratio of green signal time increases, up to a point where it reaches 0.5. Beyond this threshold, the capacity stabilizes. This observation suggests that an optimal balance between green and red signal periods is crucial for maximizing the flow of vehicles through the roundabout. By fine-tuning the duration of green signal time relative to the overall cycle time, traffic engineers can effectively manage congestion and ensure smooth traffic flow. Moreover, reaching a stable capacity beyond the 0.5 ratio implies that there may be diminishing returns or other factors influencing traffic flow dynamics beyond a certain point, highlighting the complexity of traffic management systems and the need for further investigation into optimal signal timing strategies.

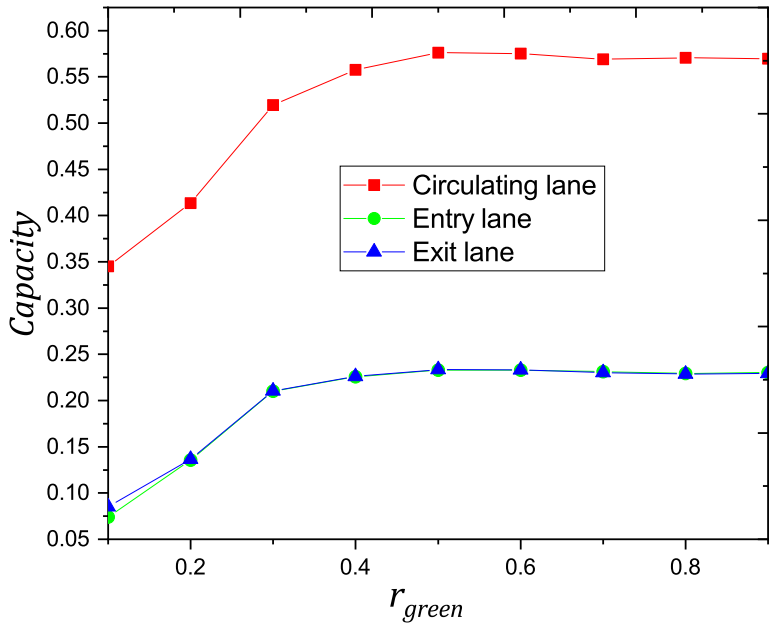

Figure 2.15: Capacity as a function of the ratio of green signal time to the cycle time T. For the three lanes of the roundabout (circulating, entry, and exit lanes).

2.5 Conclusion

Roundabouts are essential intersections that minimize vehicle conflicts without the need for traffic lights and are commonly used in traffic patterns worldwide. However, several factors can affect the efficiency of the roundabout system. One aspect that has not been adequately studied is the impact of vehicles that remain in the circulating lane of the roundabout for extended periods and how this affects other lanes. These vehicles can be

categorized into two groups: those making complete circles and those who continue to drive around the roundabout until they decide to exit. Additionally, the effect of vehicles coming from the entry lanes not respecting safety gaps when entering the circulating lane should be considered.

In this study, we examined the impact of U-turns on roundabout traffic flow and found that due to the priority rules in place, these turns typically result in increased traffic in the entry lane. As a consequence, incoming vehicles are forced to wait for a sufficient gap to form, leading to waiting lines at the entry lane and an increase in CO_2 emissions in that area. According to our findings, when the number of these vehicles increases, the maximum current phase increases, and the free flow and congestion phases decrease. Additionally, this results in a clogged section of the circulation lane.

An increase in the proportion of vehicles that consistently drive in the circulating lane increases energy dissipation and CO_2 emissions in all lanes in different ways. An analysis of energy dissipation shows that an increase in these vehicles results in a noticeable decrease in energy dissipation during the free-flow and congested periods. At these extremes, energy dissipation is reduced, indicating the appearance of local interaction, and traffic is either flowing freely or congested. The CO_2 emissions analysis shows that by preserving speed heterogeneity, a rise in the number of vehicles without a set exit stabilizes maximum emissions in the circulating lane. In contrast, higher speed heterogeneities in the entrance lanes cause an increase in CO_2 emissions, which eventually decrease when queues form and traffic flow deteriorates, resulting in fewer acceleration and deceleration occurrences. The reduction of vehicles in the exit lanes leads to improved traffic flow in this lane and consequently lower CO_2 emissions.

In summary, the presence of persistently circulating vehicles influences traffic dynamics, energy dissipation, and CO_2 emissions in varying degrees across different lanes. These observations are crucial for understanding the interplay between traffic flow, energy dissipation, and environmental impact regarding vehicle circulation within roundabouts. Furthermore, we examined how vehicles disregarding safety gaps when entering the circulating lane highlighted a significant reduction in the capacity of the circulating lane, ultimately resulting in a decrease in the system's overall capacity. To enhance the functionality of the roundabout system, we propose the introduction of traffic lights to reduce vehicle interactions. Assessing its impact on the roundabout system, we observed that the free-flow and the jammed phases decreased, while the maximum current phase increased. Additionally, congestion phases were observed across all lanes of the roundabout. Furthermore, we investigated how the difference between the durations of the green and red signal periods can affect capacity. This study emphasizes the importance of managing entry lanes in roundabout traffic flow dynamics. This resource is crucial for understanding the intricate effects of U-turns and hesitant driving on roundabout traffic patterns. It also lays the groundwork for future academic research on vehicle dynamics in multi-lane roundabouts and their relationship to the surrounding environment.

Chapter 3

Assessing the Impact of Adaptive Traffic Lights on Traffic Circle Throughput: A Simulation and Modeling Study

3.1 Introduction

Effective intersection management is essential for the smooth operation and safety of urban transportation systems [19, 104]. It involves coordinating various elements, such as vehicle and pedestrian traffic, flow patterns, safety needs, and infrastructure optimization. These factors work together in a complex manner to ensure efficient and safe transportation networks. A variety of techniques and strategies in traffic management are used to handle the challenges presented by intersections, including implementing traffic circles, roundabouts, traffic light control, and unsignalized intersections (type X or Y, T), among others [105–111]. Each of these actions contributes differently to controlling traffic and improving safety.

Traffic circles are one of the strategies that are becoming increasingly popular as an efficient way to manage intersections [90]. Compared to conventional intersections, traffic circles have several advantages, including increased capacity, reduced vehicle emissions, decreased delays, and improved safety. In a traffic circle, vehicles in the entry lane are given priority over others because this lane is intended to accelerate vehicle entry and enable faster passage via the circulating lane. Combining circular intersections with traffic signals further enhances throughput and reduces emissions. Despite the global popularity of traffic circles, some cities still rely on them; a notable example is the Arc De Triomphe in Paris. Intelligent control of entry lanes, based on circulating lane traffic conditions, is a technique that could enhance throughput quality and prevent gridlock within the traffic circle system.

In this chapter, we will assess the impact of adaptive traffic lights on the throughput of the traffic circle system. Our solution preserves the key feature of traffic circles—the priority rules enabling uninterrupted traffic flow. However, the traffic lights in the entry lanes turn red based on the traffic situation in the circulation lane to prevent deadlock resulting from mutual obstruction, only turning red when traffic flow worsens. We will evaluate several control parameters, including traffic density, satisfaction rate, average speed, time headway, and the density of stopped cars. To calculate these parameters, we will install sensors in the circulating lane. Subsequently, based on sensor results, the traffic lights in the entry lanes will turn red until traffic conditions in the circulating lane no longer pose a deadlock risk.

3.2 Model Development and Simulation

3.2.1 The motion rules

We are examining a traffic circle with three lanes: an entry lane, an exit lane, and a circulation lane. The circulation lane is considered a one-dimensional lattice with periodic boundary conditions. Each vehicle is only permitted to occupy one cell, and the size of the circulation lane is given by L_1 cells, which also represents the maximum number of vehicles that can be accommodated in the circulation lane. Each cell is assumed to be 7.5 meters in length, and we set the time step to be equal to 1 second. The circulating lane is connected to one end of the entry/exit lanes, which consists of L_2 cells. The other end is regulated by the rates of injection and extraction, with each lane considering an open boundary.

At every time step, a vehicle is identified by its position and speed. Updates to vehicle positions and speeds are carried out simultaneously following the guidelines of the NaSch model [16]. In the circulating lane, vehicles move counterclockwise. Each cell may contain one or more vehicles, and the speed of each vehicle can be an integer between zero and its maximum speed ($V_i = 0, 1, 2, ..., V_{\max}$). The number of entry and exit lanes in this study is $N = 4$, where N is the total number of entry and exit lanes.

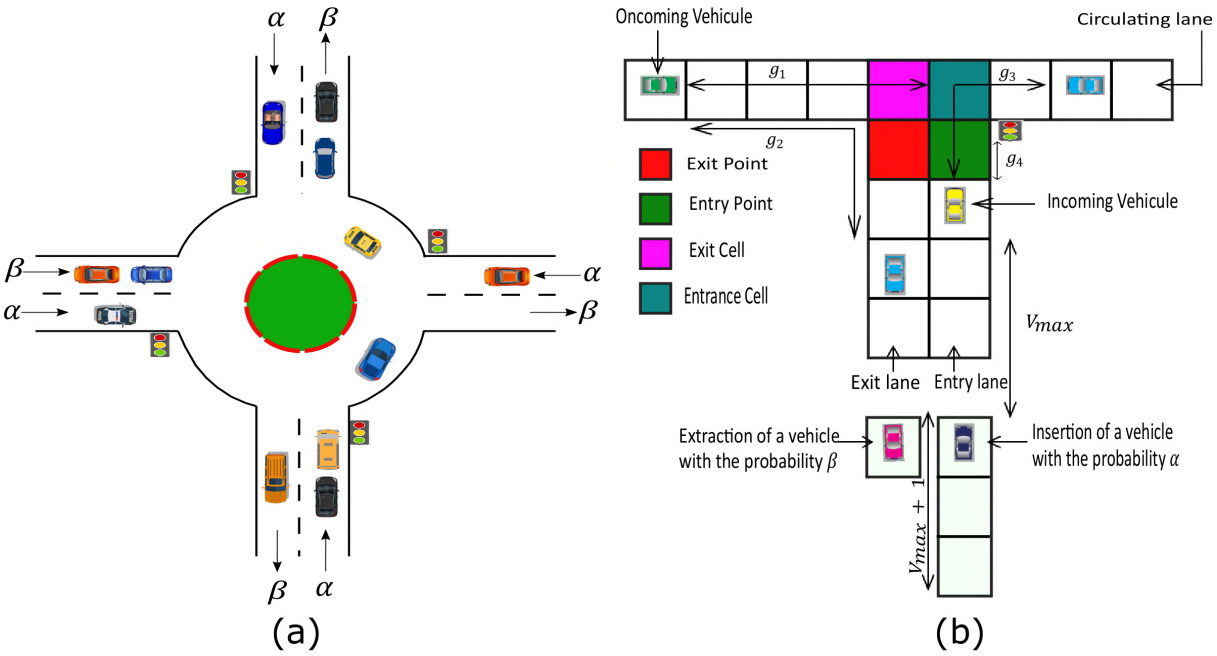

Figure 3.1: (a) Sketch of the traffic circle system, (b) Regulations for entry and exit.

3.2.2 The priority rules

In a traffic circle, incoming vehicles have the right of way. Approaching vehicles that were previously in the circulation lane near the entry cell yield to the incoming vehicle, as shown in Figure 3.1(b). The number of empty cells g_1 between the entry cell and the approaching vehicle in the circulation lane is used to determine the speed of the incoming vehicles.

The following rules apply to incoming vehicles (i.e., vehicles at the entry point) and their right of way in a traffic circle:

- If the traffic lights at entry lanes are not red, the second rule of the NaSch model is modified to $v_i = \min(v_i, g_3)$. Here, g_3 denotes the distance between the incoming vehicle and the first vehicle to the right of the entrance cell in the circulating lane (see Figure 3.1(b)).
- If the traffic light is red or the cell connecting the entrance point and the circulating lane is occupied, the second rule of the NaSch model becomes $v_i \rightarrow \min(v_i, g_4)$. Here, g_4 represents the number of unoccupied cells between the entering vehicle and the traffic signal ahead (see Figure 3.1(b)).

The following rules determine the exit from the circulating lane:

- A vehicle approaching its targeted exit (which was previously in the circulating lane) must determine the number of empty cells (g_2) between it and the first vehicle in the desired exit lane (refer to Figure 3.1(b)). If this is done, the vehicle's speed is adjusted to $v_i \rightarrow \min(v_i + 1, g_2, v_{\max})$.
- If $v_i > g_2$ and at least the first cell in the exit lane is empty, the vehicle exits the circulating lane.
- If the first cell in the exit lane is not empty, the vehicle continues traveling in the circulating lane until it reaches the intended exit.

Vehicles are inserted into and removed from the system according to the rules of the expanded open boundary conditions mentioned in Chapter 1.

3.2.3 Traffic lights rules

Adaptive traffic lights positioned at the entry lanes regulate the traffic circle system; they activate only when the circulating lane's traffic flow reaches a certain threshold. When the traffic condition exceeds a critical parameter, such as density, satisfaction rate, average speed, time headway, or the density of stopped cars, the traffic lights in the entry lanes turn red until the system eases to reduce the number of vehicles in the circulating lane, at which point the system resumes normal operation. Under normal circumstances, the entry rules of the traffic circle, which prioritize incoming vehicles, are followed.

3.2.4 Time-to-Collision Concept

In this study, we have elaborated on a safety metric that was initially based on the concept of Time-to-Collision (TTC) [112]. TTC refers to the duration within which two consecutive vehicles, traveling at a certain speed difference, could potentially collide. The TTC for a vehicle i in relation to a preceding vehicle $i + 1$ at a particular time step t, can be computed using the following equation:

$$\mathrm{TTC}(i,t) = \frac{d(i,t)}{V(i,t) - V(i+1,t)} \quad \forall\, V(i,t) > V(i+1,t) \tag{3.1}$$

An evaluation of the time until a potential collision can only be done when there is a difference in the speed of two vehicles traveling one after the other. In this scenario, $V(i,t)$ signifies the speed of the vehicle i at a specific moment in time t, and $d(i,t)$ denotes the actual distance between the vehicle i and the one in front of it at the same time step t.

3.2.5 Simulation Parameters

The parameters used in our computational studies are provided in Table 3.1. In this investigation, we examined the carbon dioxide (CO_2) emissions that cause pollution. It was assumed that petrol was the fuel used in all of the vehicles in the simulation.

Table 3.1: Parameters of the model used in the simulation

Parameter	Symbol	Value
Size of the circulating lane	L_1	40
Size of the entry/exit lanes	L_2	100
NaSch braking probability	P	0.1
Maximum permissible speed	$v_{\max}$	2
Maximum Time Limit of Monte Carlo	T_{Max}	40 000
Calibration Time of Monte Carlo	T_{Cal}	20 000
Number of Independent Runs	T	100

3.3 Unsignalized traffic circle

In the first step, we analyze the traffic flow in the circulating lane of the traffic circle. The circulating lane states in the traffic circle are thought to be the primary cause of fluctuations in the traffic flow of the entry/exit lanes. Therefore, we show the current in the circulating lane in Figure 3.2 (a) as a function of the injection α and extraction β rates. The corresponding phase diagram (Figure 3.2 (b)) reveals the phases of free flow, congestion, and gridlock. In a free-flow phase, traffic moves freely and unhindered, while in a congested phase, traffic moves more slowly as new vehicles enter the flow and impede the movement of existing ones.

As we can see in Figure 3.3, as the injection rate α increases, so does the density in the circulating lane during the congestion phase. This is where the incoming traffic from the entry lanes creates a line of stopped vehicles close to the entry points, increasing the traffic density in the circulation lane. When traffic reaches a higher level during the gridlock phase, stopped vehicles in the circulating lane prevent new vehicles from entering, bringing all entry lanes to a complete halt.

Since the traffic circle exhibits an excessively large period of gridlock (approximately nine times the size of the free-flow phase), it can be concluded that the probability of gridlock is higher than that of free-flow. Therefore, the primary goal of this study is to improve the traffic situation in the traffic circle. In the next subsection, we will examine the effects of adaptive traffic lights on the throughput of the traffic circle system.

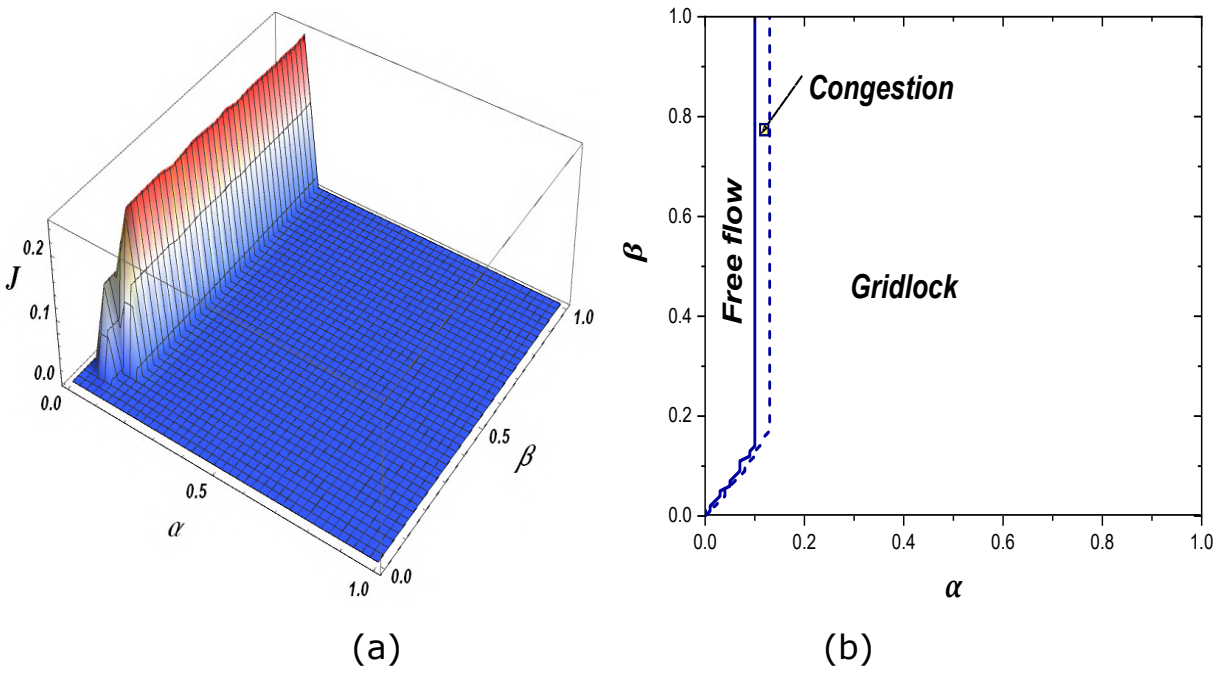

Figure 3.2: (a) Current as a function of injection α and extraction β rates in a circulating lane, (b) Phase diagram in the (α,β) plane.

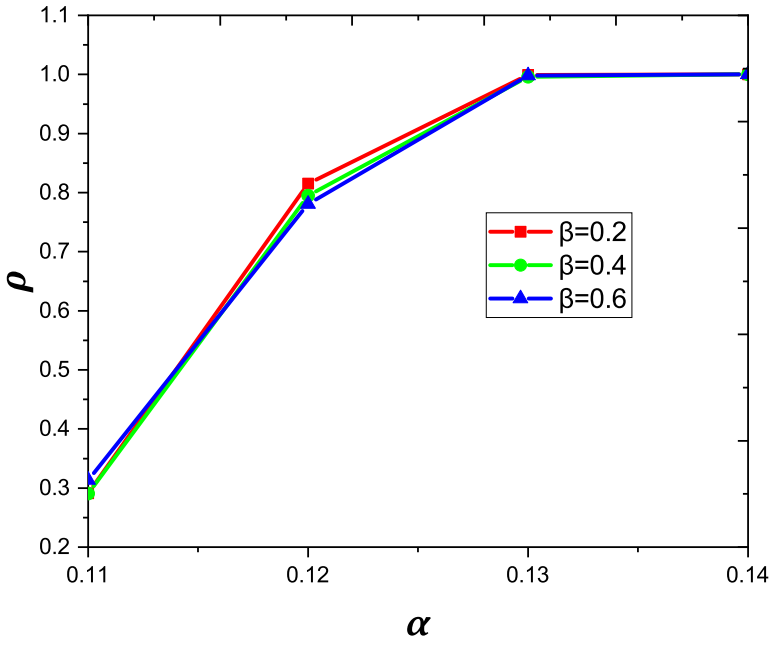

Figure 3.3: Density in the circulating lane as a function of α for $\beta = 0.2$, $\beta = 0.4$, and $\beta = 0.6$.

3.4 Effects of adaptive traffic lights

In this section, we will investigate the effects of adaptive traffic lights on the performance of a traffic circle system. To accomplish this, we will conduct a thorough analysis of various control parameters.

Firstly, we will examine the relationship between traffic density and satisfaction rate, and their impact on several critical aspects of traffic flow. These aspects include traffic phases, the microscopic interactions between vehicles, the system's overall capacity, and the duration of red lights. For this part of the study, we will limit the maximum allowable speed for vehicles to 2 ($V_{\max} = 2$).

Secondly, we will investigate the influence of average vehicle speed, time headway (the time gap between two consecutive vehicles), and the density of stopped cars on various traffic characteristics. These characteristics include traffic phases, the quantity of CO_2 emissions generated, the time to collision, the duration of red lights, and the system's overall capacity. For this part of the analysis, we will limit the maximum allowable speed for vehicles to 3 ($V_{\max} = 3$).

By analyzing these parameters, we aim to obtain a deeper understanding of how adaptive traffic lights affect traffic flow, safety, and environmental impact within a traffic circle system.

3.4.1 Effect of density

To prevent a situation where all entry lanes are completely stopped, it is essential to monitor the traffic in the circulating lane. The density of the circulating lane is one of the easiest parameters to monitor. If the density reaches a certain threshold, all traffic lights for the entry lanes turn red to stop the flow of vehicles entering the lanes. The following is the method to calculate the density in the circulating lane:

$$\rho = \frac{N_V}{L_1} \tag{3.2}$$

The number of vehicles in the circulating lane is denoted as N_V.

To observe how traffic control affects throughput in the traffic circle system, Figure 3.4 displays the current in the circulating lane as a function of the injection (α) and extraction (β) rates, along with the corresponding phase diagram in the (α, β) plane for a range of critical density values ($\rho_c = 0.8$, $\rho_c = 0.6$, and $\rho_c = 0.4$). One noteworthy observation is that the jamming and maximum current phases occur when the gridlock dissipates. The congestion phase vanishes as the critical density decreases, but the free flow and jamming phases expand at the expense of the maximum current phase. This suggests that when the control technique is implemented, the way that vehicles interact in the circulating lane changes significantly. The reason for the expansion of the free flow phase when ρ_c decreases is that there are fewer vehicles in the circulating lane, which results in less interaction and improves traffic flow conditions.

The space-time diagrams are shown in Figure 3.5 (for $\rho_c = 0.8$) to help visualize the microscopic interactions between the vehicles in the circulating lane. The vehicles (represented by the black dots in the space-time diagram) move freely and without obstruction during the free-flow phase. The traffic lights do not turn red for entering lanes because the density in the circulation lane is significantly below the critical density $\rho_c = 0.8$. However, as one approaches the border of the free flow phase, the disturbance

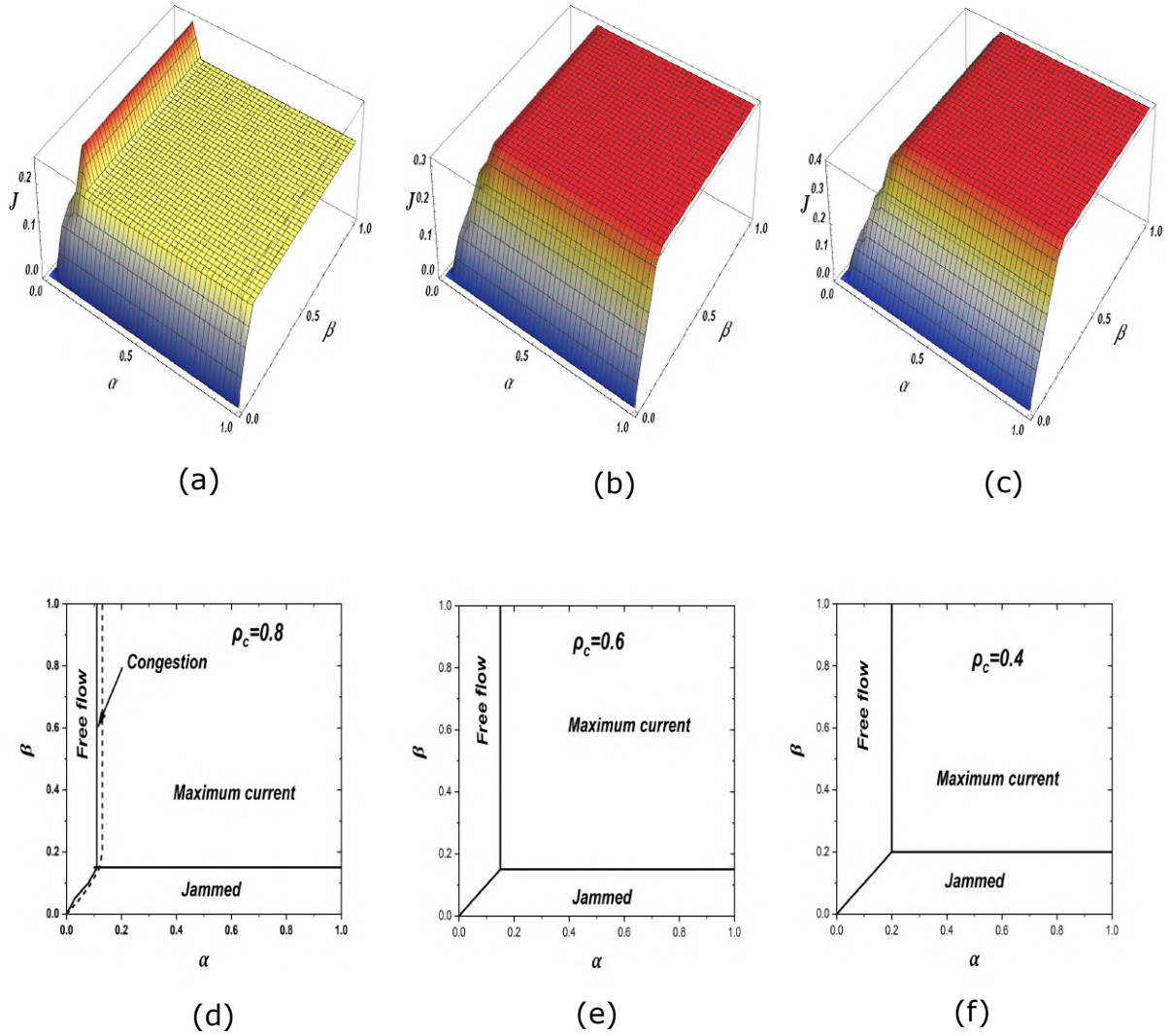

Figure 3.4: Current as a function of α for various β, when the circulating lane's density values are varied and the adaptation criterion is applied: (a) $\rho_c = 0.8$, (c) $\rho_c = 0.6$, and (e) $\rho_c = 0.4$. Phase diagrams for (b) $\rho_c = 0.8$, (d) $\rho_c = 0.6$, and (f) $\rho_c = 0.4$ in the (α, β) plane.

caused by incoming cars slightly increases the density in the circulating lane. At that point, traffic lights function to lessen the flow of vehicles entering the entry lanes, increasing the free flow at the expense of the congestion and gridlock phases (Figure 3.4 (b) in contrast to Figure 3.2 (b)).

During the congested period (refer to Figure 3.5 (b)), there is a modest decrease in traffic in the entry and circulating lanes, and there are minor disruptions in the circulating lane that cause a slight decrease in throughput (Figure 3.5 (b)). The cluster of stopped vehicles in the circulating lane appears for the Maximum current (Figure 3.5 (c)). The traffic lights then function to keep the system from entering a state of gridlock. Traffic in the circulating and entrance lanes exhibits similar characteristics to those seen in the maximum current periods during the jammed phase (Figure 3.5 (d)). The traffic lights improve traffic flow and prevent gridlock by reducing interaction in the circulating lane. While the traffic situation in the exit lanes is quite similar for all phases, an exception is observed in the jammed phase where a small cluster of stopped vehicles is present

at the right limit of the lattice. This is due to the low value of the extraction rate β, which hinders vehicles from exiting the system. This scenario mimics the traffic state at the destination, where a low β value corresponds to jammed traffic, and a high β value corresponds to free-flowing traffic.

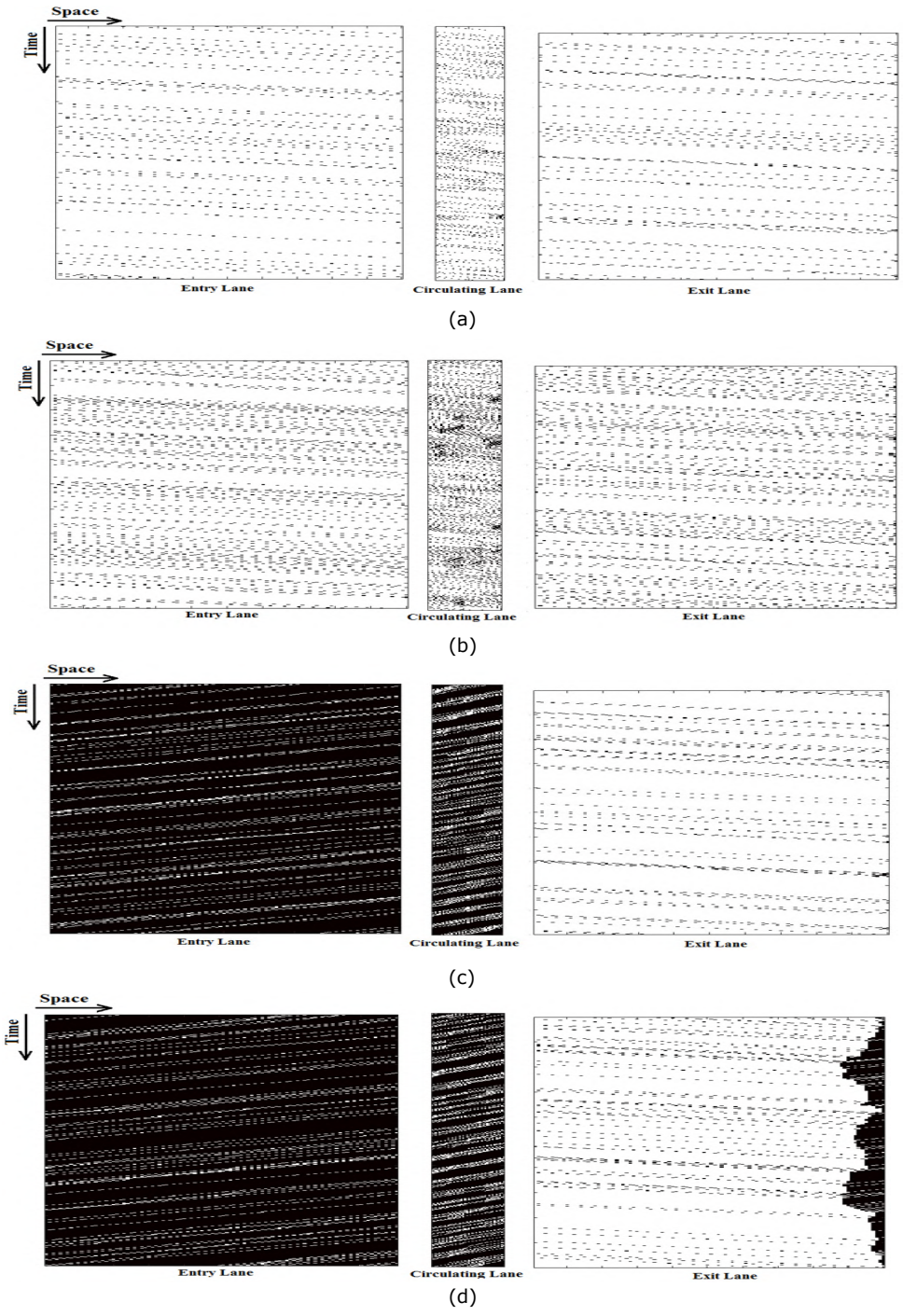

Figure 3.5: Space-time diagrams for the traffic circle system with density $\rho_c = 0.8$ for: (a) $\beta = 0.6$ and $\alpha = 0.05$, (b) $\beta = 0.12$ and $\alpha = 0.6$, (c) $\beta = 0.6$ and $\alpha = 0.6$, and (d) $\beta = 0.1$ and $\alpha = 0.6$. White color represents free space, whereas black color represents vehicles.

Next, we will assess the relationship between the critical density ρ_c in lanes of the traffic circle (the entry/exit and circulating lanes) and the capacity or the maximum current that

can be obtained in the lane. As we can see from Figure 3.6, the capacity increases with density until it reaches a critical value, at which point it starts to decrease. In this case, an increase in ρ_c results in denser traffic conditions in the circulating lane, which in turn lowers the system's capacity.

Furthermore, the capacity in the circulating lane is higher than in the entry/exit lanes due to the vehicles arriving from multiple entry lanes. Since the maximum number of vehicles that can pass from a lattice point for a given time is the same for both lanes, the capacity in the entry and exit lanes exhibits a similar feature.

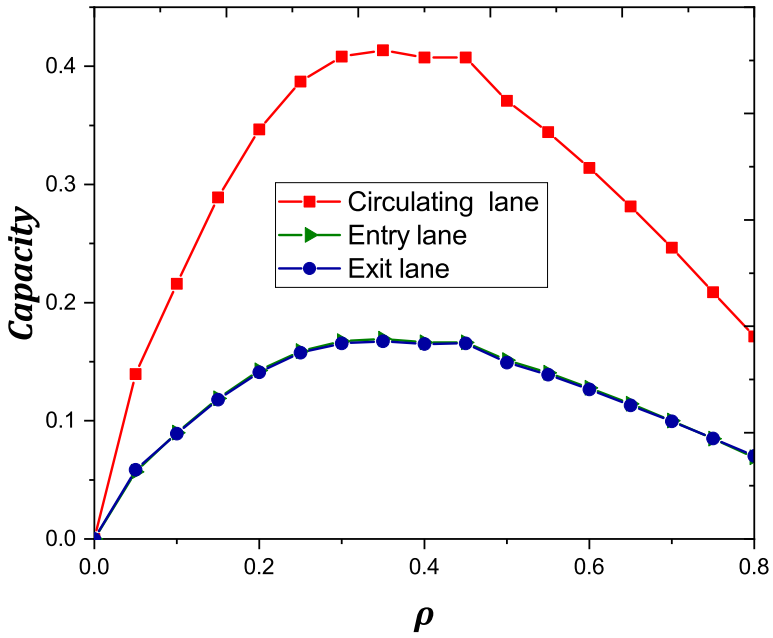

Figure 3.6: The capacity of the entry/exit and circulation lanes as a function of density ρ_c.

As we observed, adaptive traffic management improves traffic flow in the circulating lane, indicating that traffic control can increase throughput in the traffic circle system. However, one might wonder, for what length of time do the traffic lights remain in the red state?

In our study, the answer to this question is crucial because adopting longer red cycle lengths to improve traffic flow conditions is pointless without proper understanding. We examine the durations of these red cycle lengths, during which the red light remains lit at the entry lanes, to verify the efficacy of adaptive traffic signals and to comprehend their impact on the traffic flow in the entry lanes. Figure 3.7 displays the findings. For $\rho_c = 0.8$, the longest duration for which the red light stays on is approximately 8 time steps. For $\rho_c = 0.6$, the maximum number of time steps that the red light can remain lit is 11. Consequently, for $\rho_c = 0.4$, the red light can remain lit for a maximum of 16 time steps. The time required to reduce the number of vehicles in the circulating lane increases as the critical density decreases, resulting in longer red cycle durations. As observed in a previous study [113], the maximum duration of the red light's illumination at a typical signalized intersection is shorter. By assessing and utilizing the critical density of the circulating lane as feedback, its usage frequency could be increased, thereby improving

traffic flow from the entry lanes. However, the traffic circle system's performance can be more effectively enhanced by evaluating other parameters as feedback. In the following section, we will examine the satisfaction rate as a feedback control parameter to regulate the entry-lane adaptive traffic signals.

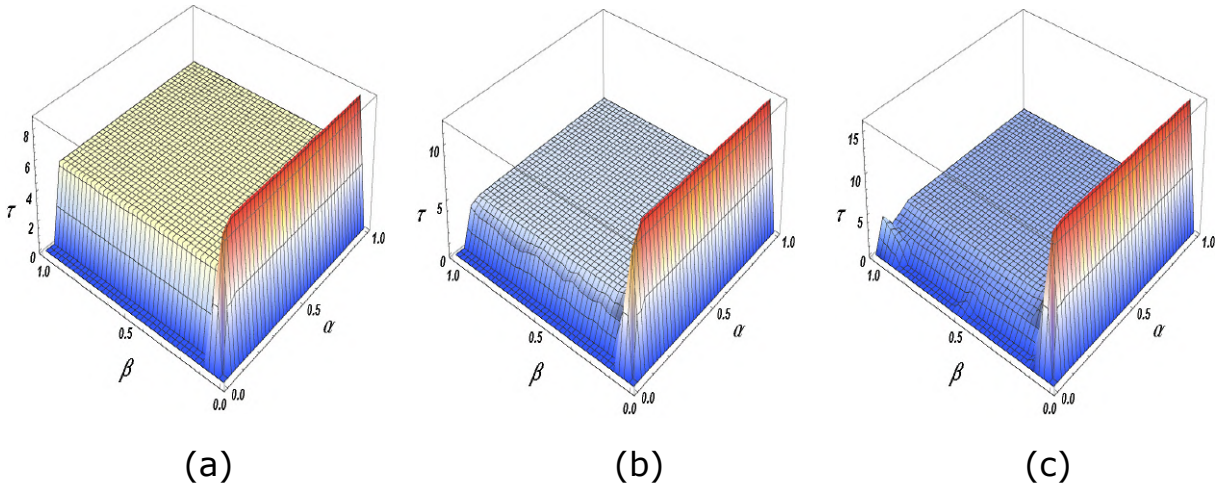

Figure 3.7: The duration of the red light in each entry lane, as a function of α and β, for the following cases: (a) $\rho_c = 0.8$, (b) $\rho_c = 0.6$, and (c) $\rho_c = 0.4$.

3.4.2 Effect of satisfaction rate

The satisfaction rate is another metric that can be used to assess the traffic condition of the circulating lane. It measures the proportion of vehicles that travel at their intended speed. We define the satisfaction rate η as follows:

$$\eta = \frac{v_i}{v_{\max}} \tag{3.3}$$

Here, $v_{\max}$ represents the desired or maximum speed, and v_i represents the actual speed of vehicle i.

The satisfaction rate is a parameter that depends on the speeds of the vehicles. A vehicle i in the circulating lane is considered unsatisfied (i.e., $\eta < 1$) when it is unable to move at its desired speed (i.e., $v_i < v_{\max}$). The response of the traffic lights to changes in the satisfaction rate η is as follows: at each iteration of the simulation, the mean satisfaction rate for vehicles already in the circulating lane is computed. If the average satisfaction rate $\langle\eta\rangle$ (calculated as the mean of the satisfaction rates for all vehicles in the circulating lane) is greater than or equal to the critical satisfaction rate η_c, then the traffic lights for all entry lanes turn red.

Figure 3.8 displays the current as a function of α and β rates for various values of the critical satisfaction rate ($\eta_c = 0.2$, $\eta_c = 0.5$, and $\eta_c = 0.75$), along with the associated phase diagram in the (α, β) plane. It is evident that the traffic situation was improved by the control method that used the satisfaction rate to inform entry-lane traffic light timing. We recall that gridlock occurs only when $\beta = 0$. For $\eta_c = 0.2$, the maximum current and jammed phases are present, and the gridlock phase disappears. As η_c increases, the maximum current phase shrinks at the expense of an expansion in the free flow and jammed phases. This difference can be explained by the fact that high values of η_c indicate that there are many satisfied vehicles in the circulating lane, which causes the maximum

current phase to decrease because the traffic situation becomes more dependent on the boundary conditions. It should be noted that while the phase diagrams of $\eta_c = 0.5$ and $\eta_c = 0.75$ exhibit similar features, the two cases differ in that the maximum current values are larger in the case of $\eta_c = 0.5$ than in the case of $\eta_c = 0.75$.

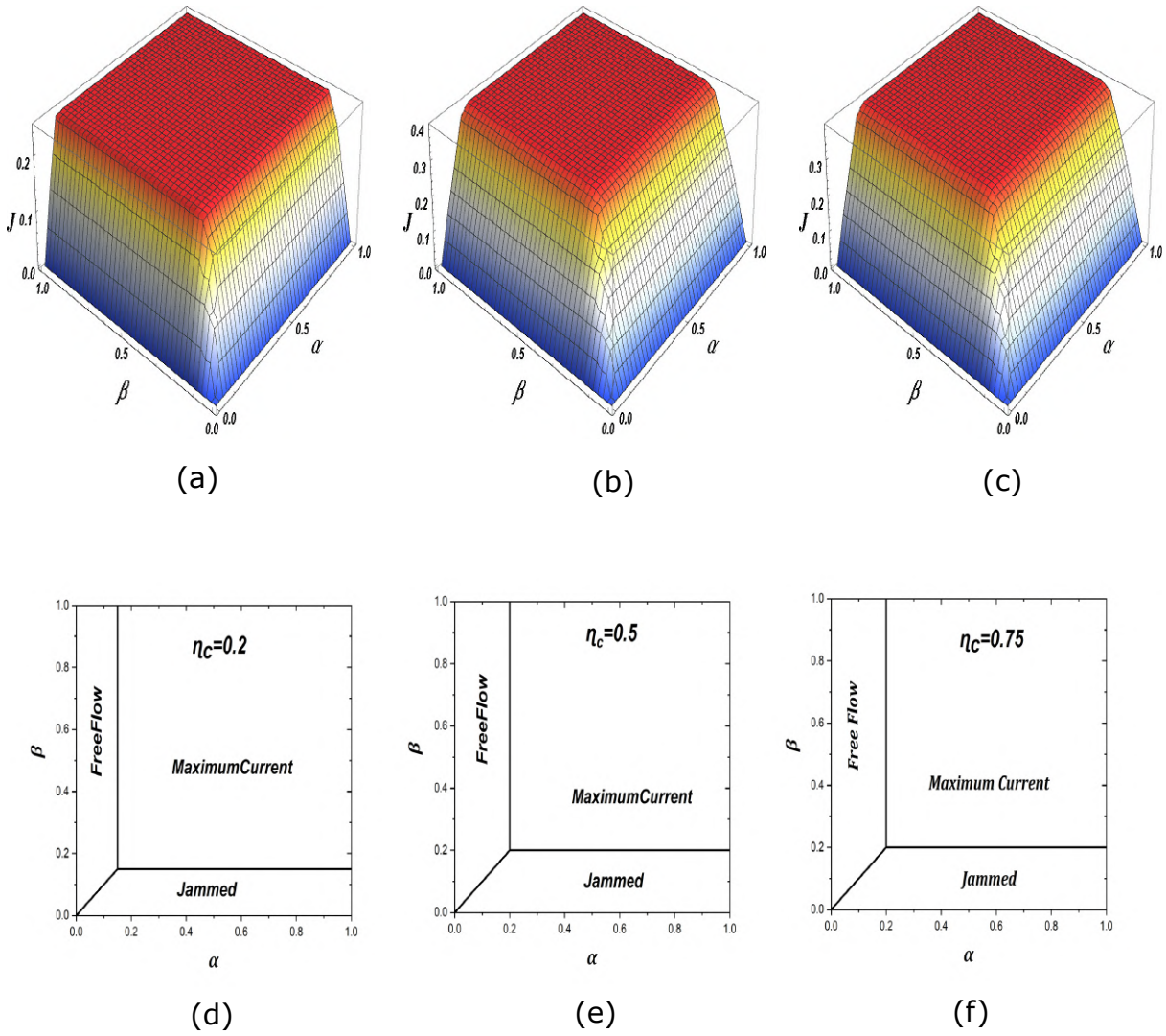

Figure 3.8: Current as a function of α for various β, when the circulating lane's satisfaction rate values are varied and the adaptation criterion is applied: (a) $\eta_c = 0.2$, (c) $\eta_c = 0.5$, (e) $\eta_c = 0.75$. Phase diagrams for (b) $\eta_c = 0.2$, (d) $\eta_c = 0.5$, (f) $\eta_c = 0.75$ in the (α, β) plane.

To understand the microscopic interactions among vehicles in each phase, the space-time configurations for all three phases and $\eta_c = 0.2$ are displayed in Figure 3.9. In the free flow phase, traffic in all lanes exhibits the same characteristics: vehicles travel at their desired speeds. During the maximum current phase, when there is heavy traffic in the entry lane, the white area moves backward in the opposite direction of the traffic flow, indicating a stop-and-go traffic condition. An increase in traffic from the entry lanes may impact the circulating lane, as evidenced by the appearance of dark patches in this lane. Since mutual obstruction in the circulating lane is the primary factor contributing to the system's decreased throughput, the increase in injection rate has little effect on the traffic conditions in the exit lanes. In this instance, the entry lane traffic lights were turned red to prevent the system from entering a state of gridlock. Conversely, lines of halted cars

are another feature of the packed phase. The low value of the extraction rates in the exit lane is what causes the line of stopped cars. When it comes to the entry lane, however, the congestion in the circulating lane prevents vehicles from entering, causing the traffic lights to turn red in order to minimize the number of vehicles in the circulating lane.

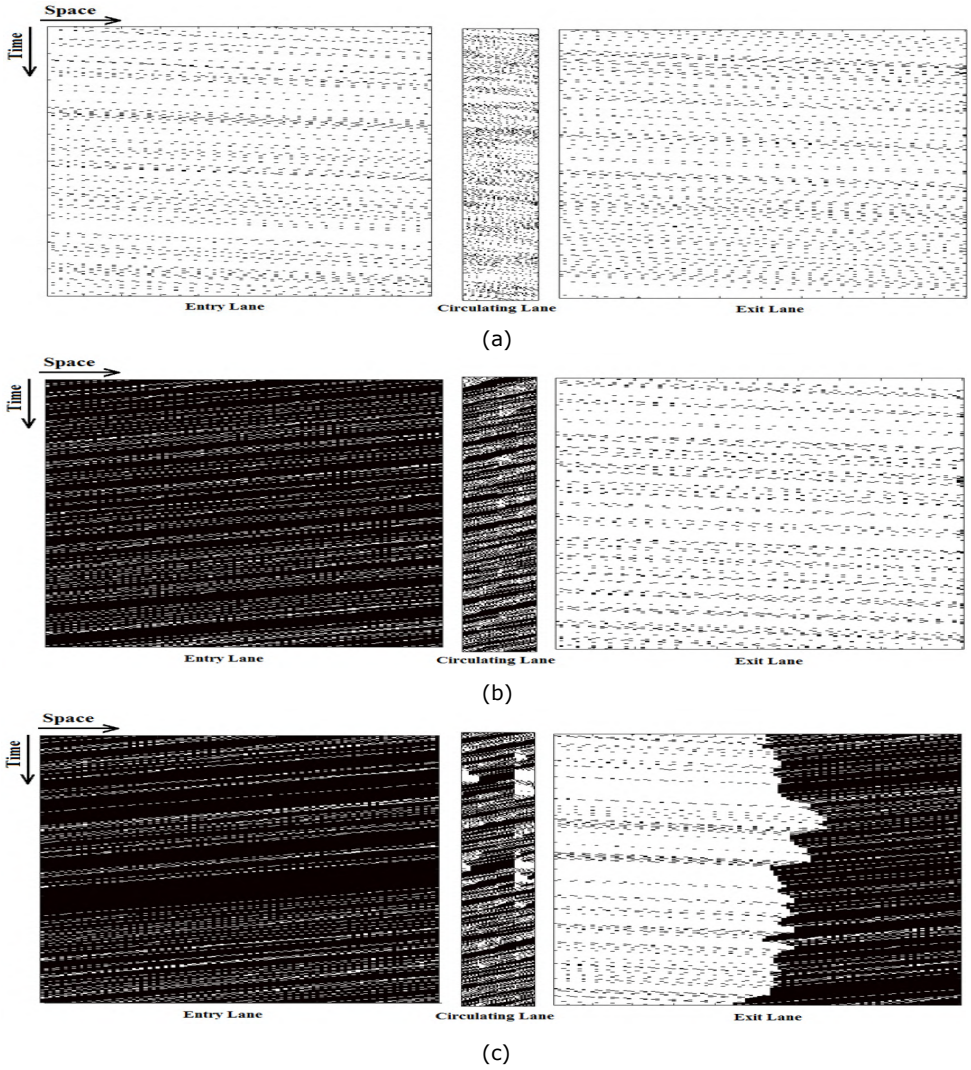

Figure 3.9: Space-time diagrams for the traffic circle system with satisfaction rate $\eta_c = 0.2$ for (a) $\alpha = 0.05$ and $\beta = 0.5$, (b) $\alpha = 0.5$ and $\beta = 0.5$, (c) $\alpha = 0.05$ and $\beta = 0.5$. White color represents free space, whereas black color represents vehicles.

To gain a more comprehensive understanding of the throughput for various values of η_c, the traffic circle system's capacity was assessed. Figure 3.10 shows the capacity evolution for the circulating lane and entry/exit lanes as a function of the critical satisfaction rate. According to the data, the capacity rises steadily as η_c increases, reaching values of 0.39 for the circulation lane and 0.16 for the entry/exit lanes. After that, it appears to be nearly stable before gradually declining. Furthermore, since traffic from various entering lanes raises the maximum current in the circulating lane, its capacity is superior to that of the entry/exit lanes.

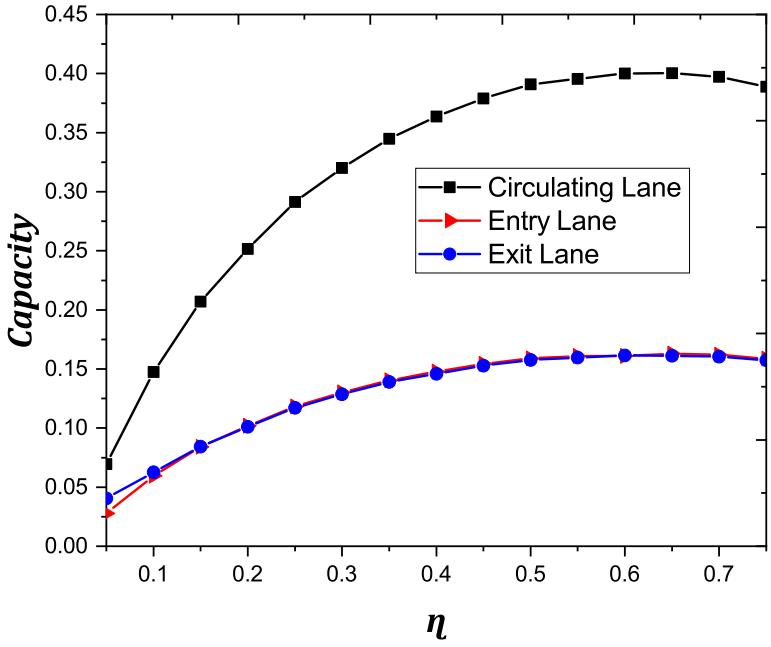

Figure 3.10: The capacity of the entry/exit and circulation lanes as a function of the critical satisfaction rate η_c.

We examine the red cycle lengths (Figure 3.11) where the red light remains lit at the entry lanes to verify the efficacy of adaptive traffic systems. The relationship between the maximum duration that the red lights remain lit and the increase in η_c is found to be nonlinear. The capacity exhibits similar characteristics, as it first rises, reaches a maximum, and then falls. Examining the maximum region—which corresponds to the jammed phase for every graph in Figure 3.11—tells us that the situation is similar in this instance. To fulfill the key criterion (here, the satisfaction rate, which depends on vehicle speed), the system must adjust itself to decrease the number of incoming vehicles. The red light will remain lit for a maximum of approximately 36-time steps for $\eta_c = 0.2$. In this instance, the red signal duration is longer than for traffic lights governed by the critical density. To understand this, we should consider the traffic situation in the circulating lane. Here, we need to ensure that vehicle speeds are higher to achieve satisfaction rates, which takes longer to accomplish than when analyzing vehicle density in the circulating lane. However, the longest the red light remains lit is approximately 45-time steps for $\eta_c = 0.5$. If $\eta_c = 0.5$ is exceeded, the traffic lights in this instance function effectively. However, since it depends on how vehicles are distributed along the circulating lane, and there are many different combinations of parameters that satisfy this criterion, we cannot say that this corresponds to 50% of vehicles moving at their desired speed or that all vehicles in the circulating lane move at a speed of 1. In this instance, there is more mutual blocking, and the arrangement of vehicles influences how long the traffic lights remain red. Meanwhile, the maximum duration that the red light remains lit for $\eta_c = 0.75$ is around 28-time steps. In this case, the system adjusts itself from the start to minimize incoming vehicles in order to ensure a better satisfaction rate in the circulating lane, which impacts the traffic in the entry lanes. As a result, the maximum duration that the traffic lights remain red is decreased.

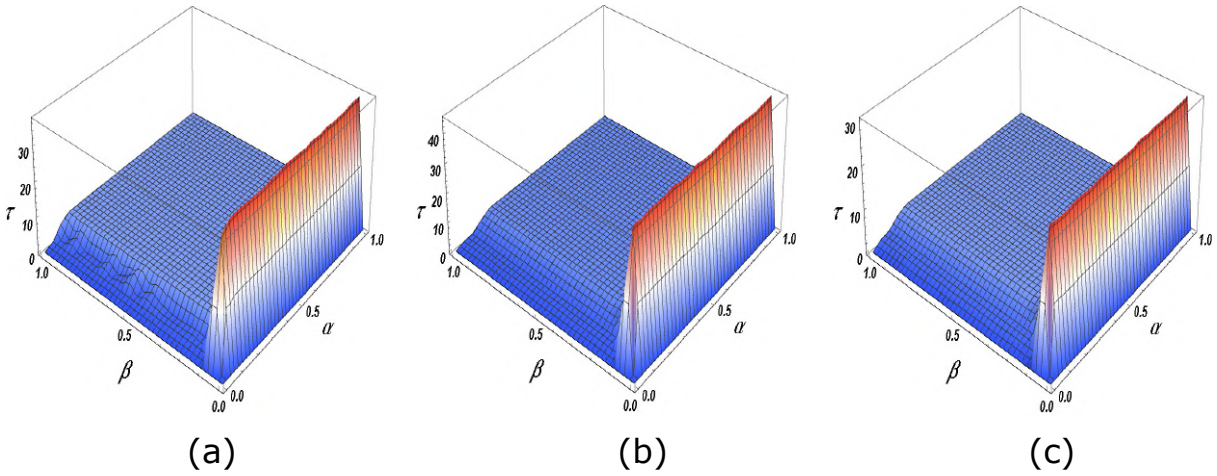

Figure 3.11: The duration of the red light in each entry lane, as a function of α and β, for the following cases: (a) (a) $\eta_c = 0.2$, (b) $\eta_c = 0.5$, and (c) $\eta_c = 0.75$.

3.4.3 Effect of average speed

The average speed of vehicles in the circulating lane is a useful parameter to evaluate its state. If the average speed exceeds a certain limit, an automatic response should be triggered to turn the traffic lights in all entry lanes red. This stops incoming vehicles from these lanes and allows traffic in the circle to continue flowing smoothly.

The average speed in the circulating lane is calculated using the following formula:

$$\langle V \rangle = \frac{1}{N} \sum_{i=1}^{N} V_i \tag{3.4}$$

In this context, V_i represents the instantaneous speed of vehicles at a specific moment, while N refers to the count of vehicles that pass by a sensor or detector within a predetermined time period T.

To evaluate the effects of traffic control strategies on the efficiency of a traffic circle system, Figure 3.12 presents the current within the circulating lane, depending on the α and β rates. Additionally, it displays the corresponding phase diagram in the (α, β) plane, taking into account various critical mean velocity values, such as $\langle V \rangle_c = 1.4$, $\langle V \rangle_c = 2.5$, $\langle V \rangle_c = 3$. For $\langle V \rangle_c = 1.4$, the traffic flow phases remain unchanged compared to the traffic circle without adaptive traffic lights. However, for $\langle V \rangle_c = 2.5$, both the jammed and maximum current phases appear, effectively eliminating gridlock and congestion phases while expanding the free flow phase. For $\langle V \rangle_c = 3$, the maximum current phase increases, accompanied by a decrease in free flow and jammed phases as the maximum current value is reduced. The reduction in the maximum current value can be attributed to a monitoring system installed within the circulating lane. When the critical mean velocity reaches 3, fewer vehicles enter the circulating lane, resulting in a decrease in the maximum current value.

.

In the next step, we will examine how the capacity (i.e., the highest flow of vehicles in the lane) changes with the critical mean velocity ($\langle V \rangle_c$) in both the entry/exit and circulating lanes. Figure 3.13 shows that the capacity remains constant for both the entry/exit and circulating lanes until it starts to increase at $\langle V \rangle_c = 1.7$, reaches its maximum at $\langle V \rangle_c = 2.2$, and then begins to decrease. Initially, at low values of $\langle V \rangle_c$, the

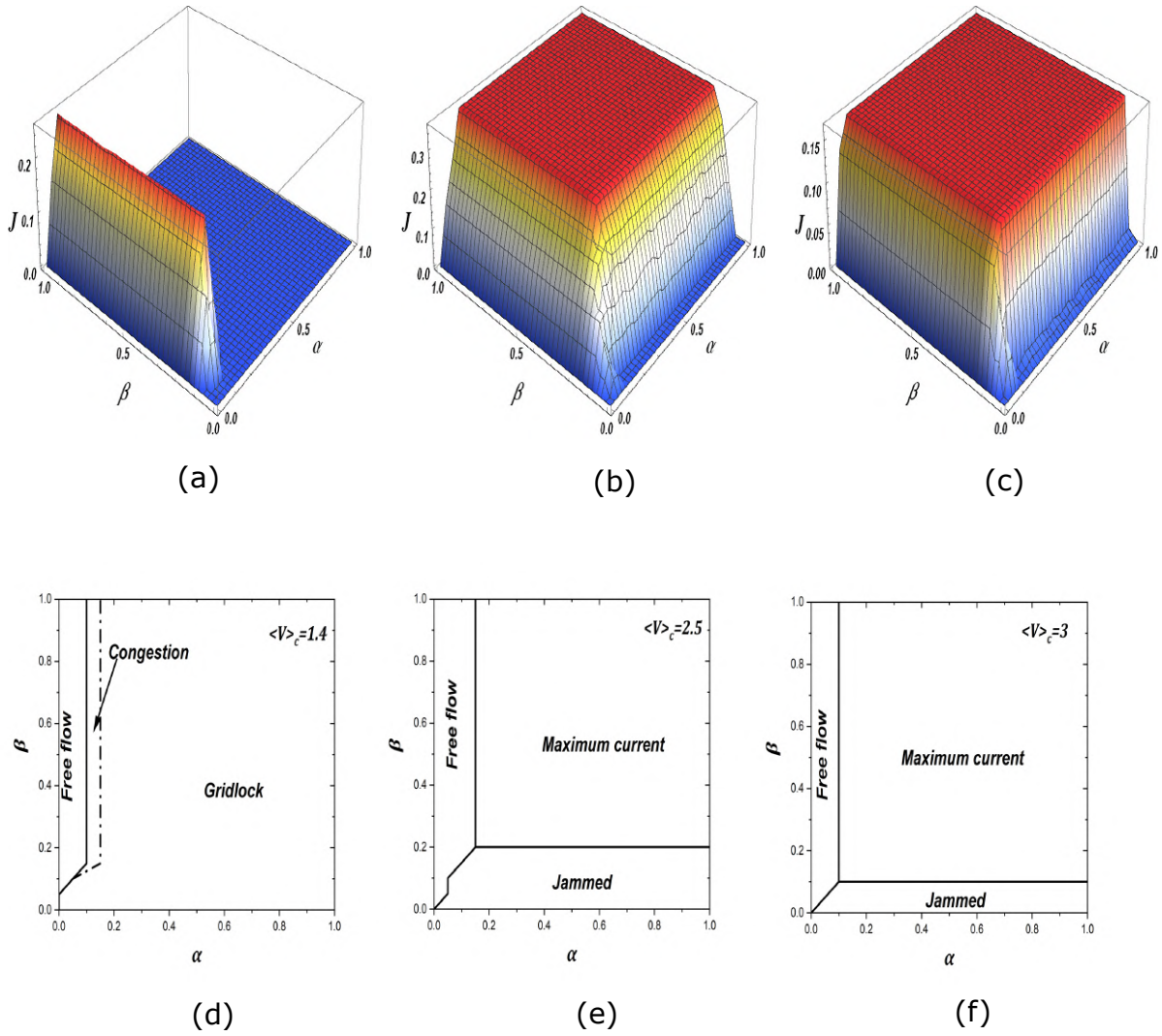

Figure 3.12: Current as a function of α for different β where the adaptation criterion is done with different mean velocity values in circulating lane (a) $\langle V\rangle_c = 1.4$, (c) $\langle V\rangle_c = 2.5$, (e) $\langle V\rangle_c = 3$. Phase diagram in the (α, β) plane (b) $\langle V\rangle_c = 1.4$, (d) $\langle V\rangle_c = 2.5$, (f) $\langle V\rangle_c = 3$.

capacity is stable because the flow of vehicles is consistent. This stability is due to the relatively low speeds, which allow a steady stream of vehicles to move through the system without significant disruptions. Vehicles can enter and exit the traffic circle smoothly, maintaining a constant flow rate. As the critical mean velocity ($\langle V\rangle_c$) increases, the system maintains relatively high speeds and a low number of vehicles entering the circulating lane, which increases the overall throughput of the traffic circle. This is because higher speeds allow vehicles to move through the traffic circle more quickly, reducing the time each vehicle spends in the system and allowing more vehicles to pass through over a given period. The capacity reaches its peak at $\langle V\rangle_c = 2.2$. At this point, the traffic system is operating at its most efficient, with vehicles moving at optimal speeds that maximize the flow rate. This peak efficiency occurs because the balance between vehicle speed and the number of vehicles entering the circulating lane is optimal, ensuring smooth and continuous traffic flow without significant delays or congestion. Beyond the peak at $\langle V\rangle_c = 2.2$, capacity begins to decrease. This decrease happens because as vehicles move at even higher speeds, the gaps between them increase, making it harder for new vehicles to enter the circulating lane. The reduced number of entering vehicles lowers the overall

flow rate despite the higher individual vehicle speeds. In essence, the system becomes less efficient at very high speeds because the increased spacing between vehicles limits the number of vehicles that can circulate through the traffic circle simultaneously. Notably, the capacity in the circulating lane is consistently higher than in the entry/exit lanes. This difference can be attributed to the merging of traffic from multiple entry lanes into the circulating lane. When vehicles from different entry points merge into the circulating lane, the combined flow results in a higher overall capacity. The circulating lane can handle a larger volume of traffic because it integrates flows from various sources, enhancing the total throughput of the traffic circle.

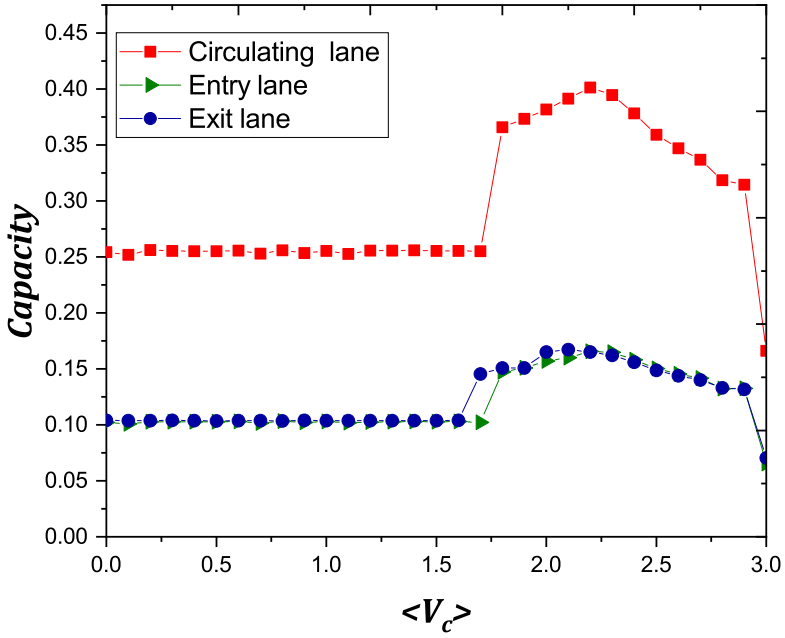

Figure 3.13: Capacity as a function of mean velocity $\langle V \rangle_c$ for the circulating lane and entry/exit lanes.

Figure 3.14 illustrates the carbon dioxide (CO_2) emissions in a traffic circle system equipped with adaptive traffic lights in the circulating lane. Our analysis reveals a nonlinear relationship between the maximum CO_2 emissions and the increase in average vehicle speed ($\langle V \rangle_c$). The capacity exhibits similar behavior, initially stabilizing, reaching a peak, and then declining, as shown in Figure 3.13. When the average vehicle speed ($\langle V \rangle_c$) is 1.4, CO_2 emissions reach a peak of 8.45 (g/m) under free-flowing traffic conditions, denoted by ($\alpha \ll \beta$). In this phase, vehicles move smoothly with minimal interruptions, resulting in moderate CO_2 emissions. However, as traffic congestion increases and vehicles come to a halt during gridlock, emissions drop to zero since stationary vehicles do not produce additional CO_2. For an average vehicle speed ($\langle V \rangle_c$) of 2.5, CO_2 emissions increase to a maximum value of 16.48 (g/m) before entering a plateau region. This plateau occurs due to the heterogeneity in vehicle speeds within the traffic circle. Variations in individual vehicle speeds lead to stop-and-go conditions, which in turn cause increased fuel consumption and higher CO_2 emissions. When the average vehicle speed ($\langle V \rangle_c$) reaches 3, CO_2 emissions decrease again, peaking at 8.35 (g/m) before stabilizing in a new plateau region. This reduction in emissions is attributed to the fact that most vehicles are moving at their

optimal speeds with minimal acceleration and deceleration. At this optimal speed, the engine efficiency is higher, and fuel consumption—and thus CO_2 emissions—are lower. Overall, the observed trends highlight the complex dynamics between vehicle speed, traffic flow, and CO_2 emissions. Adaptive traffic lights play a crucial role in managing these dynamics by optimizing traffic flow and minimizing congestion, ultimately reducing CO_2 emissions.

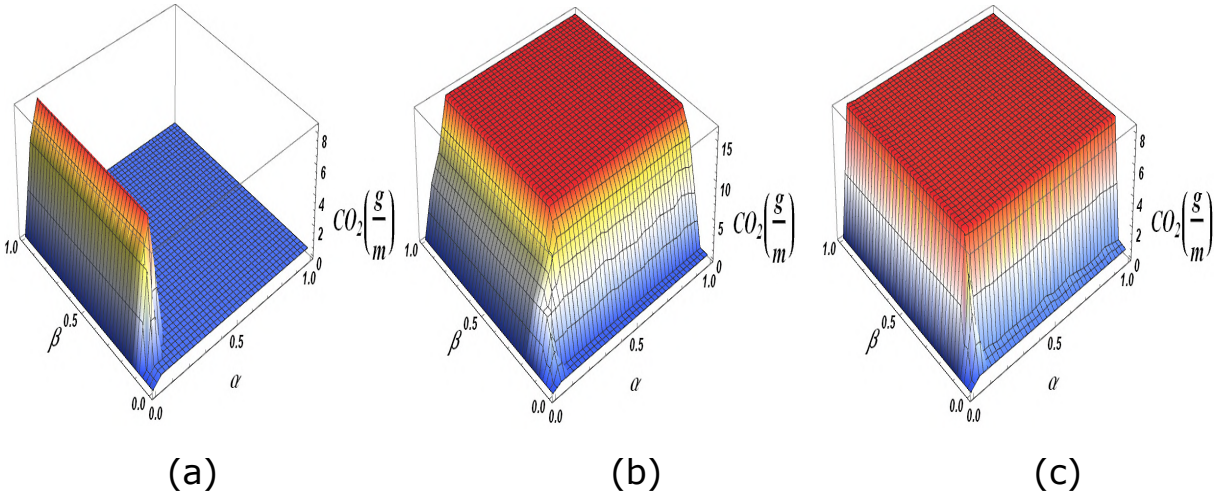

Figure 3.14: Carbon dioxide emission as a function of α and β where the adaptation criterion is done with different mean velocity values in circulating lane (a) $\langle V \rangle_c = 1.4$, (b) $\langle V \rangle_c = 2.5$ (c) $\langle V \rangle_c = 3$.

Next, we will discuss the distributions of time-to-collision (TTC) for different values of the critical mean velocity in Figure 3.15. As the critical mean velocity ($\langle V \rangle_c$) increases, the system experiences different impacts on time-to-collision (TTC) distributions, influencing the probability and severity of accidents. At lower mean velocities ($\langle V \rangle_c = 1.4$) (see Figure 3.15 (a)), traffic density is high, as shown in the space-time diagram in Figure 3.16 (a). This leads to frequent stops and starts, resulting in lower TTC values and a higher risk of minor collisions due to close vehicle proximity. At moderate velocities ($\langle V \rangle_c = 2.5$) (see Figure 3.15 (b)), the system reaches an efficient balance, maintaining moderate density and flow. The space-time diagram in Figure 3.15 (b) helps clarify this. However, there are still significant low TTC values, indicating potential minor collisions. At higher velocities ($\langle V \rangle_c = 3$) (see Figure 3.15 (c)), traffic density decreases, leading to higher TTC values with vehicles spaced further apart. This reduces the immediate risk of collisions but increases the severity of any that occur due to higher speeds. These dynamics underscore the importance of adaptive traffic control strategies to optimize safety and efficiency in traffic circle systems by managing vehicle speeds and traffic density effectively.

We will analyze the duration of red cycles, during which the red light is active at the entry lanes, to optimize the performance of adaptive traffic lights. Figure 3.17 provides a clear view of the red signal durations for different critical mean velocities ($\langle V \rangle_c$). At $\langle V \rangle_c = 1.4$, the red signal lasts for approximately 1 time step. For $\langle V \rangle_c = 2.5$, this duration extends to 8 time steps, and at $\langle V \rangle_c = 3$, it further increases to a maximum of 13 time steps. As the critical mean velocity increases, the time needed to clear vehicles from the circulating lane also increases, leading to longer red cycle durations. This is because higher velocities result in faster circulation within the traffic circle, causing vehicles to accumulate

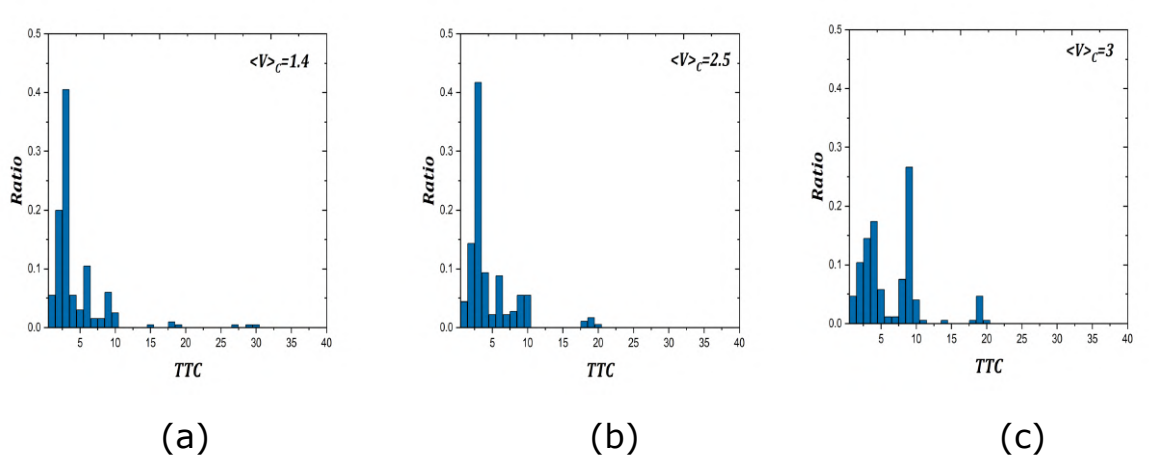

Figure 3.15: Time-to-collision distributions under various critical mean velocity values in the circulating lane (a) $\langle V \rangle_c = 1.4$, (b) $\langle V \rangle_c = 2.5$, (c) $\langle V \rangle_c = 3$.

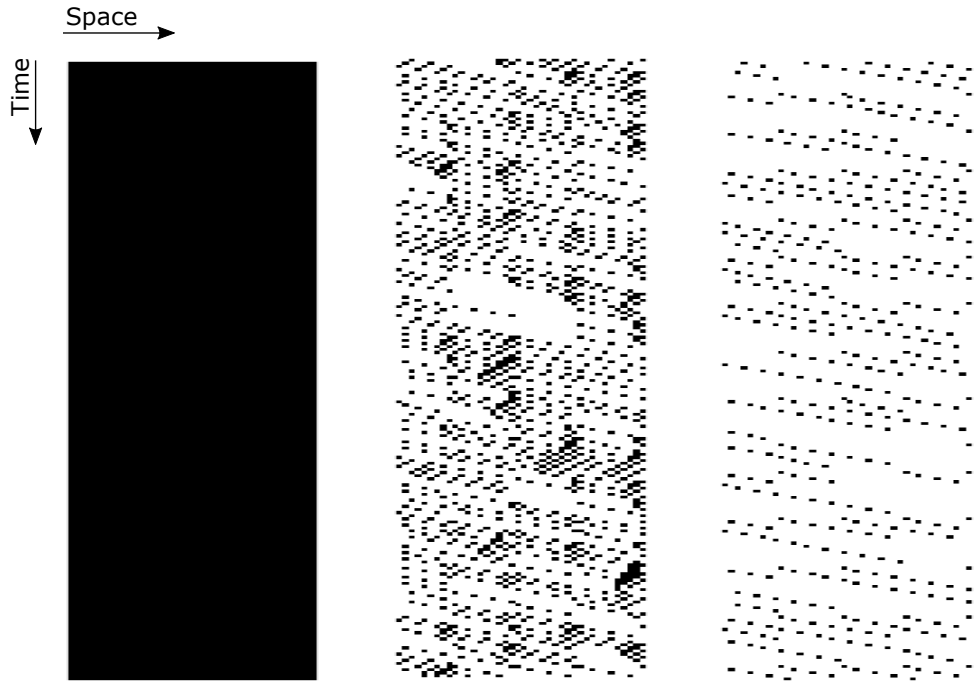

Figure 3.16: Space-time diagram for ($\alpha = 0.5$ and $\beta = 0.5$) where the adaptation criterion is done with different mean velocity values in the circulating lane (a) $\langle V \rangle_c = 1.4$, (b) $\langle V \rangle_c = 2.5$, (c) $\langle V \rangle_c = 3$. Black color corresponds to vehicles while free space is presented by white color.

more rapidly at the entry points. Consequently, longer red light periods are required to manage the flow effectively and prevent gridlock. The extended red cycles allow the circulating lane to clear out sufficiently before allowing more vehicles to enter, thereby maintaining a smooth and controlled traffic flow. By optimizing red cycle durations based on critical mean velocities, adaptive traffic lights can enhance overall traffic efficiency and reduce congestion within the traffic circle.

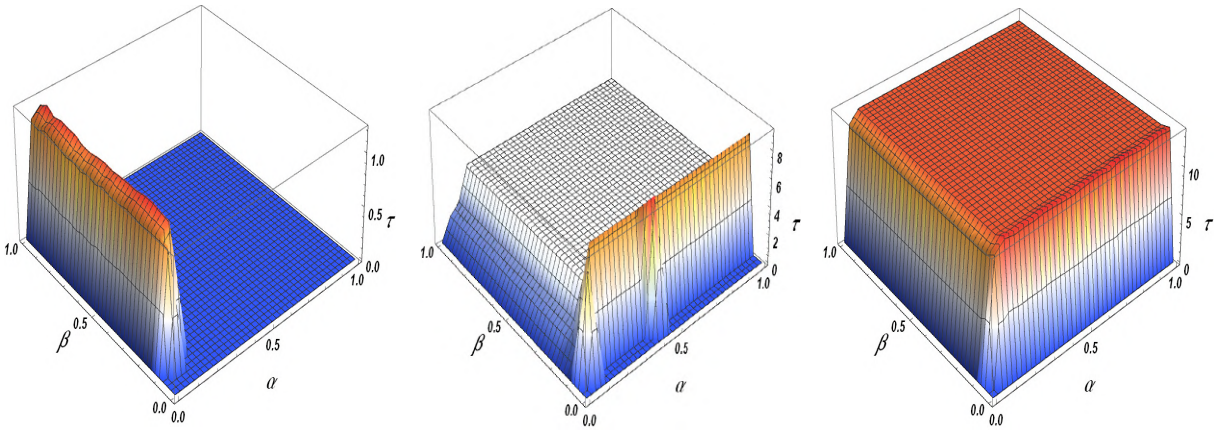

Figure 3.17: The time needed to remain red light in all entry lanes as a function of α and β, for (a) $\langle V \rangle_c = 1.4$, (c) $\langle V \rangle_c = 2.5$, (e) $\langle V \rangle_c = 3$.

3.4.4 Effect of time headway

The traffic condition within the circulating lane can be evaluated using the time headway, which represents the time interval between the arrivals of the front edge of two consecutive vehicles. This time difference indicates the gap between the passage of two successive vehicles i and $i+1$. The time headway can be expressed using the following relation:

$$t_{h(i+1,i)} = t_{i+1} - t_i \tag{3.5}$$

In general, the unit for measuring the flow of vehicles is given as (vehicles/second). The relationship between the mean time headways $\langle t_{h(i+1,i)} \rangle$ and the current vehicle flow J can be established using the following formula:

$$J = \frac{1}{\langle t_{h(i+1,i)} \rangle} \tag{3.6}$$

The traffic signal system adjusts to changes in the time headway in the following way: during each step of the simulation, the averge time headway for vehicles already present in the circulating lane, denoted as t_h, is calculated. If t_h is equal to or greater than the critical time headway t_{hc}, the traffic signals switch to red across all entry lanes.

Figure 3.18 shows the current as a function of the α and β rates, along with the associated phase diagram plotted in the (α, β) plane. For various values of the critical time headway ($t_{hc} = 3$, $t_{hc} = 8$, $t_{hc} = 15$), the following observations can be made: When the headway time t_{hc} is set to 15, there are no changes in the traffic flow phases compared to the traffic circle without adaptive traffic lights. For $t_{hc} = 8$, the jammed and the maximum current phases occur, effectively eliminating gridlock (which only occurs when $\beta = 0$). As t_{hc} decreases (see the case of $t_{hc} = 3$), the maximum current phase increases, accompanied by a decrease in jammed phase and the disappearance of the congestion phase. This change can be explained by the fact that lower t_{hc} values indicate the presence of a large flow of vehicles in the circulating lane, causing the traffic dynamics to be more dependent on boundary conditions (i.e., the inflow and outflow of vehicles). This ultimately increases the maximum current phase.

To better understand the throughput at various t_{hc} values, we assessed the traffic circle

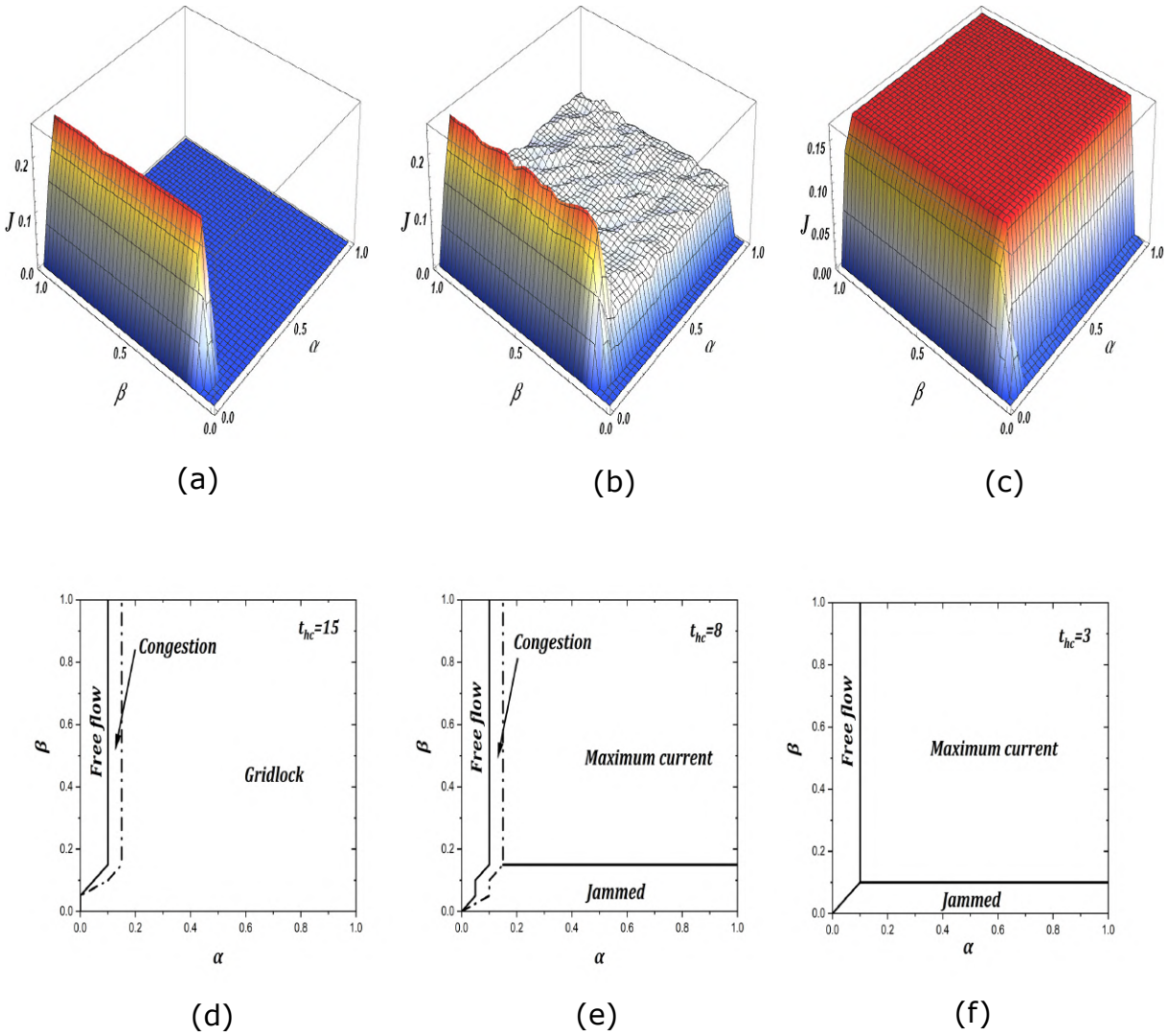

Figure 3.18: Current as a function of α for different β where the adaptation criterion is done with different time headway values in circulating lane (a) $t_{hc} = 15$, (c) $t_{hc} = 8$, (e) $t_{hc} = 3$. The phase diagram in the (α, β) plane (b) $t_{hc} = 15$, (d) $t_{hc} = 8$, (f) $t_{hc} = 3$.

system's capacity. Figure 3.19 shows how the capacity changes in relation to the critical time headway (t_{hc}) for both the circulating lane and the entry/exit lanes. The results indicate that the capacity increases steadily with the increase of t_{hc} until it reaches 0.25 for the circulating lane and 0.10 for the entry/exit lanes, after which it remains stable. This stability can be explained by the fact that when the critical time headway value exceeds 10, the system reaches its maximum flow rate. The critical time headway (t_{hc}) represents the minimum time gap between successive vehicles that the system can handle while maintaining optimal traffic flow. When t_{hc} is small, vehicles are too close together, leading to potential congestion and reduced capacity. As t_{hc} increases, vehicles are spaced out more evenly, allowing for smoother flow and higher throughput. Once t_{hc} surpasses 10, the time gaps between vehicles become sufficient to ensure that vehicles can enter, circulate, and exit the traffic circle without causing deadlock. This optimal spacing means that the system can handle the maximum number of vehicles efficiently, and any further increase in t_{hc} does not contribute to a significant improvement in capacity. At this point, the traffic system operates at its peak efficiency, where the time gaps between vehicles

are just right to maintain a continuous and smooth flow. Consequently, even when the traffic light switches to red, the flow rate remains stable because the system has already optimized the entry and circulation of vehicles. The red light intervals are calibrated to ensure that vehicles can clear the circulating lane without causing backlogs at the entry points. Notably, the circulating lane has a higher capacity compared to the entry/exit lanes. This can be attributed to the increased maximum flow rate resulting from the merging of traffic from multiple entry lanes into the circulating lane.

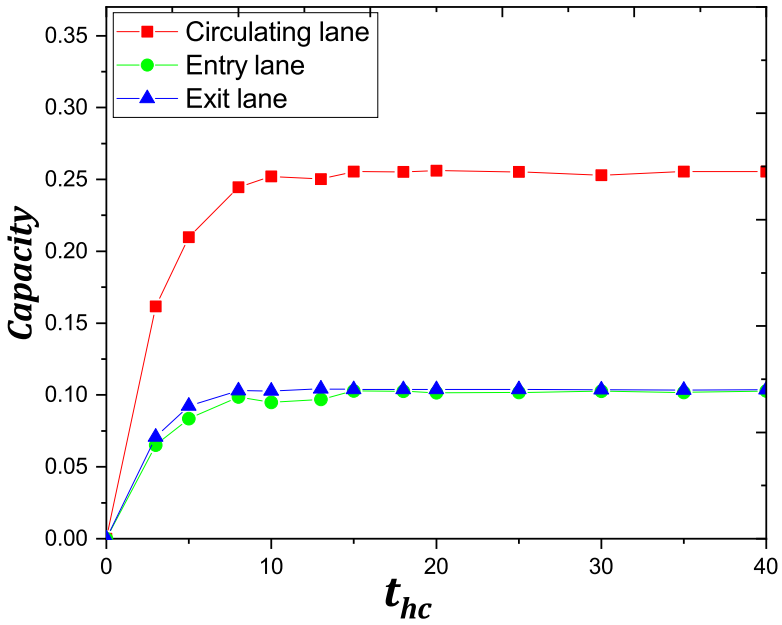

Figure 3.19: Capacity as a function of time headway t_{hc} for the circulating lane and entry/exit lanes.

Next, we will analyze the CO_2 emissions within the traffic circle system with adaptive traffic lights in the circulating lane (see Figure 3.20 (a)) for different critical time headways. For $t_{hc} = 15$, free-flowing traffic conditions result in a peak CO_2 emission of 8.41 (g/m), represented by ($\alpha \ll \beta$). Moderate CO_2 emissions are produced during this phase by vehicles moving steadily and with few interruptions. However, as traffic congestion worsens and cars stop moving during a jam, emissions decrease to zero since stationary vehicles don't emit any more CO_2. For $t_{hc} = 8$ (Figure 3.20 (b)), CO_2 emissions reach a peak of 8.24 g/m under free-flow conditions. However, as traffic density increases and the system approaches more congested conditions, CO_2 emissions start to decrease. This decrease can be attributed to the reduced speed and more frequent stopping of vehicles, which lower fuel consumption rates compared to the higher speeds of free-flowing traffic. As vehicles slow down and the traffic density continues to rise, emissions stabilize and form a plateau region at approximately 2.6 (g/m). This plateau indicates that the emissions have reached a relatively steady state, where the combination of lower speeds and stop-and-go traffic results in a consistent, albeit lower, level of CO_2 emissions compared to the peak observed during free flow. When the critical time headway decreases further, as in the case of $t_{hc} = 3$ (Figure 3.20 (c)), CO_2 emissions reach their maximum of 8.36 (g/m) for all values of α and β. This suggests that very short time headways lead to high vehicle

density and significant emissions due to frequent stops and starts, which are typical in congested traffic conditions. It is important to note that CO_2 emissions cease completely when $\beta = 0$, meaning no vehicles are leaving the circulating lane, indicating a complete traffic standstill.

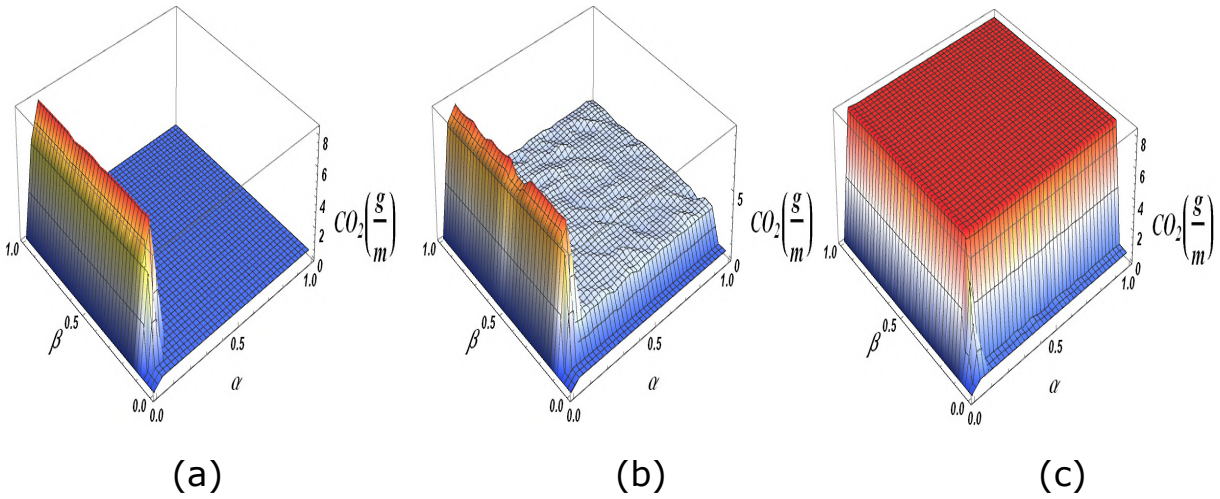

Figure 3.20: Carbon dioxide emission as a function of α and β where the adaptation criterion is done with different time headway values in circulating lane (a) $t_{hc} = 15$, (b) $t_{hc} = 8$, (c) $t_{hc} = 3$.

We will now present the distributions of time-to-collision (TTC) for various values of the critical time headway ($t_{hc} = 15$, $t_{hc} = 8$, $t_{hc} = 3$). The results in Figure 3.21 show that as the critical time headway increases (for $t_{hc} = 15$ and $t_{hc} = 8$), the frequency of low TTC values also rises. This suggests a negative effect on traffic safety, implying a heightened risk of collisions if vehicles attempt to move without sufficient spacing between them, as depicted in the space-time diagrams (see Figure 3.22(a, b)). The diagrams reveal clusters of stopped vehicles, indicating increased interactions and potential for accidents. These clusters highlight the congestion and risk associated with insufficient spacing between vehicles. Conversely, a reduction in the critical time headway (as seen for $t_{hc} = 3$ in Figure 3.21 (c)) leads to an increase in the frequency of higher TTC values. This indicates an enhancement in safety and smoother traffic flow, as shown in Figure 3.22 (c). Shorter critical time headways allow vehicles to maintain safer distances more consistently, reducing the probability of sudden braking or collisions.

To ensure the efficiency of adaptive traffic lights, we analyze the red cycle lengths, during which the red light remains active at the entry lanes (see Figure 3.23). The results show that for $t_{hc} = 15$, the maximum duration that the red light stays lit is about 1 time step. For $t_{hc} = 8$, this duration increases to up to 8 time steps. For $t_{hc} = 3$, the red light remains active for up to 13 time steps. As the critical time headway decreases, the time needed to reduce the number of vehicles in the circulating lane increases, which in turn extends the red cycle lengths. This phenomenon can be explained by the increased traffic density and flow dynamics within the circulating lane. When the critical time headway is shorter, vehicles have less time to safely enter and exit the circulating lane, resulting in a higher accumulation of vehicles. To prevent congestion and ensure a smooth flow of traffic, the traffic lights must stay red for longer periods to allow the circulating lane to clear out sufficiently before new vehicles enter.

Assessing the critical time headway in the circulating lane, which is used as feedback

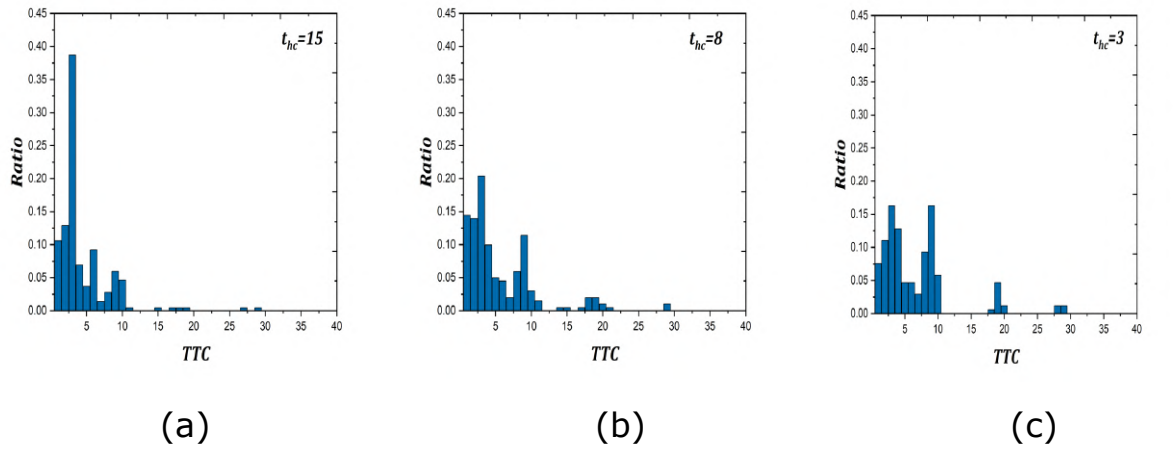

Figure 3.21: Time-to-collision distributions under various critical mean velocity values in circulating lane (a) $t_{hc} = 15$, (b) $t_{hc} = 8$, (c) $t_{hc} = 3$.

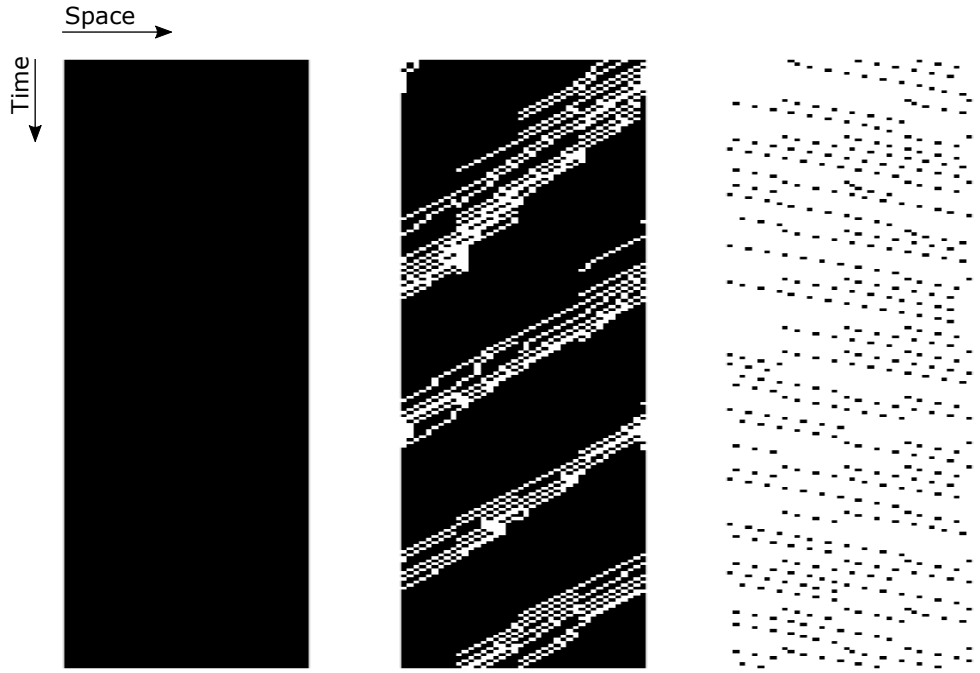

Figure 3.22: Space-time diagram for ($\alpha = 0.5$ and $\beta = 0.5$) where the adaptation criterion is done with different time headway values in circulating lane (a) $t_{hc} = 15$, (b) $t_{hc} = 8$, (c) $t_{hc} = 3$. Black color corresponds to vehicles while free space is presented by white color.

to regulate traffic from the entry lanes, can potentially enhance the usage of the traffic circle system. Nonetheless, exploring additional parameters as feedback can significantly improve the system's efficiency. In the upcoming subsection, we will focus on assessing the density of stopped cars as a feedback control parameter. This approach aims to effectively manage adaptive traffic lights at the entry lanes and improve overall traffic management within the system.

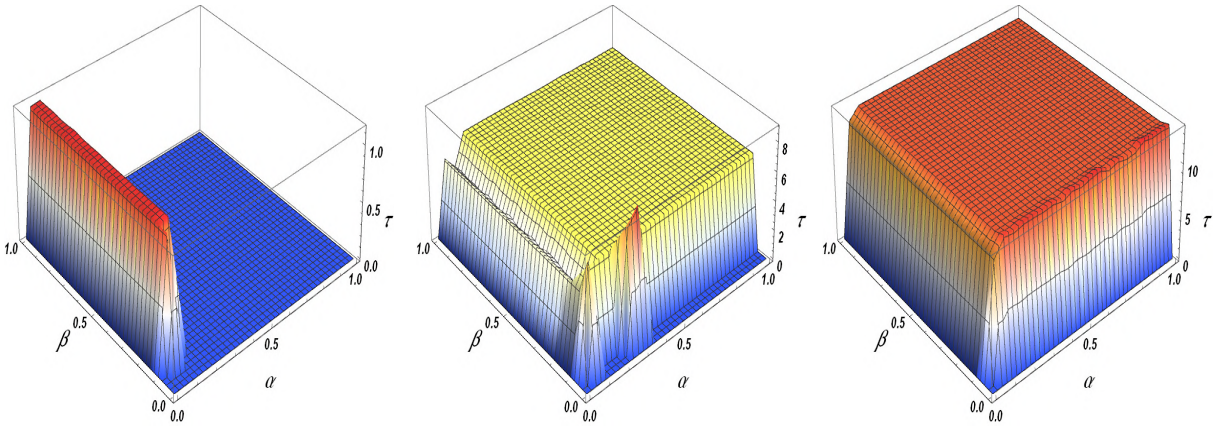

Figure 3.23: The time needed to remain the red light in all entry lanes as a function of α and β, for (a) $t_{hc} = 15$, (b) $t_{hc} = 8$, (c) $t_{hc} = 3$.

3.4.5 Effect of density of stopped cars

The traffic condition within the circulating lane can also be evaluated using the density of stopped cars. We define the density of stopped cars, represented as ρ_{SC}, with the following formula:

$$\rho_{\mathrm{SC}} = \frac{N'_V}{L_1} \tag{3.7}$$

In this analysis, we use N'_V to represent the number of stopped vehicles in the circulating lane. To understand the impact of traffic control on throughput within the traffic circle system, we examine the current as a function of the α and β rates in Figure 3.24. We also present the corresponding phase diagram on the (α, β) plane. This analysis covers a diverse range of the critical density of stopped cars ($f = 80\,\%, f = 55\,\%, f = 20\,\%$).

A notable observation is the complete elimination of gridlock, allowing the maximum current and jamming phases to be more prominent. As the critical density of stopped cars declines, the free flow and jamming phases expand at the expense of the maximum current phase, effectively eliminating congestion. This implies a significant change in vehicle interactions within the circulating lane due to the integration of the control strategy. We attribute the expansion of the free flow phase, resulting from a reduction in the percentage of the critical density of stopped cars f, to the decrease in the number of vehicles within the circulating lane. This reduction diminishes interactions between vehicles, thereby improving traffic flow conditions.

To better understand the throughput for various f values, we evaluated the traffic circle system's capacity. Figure 3.25 shows the progression of capacity as a function of the percentage of the critical density of stopped cars for both the circulating lane and entry/exit lanes. The results indicate that the capacity reaches a peak of 0.41 for the circulating lane and 0.17 for the entry/exit lanes, followed by gradual decreases before stabilizing. This behavior can be explained by the fact that an increase in stationary vehicles leads to a decline in capacity. As the number of stopped vehicles grows, the effective flow of traffic is impeded, causing a reduction in overall capacity. Once the lanes become saturated with stationary vehicles, the capacity stabilizes because the system cannot accommodate additional traffic, and the flow reaches a point of equilibrium. Notably, the circulating

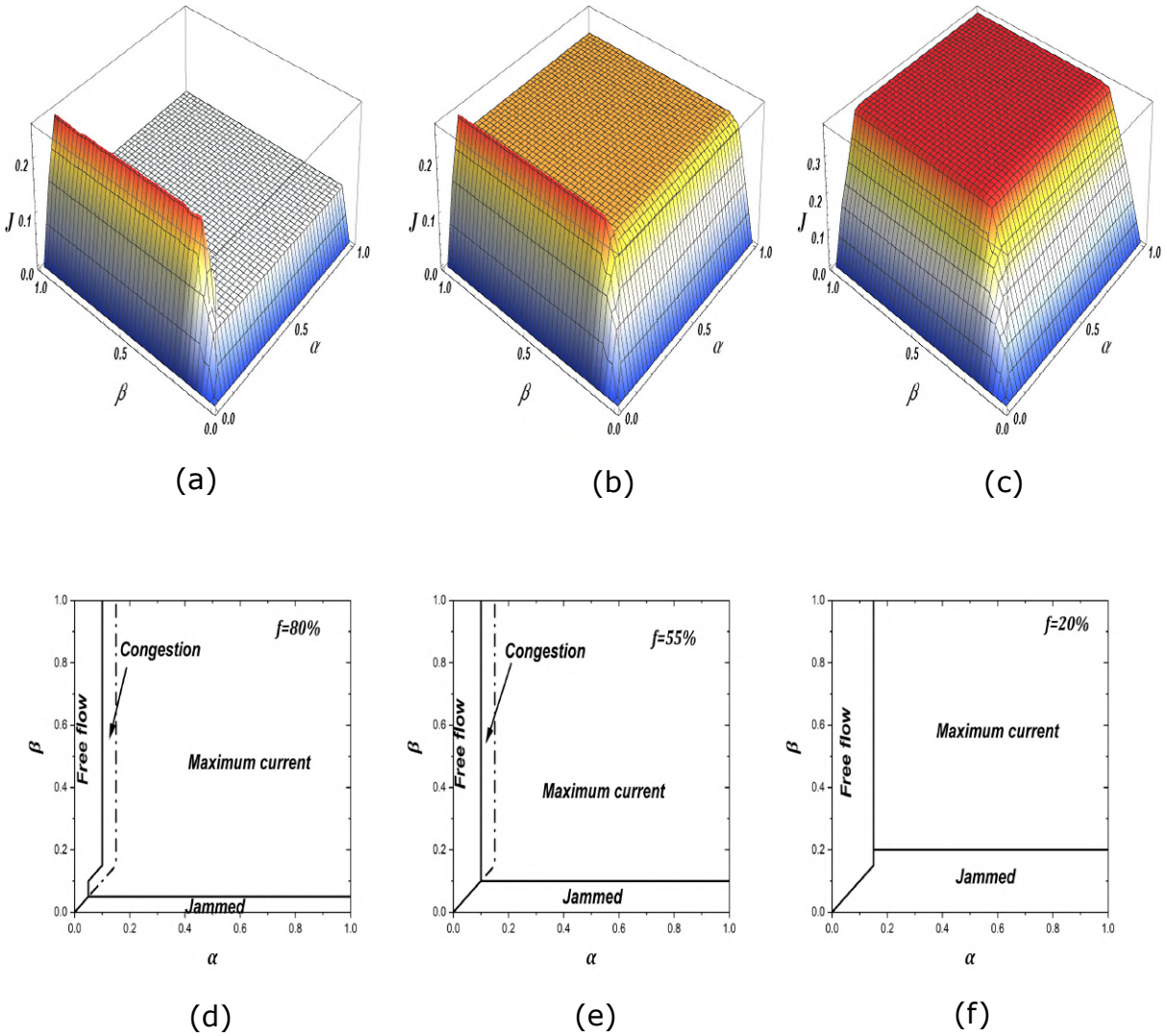

Figure 3.24: Current as a function of α for different β where the adaptation criterion is done with different density of stopped cars values in circulating lane (a) $f = 80\,\%$, (c) $f = 55\,\%$, (e) $f = 20\,\%$. The phase diagram in the (α, β) plane (b) $f = 80\,\%$, (d) $f = 55\,\%$, (f) $f = 20\,\%$.

lane consistently has a higher capacity compared to the entry/exit lanes. This difference is attributed to the increased maximum flow resulting from the merging of traffic from multiple entry lanes into the circulating lane. The circulating lane benefits from continuous movement and higher throughput, while the entry/exit lanes experience interruptions due to vehicles entering and exiting the traffic circle.

In the following analysis, we will examine the CO_2 emissions within the traffic circle system with adaptive traffic lights in the circulating lane for different percentages of critical density of stopped cars (refer to Figure 3.26). For both Figures 3.26 (a) and 3.26 (b), CO_2 emissions reach up to 8.47 (g/m) in free-flowing traffic. This high emission level is due to vehicles moving at higher speeds and maintaining a steady flow, which typically results in higher fuel consumption and thus greater CO_2 emissions. However, as traffic flow becomes more congested, vehicles slow down or stop more frequently, leading to a reduction in overall fuel consumption and CO_2 emissions. For $f = 80\%$, emissions decline to a minimum value of approximately 2.9 (g/m), and for $f = 55\%$, they decline

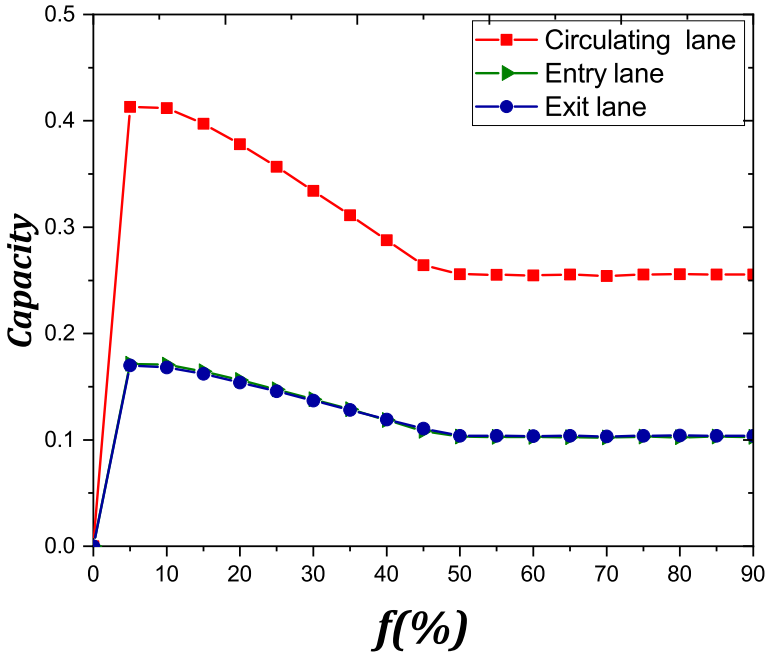

Figure 3.25: Capacity as a function of density of stopped cars f for circulating lane and entry/exit lanes.

to 6.5 (g/m). After reaching these minimum values, the emissions form a plateau region, indicating a stable emission rate despite further increases in the injection α and extraction β rates. This stability suggests that the system has reached a point where additional congestion does not significantly alter the emission levels. In contrast, for a lower density of stopped cars ($f = 20\%$), CO_2 emissions increase up to 14.16 (g/m). This increase is due to the injection α and extraction β rates of vehicles, which cause frequent stops and starts. These frequent changes in speed and stopping patterns lead to inefficient fuel usage, resulting in higher CO_2 emissions. The higher interaction between moving and stopping vehicles at this lower density contributes to the maximum emission region.

Next, we will present the time-to-collision (TTC) distributions for different percentages of the critical density of stopped cars ($f = 80\%$, $f = 55\%$, $f = 20\%$). As shown in Figure 3.27, there is no linear relationship between the increase in f and the TTC distributions for various values of f. The highest TTC frequency recorded is 0.48, observed at $f = 80\%$. This can be explained by referring to the space-time diagram presented in Figure 3.28 (a), which shows a significant increase in stopped vehicles, leading to a higher probability of car accidents due to reduced mobility and increased traffic density. Following this, a frequency of 0.45 is observed for $f = 20\%$. The space-time diagram (Figure 3.28 (b)) illustrates an increase in moving vehicles, which subsequently raises the probability of accidents between moving vehicles due to higher interaction rates. On the other hand, the lowest frequency, 0.40, is recorded for $f = 55\%$. This observation is supported by the space-time diagram (Figure 3.28 (c)), where the number of stopped and moving vehicles is approximately equal, resulting in a balanced traffic flow that reduces the possibility of collisions. These findings highlight the complex relationship between the density of stopped cars and traffic safety. A higher percentage of stopped cars can significantly increase the probability of collisions

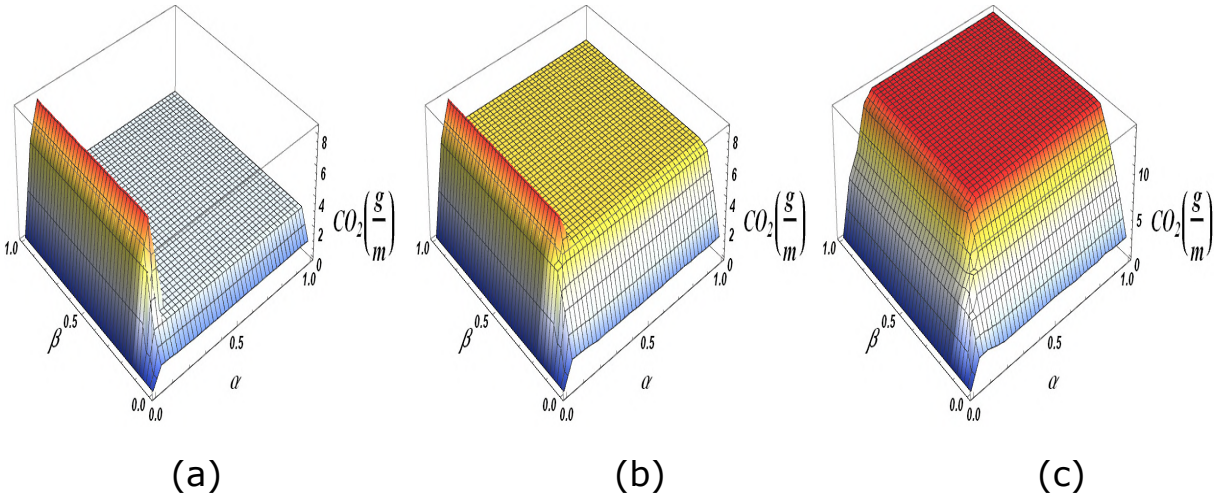

Figure 3.26: Carbon dioxide emission as a function of α and β where the adaptation criterion is done with different density of stopped cars values in circulating lane (a) $f = 80\,\%$, (b) $f = 55\,\%$, (c) $f = 20\,\%$.

due to congestion and reduced maneuverability, whereas a balanced mix of stopped and moving vehicles tends to promote safer traffic conditions. Understanding these dynamics is crucial for optimizing traffic control strategies to enhance safety and efficiency within traffic circles.

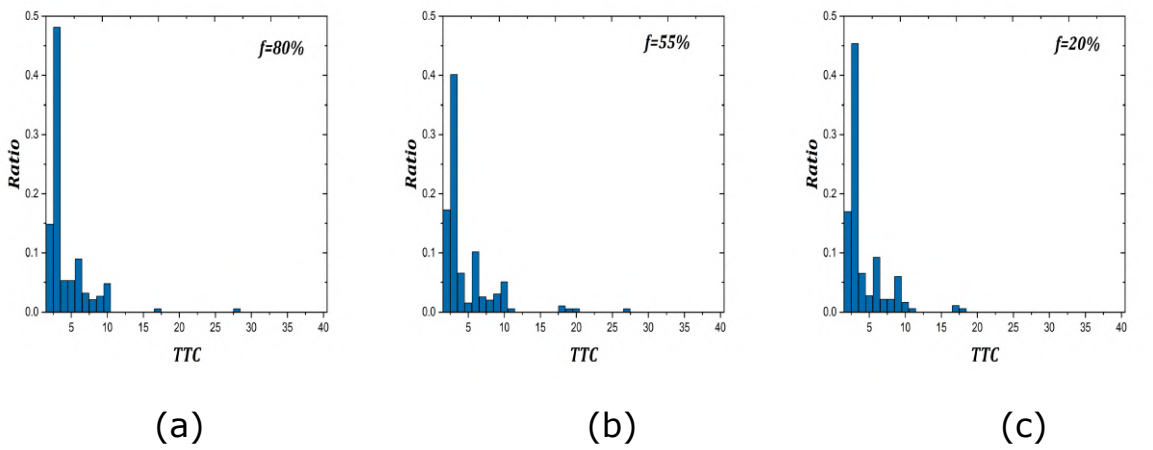

Figure 3.27: Time-to-collision distributions under various critical densities of stopped car values in circulating lane (a) $f = 80\%$, (b) $f = 55\%$, (c) $f = 20\%$.

To ensure the optimal performance of adaptive traffic lights, we analyze the red cycle lengths, during which the red light remains active at the entry lanes. From Figure 3.29, we observe that for $f = 80\%$, the maximum duration of the red signal is approximately 7 time steps. For $f = 55\%$, this duration extends up to 17 time steps, and for $f = 20\%$, it further increases to a maximum of 29 time steps. As the percentage of the critical density of stopped cars decreases, the time required to clear vehicles from the circulating lane increases, subsequently lengthening the red cycle durations. This phenomenon can be explained by examining the traffic conditions within the circulating lane. With a lower percentage of stopped cars, vehicles in the circulating lane move more freely, leading to more vehicles entering from the entry lanes. This increased influx necessitates longer red

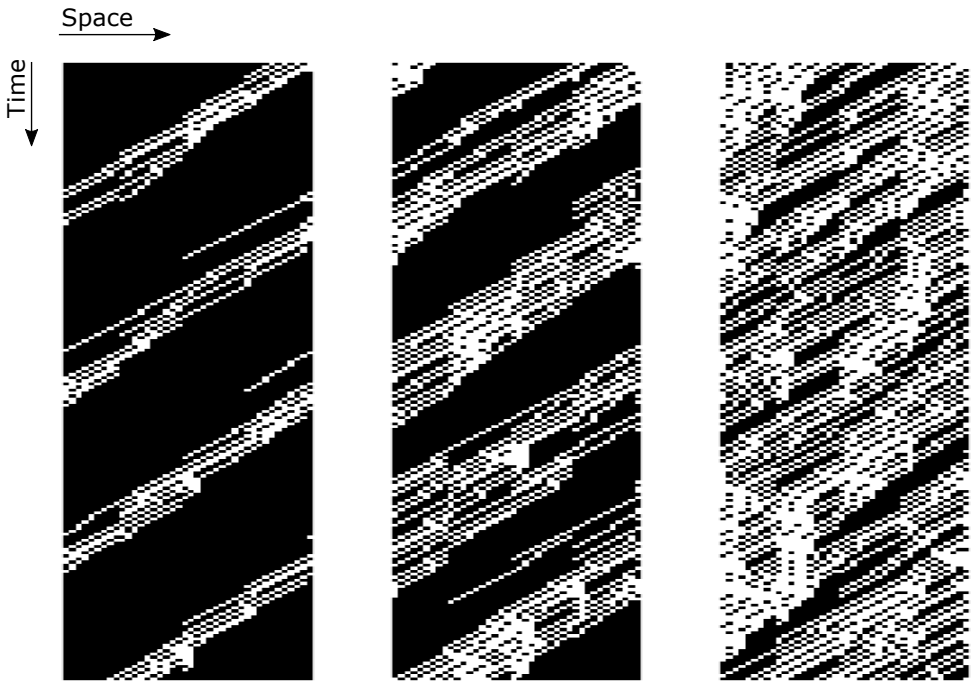

Figure 3.28: Space-time diagram for ($\alpha = 0.5$ and $\beta = 0.5$) where the adaptation criterion is done with different densities of stopped cars values in circulating lane (a) $f = 80\%$, (b) $f = 55\%$, (c) $f = 20\%$. Black color corresponds to vehicles while free space is presented by white color.

signal cycles to effectively manage and clear the circulating lane, ensuring a smooth traffic flow and preventing congestion. Additionally, a reduced percentage of stopped cars means that vehicles are moving faster, creating more dynamic and variable traffic conditions. Adaptive traffic lights need to respond to these changing conditions by extending the red signal duration to balance the inflow and outflow of vehicles, thereby maintaining an optimal flow within the traffic circle. Understanding these dynamics is crucial for designing adaptive traffic light systems that can efficiently handle varying traffic densities and maintain overall traffic efficiency.

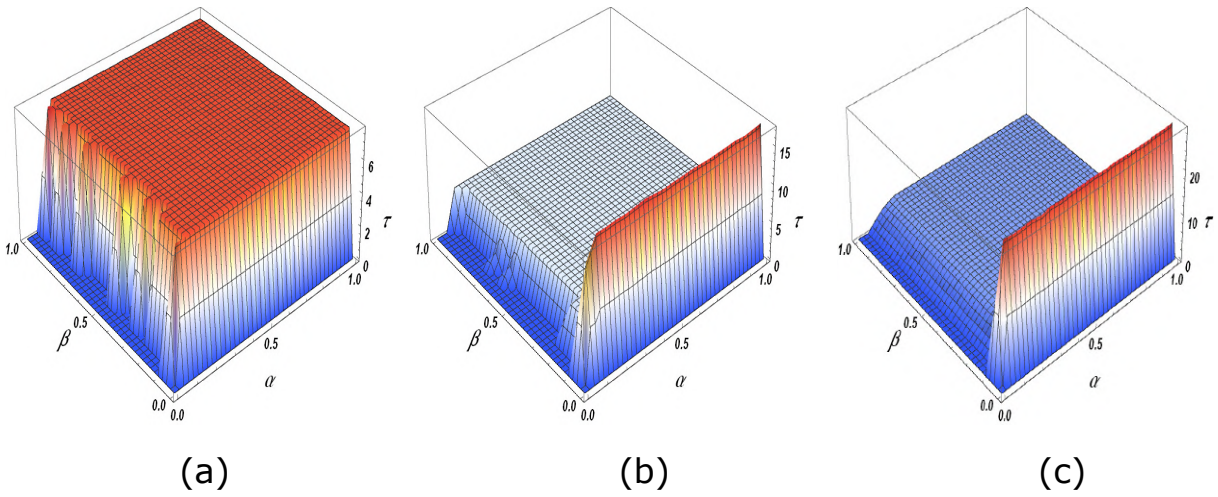

Figure 3.29: The time needed to remain red light in all entry lanes as a function of α and β, for (a) $f = 80\%$, (b) $f = 55\%$, (c) $f = 20\%$.

3.5 Conclusion

The primary challenges of an unsignalized intersection are mutual blocking and traffic congestion at the nearby intersection caused by a higher arrival rate. Adaptive traffic lights are one of the solutions available to enhance traffic control at these intersections. A hybrid system can be implemented, where traffic lights operate when traffic conditions exceed a critical threshold, and priority rules govern the intersection otherwise. In this study, we propose a hybrid traffic control cellular automaton model that combines traffic lights and priority rules. Traffic lights are used to regulate the entry lanes, and feedback from the flow of traffic in the circulating lane is utilized. The density, satisfaction rate,averge speed, time headway and density of stopped cars of the circulating lane rate provide valuable information. Our research shows that adaptive traffic lights can significantly improve the efficiency of a traffic circle system. By eliminating the gridlock phase and making the maximum current, congestion, and jammed phases more prominent, adaptive traffic lights can enhance traffic flow. We conducted a comparative analysis of various adaptation criteria. Our results indicate that the density criterion yields better outcomes in terms of of the duration of the red light in entry lanes, while the satisfaction rate criterion produces superior results in terms of capacity. Using average speed to manage emissions ensures efficient vehicle movement without excessive acceleration or deceleration. Applying critical time headway optimizes capacity and maintains a smooth flow, avoiding congestion and ensuring maximum throughput. Incorporating the density of stopped cars enhances safety by adjusting red signal durations dynamically and preventing excessive vehicle clustering. By leveraging the strengths of each parameter, traffic management systems can achieve a balanced, efficient, and safe traffic circle operation, minimizing emissions, maximizing capacity, and reducing collision risks. Although we believe there are many more factors to consider and use as input to better control the traffic circle system, this work can be seen as an effort to understand and predict the potential consequences of using adaptive traffic signals in the traffic circle system.

General conclusion

Cost-effective traffic management techniques are necessary to address transportation-related challenges, as building new infrastructure is not a solution to the underlying causes of these issues. Instead, traffic should be analyzed and managed using intelligent methods. One such method is to provide accurate models that are useful resources for understanding the complex dynamics of vehicle interactions. These models simulate the movements of multiple vehicles within a specific environment and provide a comprehensive understanding of the interactions between them and their surrounding environment. They not only identify the underlying causes of traffic congestion and other phenomena through meticulous analysis but also shed light on the multitude of variables influencing vehicle interactions. They also offer insightful information on how these relationships affect energy dissipation and environmental pollution. Through the examination of individual vehicle interactions and their contributions to the overall traffic flow, these models help in the development of more efficient and sustainable transportation systems.

The first chapter of this thesis provided a comprehensive overview of the complex subject of traffic flow theory and the tools used to study it. The evolution of traffic flow theory was meticulously tracked, and the underlying causes of traffic dynamics were extensively examined, from minute details to large-scale events. Empirical traffic flow patterns were analyzed, addressing issues such as congestion and explaining the principles of hysteresis, metastability, and fundamental diagrams. A variety of modeling techniques, including macroscopic, microscopic, and mesoscopic models, were carefully examined, addressing both theoretical concerns and realistic road traffic modeling. The intricacies and extensions of the NaSch cellular automata model were explored. After that, vital subjects linked to environmental impacts, such as energy dissipation and pollutant emissions, and the characteristics of road infrastructure components were investigated. After reading this chapter, researchers interested in this field will have a firm grasp of traffic analysis techniques and a thorough comprehension of the Monte Carlo simulation tools that are used to examine the complex dynamics that underlie traffic systems.

Circular intersections, such as roundabouts and traffic circles, are one type of intersection that can improve traffic flow and reduce congestion. They offer increased capacity, decreased delays, and improved environmental quality. For these reasons, we have chosen this type of intersection as the subject of our thesis. Our goal is to investigate and analyze various factors that affect the performance of circular intersections and the environmental sustainability of such intersections, utilizing comprehensive modeling and simulation techniques. To simulate traffic flow dynamics, we use the Nagel-Schreckenberg (NaSch) cellular automata model in this thesis. The main benefit of the NaSch model is its simplicity, which makes it easy to apply and analyze while retaining many of the complex details of actual traffic flow. These characteristics include vehicle acceleration and deceleration behaviors, various traffic phases, stop-and-go waves, hysteresis effects, and the creation and dissolving of traffic jams. A large number of characteristics, including vehicle density, speed limitations, and driver behavior, can also be included in the NaSch model. Furthermore, the NaSch model offers a helpful framework for researching how traffic flow affects energy

dissipation and carbon dioxide emissions, among other environmental effects.

Our contribution to the theory of traffic flow is evident in the second and third chapters of this thesis, where we focus on the study of traffic flow dynamics in roundabouts and traffic circle systems. In the second chapter, we identify a gap in knowledge regarding the impact of vehicles making complete turns, whether U-turns or continuous turns, within roundabouts on traffic dynamics and environmental factors, such as CO2 emissions and energy dissipation patterns. We analyze the complex links between full-turn maneuvers, traffic flow measurements, and environmental implications, revealing that such maneuvers increase congestion in the entry lane due to priority rules. This leads to waiting queues and has multiple effects on energy dissipation and CO2 emissions across all lanes. The chapter also examines the effects of vehicles not respecting the safety gap at entering the circulating lane on the capacity of the roundabout system and suggests using traffic lights to reduce these kinds of interactions. The chapter emphasizes the significance of taking environmental effects into account in transportation design by offering insights into efficiently controlling traffic flow dynamics and optimizing roundabout functionality through thorough analysis.

In the third chapter, we investigate the impact of adaptive traffic lights on the throughput of a traffic circle system. The study aims to preserve the priority rules of traffic circles while preventing deadlock resulting from mutual obstruction. One potential solution to improve traffic control at these intersections is the installation of adaptive traffic lights. We present a hybrid traffic control (traffic lights and priority rules) cellular automaton model in this chapter. In this model, entry lanes are controlled by traffic lights that utilize density, satisfaction rate, average speed, time headway, and the density of stopped cars as feedback to regulate the traffic flow in the circulating lane. The flow of traffic in the circulating lane is assessed, and based on the provided information, the traffic lights in the entry lanes switch to red to decrease incoming traffic and effectively manage the intersection. This chapter answers the pivotal question for this study: do traffic circles with adaptive lights work better? The study finds that yes, they improve traffic flow by reducing vehicle buildup in the circulating lane, which eases interactions between vehicles and allows more vehicles to pass overall. The study demonstrates the importance of managing intersections properly for urban planning and transportation administration. It offers practical ideas for making transportation networks more efficient.

While the NaSch model is a useful tool for simulating traffic flow in roundabouts and traffic circle systems, it has limitations. One of the main drawbacks of the NaSch model is its oversimplified methodology, which assumes uniform vehicle acceleration and deceleration based on predetermined criteria. This can result in inaccuracies when representing changes in traffic phases, such as the transition from uncongested to congested situations. To address these limitations, researchers can combine the NaSch model with additional modeling methods, such as macroscopic models or fluid dynamics analogies. By combining multiple modeling approaches, researchers can gain a more comprehensive understanding of roundabout traffic flow.

Finally, there is a need for more research on the environmental impact of traffic flow in roundabouts and traffic circle systems. This includes studies on energy consumption, air pollution, and noise pollution. By better understanding these impacts, we can develop more sustainable transportation systems that meet the needs of all stakeholders. This can be accomplished through the use of simulation models to test different scenarios and identify the most environmentally friendly designs and traffic management strategies. Overall, future research on traffic flow in roundabouts and traffic circle systems has the potential

to improve transportation efficiency, reduce congestion, and promote sustainability.

Besides the contributions made in this thesis, there are several perspectives for future investigation concerning traffic flow. One potential direction is studying the impact of exclusive turn lanes in roundabouts on traffic fluidity and the environment. This could provide insights into whether such designs can improve traffic flow and reduce emissions. Another area of interest is the development of adaptive traffic regulation strategies based on the state of traffic lanes and entries at roundabouts. These strategies aim to ensure smooth and secure traffic flow. Additionally, real-time optimization of traffic regulation in roundabouts using artificial intelligence could lead to efficient, safe, and eco-friendly traffic management.

Examining the effects of connected and autonomous vehicles (CAVs) on traffic flow in transportation networks is also crucial. With the increasing emergence of CAVs, it is critical to understand their interaction with traditional vehicles and how they might alter traffic patterns. CAVs have the potential to significantly improve traffic flow and reduce congestion but also present challenges in ensuring safe and efficient interaction with human-driven vehicles.

Another perspective involves investigating the effects of various road designs and geometries on traffic flow in roundabout systems. The design of these intersections can significantly impact traffic flow and congestion. By optimizing the architecture of these intersections, it may be possible to further reduce congestion and enhance traffic flow. This can be achieved through the use of simulation models, such as the NaSch model, to test different design scenarios and identify the most effective designs.

Appendix A

List of Publications and Presentations

List of Publications

1 A. Ez-Zahar, H. Ez-Zahraouy, K. Bentaleb, A. Khallouk, & N. Lakouari. (2021). "Simulation study of the traffic circle system with adaptive traffic lights". Modern Physics Letters B, 35(16), 2150268.

2 A. Ez-Zahar, N. Lakouari, O. Oubram, R. Marzoug, & H. Ez-Zahaoury. (2024). "Analyzing Single-Lane Roundabout Traffic and Environmental Impacts through Cellular Automaton: A Focus on U-Turn Effects". International Journal of Modern Physics C.

Articles in the process of publication

3 A. Ez-Zahar, N. Lakouari,O. Oubram,R. J. Guadalupe Velásquez Aguilar, & H. Ez-Zahaoury. "Adaptive Traffic Control in Traffic Circle System: A Simulation-based Comparative Study".

Contributed presentations

4 A. Ez-Zahar, N. Lakouari,O. Oubram,R. J. Guadalupe Velásquez Aguilar, & H. Ez-Zahaoury. "Simulation Analysis of Traffic Management in Roundabout Systems". Oral presentation at the 4th International Conference on Innovative Research in Applied Science, Engineering and Technology - IRASET'2024 on 16-17 may 2024 in Faculty of Sciences Dhar El Mahraz - Fez, Morocco.

5 A. Ez-Zahar, N. Lakouari, & H. Ez-Zahaoury. "The prediction of the flow in the roundabout intersection based on cellular automata (CA) and artificial neural networks (ANNs)". Oral presentation at the third annual Inter-Lab-LaMCScI-LERMA-Meeting-2022 on 15-16 December 2022 in Faculty of Sciences - Rabat, Morocco.

6 A. Ez-Zahar, N. Lakouari, & H. Ez-Zahaoury. "The effect of U-turning manoeuver on the roundabout traffic flow". Poster presentation at the second annual Inter-Lab-LaMCScI-LERMA-Meeting-2019 on 9-11 December 2022 in Faculty of Sciences - Rabat, Morocco.

Bibliography

[1] F. v. Wageningen-Kessels, H. Van Lint, K. Vuik, and S. Hoogendoorn. *EURO Journal on Transportation and Logistics*, 4(4):445–473, 2015.

[2] C. F. Daganzo. *Transportation research part B: methodological*, 28(4):269–287, 1994.

[3] S. Smulders. *Transportation Research Part B: Methodological*, 24(2):111–132, 1990.

[4] M. J. Lighthill and G. B. Whitham. *Proceedings of the royal society of london. series a. mathematical and physical sciences*, 229(1178):317–345, 1955.

[5] B. D. Greenshields. *Highway Research Board Proc., 1935*, pages 448–477, 1935.

[6] J. G. Wardrop. *Proceedings of the institution of civil engineers*, 1(3):325–362, 1952.

[7] P. I. Richards. *Operations research*, 4(1):42–51, 1956.

[8] R. Herman. In *International Symposium on the Theory of Traffic Flow, 1st, 1959, Warren, Michigan, USA*, 1961.

[9] I. Prigogine. *Theory of traffic flow*, 1961.

[10] H. J. Payne. *Mathematical Model of Public System*, pages 51–61, 1971.

[11] A. Aw and M. Rascle. *SIAM journal on applied mathematics*, 60(3):916–938, 2000.

[12] D. Helbing. *Reviews of modern physics*, 73(4):1067, 2001.

[13] C. F. Daganzo. *Transportation Research Part B: Methodological*, 29(4):277–286, 1995.

[14] M. J. Cassidy. In *Handbook of Transportation Science*, pages 151–186. Springer, 1999.

[15] M. Cremer and J. Ludwig. *Mathematics and computers in simulation*, 28(4):297–303, 1986.

[16] K. Nagel and M. Schreckenberg. *Journal de physique I*, 2(12):2221–2229, 1992.

[17] M. Treiber, A. Hennecke, and D. Helbing. *Physical review E*, 62(2):1805, 2000.

[18] B. S. Kerner. *Physica A: Statistical Mechanics and its Applications*, 333:379–440, 2004.

[19] A. Schadschneider, D. Chowdhury, and K. Nishinari. *Stochastic transport in complex systems: from molecules to vehicles*. Elsevier, 2010.

[20] L. Neubert, L. Santen, A. Schadschneider, and M. Schreckenberg. *Physical Review E*, 60(6):6480, 1999.

[21] M. Treiber and A. Kesting. *Springer-Verlag Berlin Heidelberg*, pages 983–1000, 2013.

[22] J. Treiterer and J. Myers. *Transportation and traffic theory*, 6:13–38, 1974.

[23] F. L. Hall, B. L. Allen, and M. A. Gunter. *Transportation Research Part A: General*, 20(3):197–210, 1986.

[24] W. Knospe, L. Santen, A. Schadschneider, and M. Schreckenberg. *Physical Review E*, 70(1):016115, 2004.

[25] W. Knospe, L. Santen, A. Schadschneider, and M. Schreckenberg. *Physical Review E*, 65(5):056133, 2002.

[26] B. S. Kerner. Springer, Berlin, 2004.

[27] S. Cheybani, J. Kertesz, and M. Schreckenberg. *Physical Review E*, 63(1):016108, 2000.

[28] L. I. Panis, S. Broekx, and R. Liu. *Science of the total environment*, 371(1-3):270–285, 2006.

[29] P. Kachroo and K. Krishen. *Journal of Integrated Design and Process Science*, 4(1):37–54, 2000.

[30] B. S. Kerner. Springer Science & Business Media, 2009.

[31] C. F Daganzo, M. J. Cassidy, and R. L. Bertini. *Transportation Research Part A: Policy and Practice*, 33(5):365–379, 1999.

[32] C. Systematics. Technical report, United States. Federal Highway Administration, 2004.

[33] B. S. Kerner. *arXiv preprint arXiv:0712.1728*, 2007.

[34] K. Komada, S. Masukura, and T. Nagatani. *Physica A: Statistical Mechanics and its Applications*, 388(14):2880–2894, 2009.

[35] Y. Sugiyama, M. Fukui, M. Kikuchi, K. Hasebe, A. Nakayama, K. Nishinari, S. Tadaki, and S. Yukawa. *New journal of physics*, 10(3):033001, 2008.

[36] B. Persaud, S. Yagar, and R. Brownlee. *Transportation Research Record*, 1634(1):64–69, 1998.

[37] D. P. Sullivan and R. J. Troutbeck. *Traffic engineering & control*, 35(7/8), 1994.

[38] B. S. Kerner and H. Lieu. *Physics Today*, 58(11):54–56, 2005.

[39] R. Barlovic, L. Santen, A. Schadschneider, and M. Schreckenberg. *The European Physical Journal B-Condensed Matter and Complex Systems*, 5:793–800, 1998.

[40] R. Barlovic, T. Huisinga, A. Schadschneider, and M. Schreckenberg. *Physical Review E*, 66(4):046113, 2002.

[41] R. Barlovic, A. Schadschneider, and M. Schreckenberg. *Physica A: Statistical Mechanics and its Applications*, 294(3-4):525–538, 2001.

[42] B. S. Kerner and S. L. Klenov. *Physical Review E*, 68(3):036130, 2003.

[43] B. S. Kerner and H. Rehborn. *Physical review E*, 53(2):R1297, 1996.

[44] M. Schönhof and D. Helbing. *Transportation Research Part B: Methodological*, 43(7):784–797, 2009.

[45] D. Zhong and S. Chen. In *2009 IEEE International Conference on Grey Systems and Intelligent Services (GSIS 2009)*, pages 1734–1738. IEEE, 2009.

[46] S. P. Hoogendoorn and P. H. Bovy. *Proceedings of the Institution of Mechanical Engineers, Part I: Journal of Systems and Control Engineering*, 215(4):283–303, 2001.

[47] L. A. Pipes. *Journal of applied physics*, 24(3):274–281, 1953.

[48] R. Herman, E. W. Montroll, R. B. Potts, and R. W. Rothery. *Operations research*, 7(1):86–106, 1959.

[49] M. Bando, K. Hasebe, A. Nakayama, A. Shibata, and Y. Sugiyama. *Physical review E*, 51(2):1035, 1995.

[50] S. Wolfram. *World Scientific*, 1986.

[51] T. Nagatani. *Physical Review E*, 48(5):3290, 1993.

[52] O. Biham, A. A. Middleton, and D. Levine. *Physical Review A*, 46(10):R6124, 1992.

[53] D. Buckley. *Transportation Science*, 2(2):107–133, 1968.

[54] D. Branston. *Transportation Science*, 10(2):125–148, 1976.

[55] I. Prigogine and R. Herman. Technical report, 1971.

[56] J. V. Neumann. In *Systems research for behavioral science*, pages 97–107. Routledge, 2017.

[57] S. Wolfram. *Reviews of modern physics*, 55(3):601, 1983.

[58] P. H. Kourtz and W. G. O'Regan. *Forest science*, 17(2):163–169, 1971.

[59] C. J. Boulter and G. Miller. *Physical Review E*, 71(1):016119, 2005.

[60] G. Qiu, D. Kandhai, and P. M. A. Sloot. *Physical Review E*, 75(4):046116, 2007.

[61] Q. X. Liu, Z. Jin, and M.X. Liu. *Physical Review E*, 74(3):031110, 2006.

[62] R. M. Z. Santos and S. Coutinho. *Physical Review Letters*, 87(16):168102–168102, 2001.

[63] T. Toffoli. *Physica D: Nonlinear Phenomena*, 10(1-2):117–127, 1984.

[64] D. Chowdhury, L. Santen, and A. Schadschneider. *Physics Reports*, 329(4-6):199–329, 2000.

[65] N. Rajewsky, L. Santen, A. Schadschneider, and M. Schreckenberg. *Journal of statistical physics*, 92:151–194, 1998.

[66] K. Jetto. Université Mohammed V-Agdal, Faculté des Sciences, Rabat 2010.

[67] K. Nagel. In *Traffic and Granular Flow*, pages 41–56. World Scientific Singapore, 1996.

[68] Y. Xue, L. y. Dong, L. Li, and S. Dai. *Physical Review E*, 71(2):026123, 2005.

[69] K. Nagel and P. Nelson. In *Transportation and Traffic Theory. Flow, Dynamics and Human Interaction. 16th International Symposium on Transportation and Traffic TheoryUniversity of Maryland, College Park*, 2005.

[70] V. Popkov, L. Santen, A. Schadschneider, and G. M. Schütz. *Journal of Physics A: Mathematical and General*, 34(6):L45, 2001.

[71] B. S. Kerner, S. L. Klenov, and D. E. Wolf. *Journal of Physics A: Mathematical and General*, 35(47):9971, 2002.

[72] M. Fukui and Y. Ishibashi. *Journal of the Physical Society of Japan*, 65(6):1868–1870, 1996.

[73] S. C. Benjamin, N. F. Johnson, . PM Hui. *Journal of Physics A: Mathematical and General*, 29(12):3119, 1996.

[74] W. Knospe, L. Santen, A. Schadschneider, and M. Schreckenberg. *Journal of Physics A: Mathematical and general*, 33(48):L477, 2000.

[75] W. Zhang and X. Yang. *Physica A: Statistical Mechanics and its Applications*, 387(18):4657–4664, 2008.

[76] W. X. Zhu and L. D. Zhang. *International Journal of Modern Physics C*, 25(07):1450018, 2014.

[77] A. Laarej, A. Karakhi, A. Khallouk, N. Lakouari, and H. Ez-Zahraouy. *Chinese Journal of Physics*, 71:62–71, 2021.

[78] W. X. Zhu. *International Journal of Modern Physics C*, 24(07):1350046, 2013.

[79] T. Li, J. Wu, A. Dang, L. Liao, and M. Xu. *Journal of cleaner production*, 206:688–700, 2019.

[80] M. Nyhan, S. Sobolevsky, Ch. Kang, P. Robinson, A. Corti, M. Szell, D. Streets, Z. Lu, R. Britter, S. RH. Barrett, et al. *Atmospheric environment*, 140:352–363, 2016.

[81] X. Wang, Y. Xue, B. l. Cen, P. Zhang, et al. *Physica A: Statistical Mechanics and its Applications*, 537:122686, 2020.

[82] N. Wu and W. Brilon. In *Transportation and Traffic Theory, Papers presented at the Abbreviated Presentation Sessions of the 14th International Symposium on Transportation and Traffic Theory, Jerusalem*, 1999.

[83] B. S. Kerner, S. L. Klenov, and M. Schreckenberg. *Physical Review E*, 84(4):046110, 2011.

[84] K. Ma and H. Wang. *IEEE Access*, 7:50168–50178, 2019.

[85] X. G. Li, Z. Y. Gao, B. Jia, and X. M. Zhao. *International Journal of Modern Physics C*, 20(04):501–512, 2009.

[86] M. K. Singh and K. Ramachandra Rao. *IET Intelligent Transport Systems*, 14(12):1507–1516, 2020.

[87] T. Nagatani. *Journal of Physics A: Mathematical and General*, 26(23):6625, 1993.

[88] R. Marzoug, H. Ez-Zahraouy, and A. Benyoussef. *Physica Scripta*, 89(6):065002, 2014.

[89] E. Brockfeld, R. Barlovic, A. Schadschneider, and M. Schreckenberg. *Physical review E*, 64(5):056132, 2001.

[90] N. Lakouari, H. Ez-Zahraouy, and A. Benyoussef. *Physics Letters A*, 378(43):3169–3176, 2014.

[91] M. Hossain. *Transportation research part a: policy and practice*, 33(1):47–61, 1999.

[92] M.A. De Leeuw, H. Botma, and P. H. Bovy. *Transportation research record*, 1678(1):55–63, 1999.

[93] M. Mamlouk and B. Souliman. *Journal of Transportation Safety & Security*, 11(4):430–442, 2019.

[94] A. Várhelyi. *Transportation Research Part D: Transport and Environment*, 7(1):65–71, 2002.

[95] N. Lakouari, O. Oubram, A. Bassam, S. E. P. Hernandez, R. Marzoug, and H. Ez-Zahraouy. *Journal of Computational Science*, 40:101072, 2020.

[96] N. Metropolis and S. Ulam. *Stat. Assoc*, 44:335, 1949.

[97] M. Kastner. *Communications in Nonlinear Science and Numerical Simulation*, 15(6):1589–1602, 2010.

[98] K. Murthy. Universities Press, 2004.

[99] L. Rodegerdts, M. Blogg, E. Wemple, E. Myers, M. Kyte, M. P. Dixon, G. List, A. Flannery, R. Troutbeck, W. Brilon, et al. Appendixes to nchrp report 572: Roundabouts in the united states. Technical report, 2007.

[100] M. E. Fouladvand, Z. Sadjadi, and M. R. Shaebani. *Physical Review E*, 70(4):046132, 2004.

[101] H. Echab, N. Lakouari, H. Ez-Zahraouy, and A. Benyoussef. *Physics Letters A*, 380(9-10):992–997, 2016.

[102] N. P. Belz, L. Aultman-Hall, and J. Montague. *Transportation research part C: emerging technologies*, 69:134–149, 2016.

[103] R. Wang and H. J. Ruskin. *International Journal of Modern Physics C*, 17(05):693–710, 2006.

[104] T. Nagatani and N. Sugiyama. *Physica A: Statistical Mechanics and its Applications*, 392(4):851–856, 2013.

[105] X. B. Li, R. J., and Q. S. Wu. *International Journal of Modern Physics B*, 18(17n19):2703–2707, 2004.

[106] R. Marzoug, H. Ez-Zahraouy, and A. Benyoussef. *International Journal of Modern Physics C*, 26(01):1550007, 2015.

[107] M. Rickert, K. Nagel, M. Schreckenberg, and A. Latour. *Physica A: Statistical Mechanics and its Applications*, 231(4):534–550, 1996.

[108] K. Małecki and J. Wątróbski. *Applied Sciences*, 7(7):742, 2017.

[109] K. Komada, K. Kojima, and T. Nagatani. *Physica A: Statistical Mechanics and its Applications*, 390(5):914–928, 2011.

[110] Y. Hino, K. Tobita, and T. Nagatani. *Physica A: Statistical Mechanics and its Applications*, 392(15):3223–3230, 2013.

[111] S. Belbasi and M. E. Foulaadvand. *Journal of Statistical Mechanics: Theory and Experiment*, 2008(07):P07021, 2008.

[112] L. Ye and T. Yamamoto. *Physica A: Statistical Mechanics and its Applications*, 526:121009, 2019.

[113] Highway Capacity Manual. *Washington, DC*, 2(1):1, 2000.